UC Riverside

UC Riverside Electronic Theses and Dissertations

Title

Capillary Electrophoresis-based Methodology Development for Biomolecule Analysis

Permalink

https://escholarship.org/uc/item/6v9403xz

Author

Li, Ni

Publication Date

2011

Peer reviewed|Thesis/dissertation

eScholarship.org Powered by the California Digital Library
University of California

UNIVERSITY OF CALIFORNIA
RIVERSIDE

Capillary Electrophoresis-based Methodology Development for Biomolecule Analysis

A Dissertation submitted in partial satisfaction
of the requirements for the degree of

Doctor of Philosophy

in

Chemistry

by

Ni Li

June 2011

Dissertation Committee:
Dr. Wenwan Zhong, Chairperson
Dr. Ryan Julian
Dr. Quan Jason Cheng

Copyright by
Ni Li
2011

The Dissertation of Ni Li is approved:

_____

_____

_____

Committee Chairperson

University of California, Riverside

Acknowledgement

The past five years have been rich and fruitful in my life: living in a different country, experiencing a completely different culture, making new friends, acquiring new knowledge, developing new skills, and obtaining advanced degree. I would not have achieved so much without the help from numerous people. Here, I would like to express my sincere gratitude to all of them. My apologies if I am missing anyone.

I own a great debt to my advisor, Prof. Wenwan Zhong, for everything I have learned in the past a few years. She encouraged me to explore a wide spectrum of research fields including separation, sensing, bio-analysis and nano-bio interface studies. Under her supervision, I was able to work on various projects and propose novel ideas to solve problems. Whenever I feel astrayed or got stuck, she is always there ready to give me advice and inspiration. I felt so lucky to be able to work with her.

I am indebted to Prof. Yadong Yin for using nanomaterials synthesized in his group with good qualities and for his thoughtful discussions. I am grateful to Prof. Hailing Jin (Department of Plant Pathology and Microbiology, UCR) for providing plant total RNA samples, valuable suggestions on the nucleic acid sensing projects and being my committee member for oral qualifying exam. Collaborating with their research groups helps me to find interesting projects to work on and broaden my knowledge and skills.

I feel obligated to Prof. Cynthia Larive and Prof. Yinsheng Wang for providing interviews for me to join the Ph.D. program here. I would like to thank Prof. Ryan Julian and Prof. Quan Jason Cheng for being on my oral qualifying exam committee and my thesis committee. Also, thanks all for your wonderful classes.

My thanks need go to my collaborators, Dr. Jishan Li (now Associate Prof. at Hunan University, China), Shang Zeng, Le He, Carolyn Jablonowski (now a Ph.D. student in Cornell University), Sonja Kress, Anh Nguyen for their hard work and contribution. I would like to thank my group members: Dr. Runtao Zhong, Lei Ren, Samantha Schachermeyer, Jingjing Yao, Jonathan Tyrone Ashby, Kenneth Flack and Jimmy Vo for the life we spent together here in UCR. I would also like to thank all my classmates and friends in UCR.

I would like to thank my previous advisor Yunqiu Yu in School of Pharmacy, Fudan University and my dear teachers, collaborators and friends there. Without the research experiences there, I would not find my interest in analytical chemistry and definitely would not be able to carry out independent research so quickly here in UCR.

Last but certainly not least, my thanks must go to my dear family members, my husband, my mother-in-law, my sister and my aunt's family, for their unconditional love and exceptional support. My husband Yonghui Wu, who has been a graduate student in Department of Computer Science and Engineering in UCR, accompanied me for the first

two years of my Ph.D. studies, and I cannot imagine how the life would be like. In the recent three years, he kept on encouraging me on research and life. This dissertation is dedicated to my dad and mom, who passed away when I was still young. You are memorized forever and we all miss you.

Copyright Acknowledgements

The text and figures in Chapter 3, in part or in full, are a reprint of the material as it appears in *Electrophoresis* 2008, *29*, pp. 424-432. The coauthor (Dr. Wenwan Zhong) listed in that publication directed and supervised the research which forms the basis of this chapter.

The text and figures in Chapter 4, in part or in full, are a reprint of the material as it appears in *Analytical Chemistry,* 2009, 81, pp. 4906-4913. The coauthor (Dr. Wenwan Zhong) listed in that publication directed and supervised the research which forms the basis of this chapter.

The text and figures in Chapter 6, in part or in full, are a reprint of the material as it appears in *Analytical Chemistry,* 2010, 82, pp. 7460-7466. The coauthor (Dr. Wenwan Zhong) listed in that publication directed and supervised the research which forms the basis of this chapter.

ABSTRACT OF THE DISSERTATION

Capillary Electrophoresis-based Methodology Development for Biomolecule Analysis

by

Ni Li

Doctor of Philosophy, Graduate Program in Chemistry
University of California, Riverside, June 2011
Dr. Wenwan Zhong, Chairperson

Capillary electrophoresis (CE) is a separation tool with wide applications in biomolecule analysis. Fast and high-resolution separation requiring minute sample volumes is advantageous to study multiple components in biological samples. Flexible modes and methods can be developed. In this thesis, I focus on developing and applying novel CE methods to study multi-target nucleic acid sensing with high sensitivity (Part I) and interactions between multiple components, i.e. proteins, nanoparticles and drugs (Part II).

In Part I (Chapter 2-4), rolling circle amplification (RCA) was combined with CE-laser induced fluorescence detection (LIF) for sensitive detection of DNA and small RNA. In Chapter 3, development of the RCA-CE method for DNA detection was systematically carried out. The obstacle of injecting long ssDNA to capillary was overcome by digesting

them into identical short ssDNA fragments. Under optimized conditions, LOD was as low as 1.6 fmol. Dual-target sensing was also demonstrated with two padlock probes. In Chapter 4, to further improve the sensitivity for small RNA sensing, the stand-alone RCA was studied. Eliminating ligation and using the target small RNA as RCA primer simplified the assay procedure and lowered the detection limit to 200- or 35- amol with good specificity. Highly reproducible detection and accurate quantification of the target small RNA in plant total RNA extracts was achieved with the complete digestion of the background RNA molecules by RNase A. Two polymerases, *Phi29* and *Bst* were compared on their performance.

In Part II (Chapter 5-7), CE was first explored as a flexible platform to quantitatively measure the dissociation constant of the nanoparticle-protein interaction. Then, mechanism studies on driving force and binding sites identification were carried out. Surface ligand pyrolysis was revealed by mass spectrometry. Desolvation was considered as a driving force which could overcome electrostatic repulsion in our systems. Peptides associated with binding site were identified by cross-linking and mass spectrometry. They were surface peptides within drug binding site 2. Ibuprofen and naproxen, drugs sharing exactly the same binding site, would suppress the binding between human serum albumin and the Fe_3O_4 NPs. Fusidic acid, binding HSA in a site remote to site 2, showed no effect.

Contents

Chapter 1. Introduction……..……1

Part I

Chapter 2. Amplification-based nucleic acid sensing……..…19

Chapter 3. Combining rolling circle amplification with CE-LIF for sensitive DNA detection

3.1 Introduction……..…25

3.2 Experimental……...….27

3.2.1 Reagents

2.2.2 Instrumentation

2.2.3 RCA templates, probes, replication primers, and reaction conditions

3.3 Results and Discussions……...30

3.3.1 Initial investigation of the RCA reaction with CE

3.3.2 Enzyme digestion of the RCA product

3.3.2 Reaction optimization

3.3.4 Target quantification and duplexed sensing

3.4 Conclusions……..……45

Chapter 4 Stand-alone rolling circle amplification combined with capillary electrophoresis for specific detection of small RNA

4.1 Introduction…….……..……47

4.2 Experimental…….……..…..…49

4.2.1 Reagents and materials

4.2.2 CE conditions

4.2.3 Circular probe generation

4.2.4 Comparison of ligation efficiency

4.2.5 Stand-alone rolling circle amplification, restriction enzyme digestion and sample clean-up

4.3 Results and Discussions……..……55

4.3.1 Design of the detection scheme

4.3.2 Specificity study

4.3.3 Standard calibration curve

4.3.4 Small RNA detection in plant total RNA extracts

4.4 Conclusions…….……71

Supporting information…….……73

Part II

Chapter 5 Analysis of the nano-bio interface……..……77.

Chapter 6 Probing nanoparticle-protein interaction by capillary electrophoresis

6.1 Introduction…….82

6.2 Experimental……..……..84

6.2.1 Reagents and materials

6.2.2 Synthesis and characterization of NPs

6.2.3 Capillary electrophoresis

6.3 Results and discussions……..…..87

6.3.1 CE modes and affinity calculation

6.3.2 Slow dissociation system

6.3.3 Fast dissociation system

6.3.4 Impact on affinity from incubation conditions

6.3.5 Understanding the interaction from K_D and n

6.4 Conclusions……...101

Supporting Information……..…….103

Chapter 7 Mechanism study on nanoparticle-protein interaction by capillary electrophoresis and mass spectrometry

7.1 Introduction……107

7.2 Experimental……..……110

7.2.1 Synthesis of PAA-Fe_3O_4 NPs

7.2.2 Capillary Electrophoresis

7.2.3 MALDI-TOF MS for PAA characterization

7.3.4 Cross-linking and MALDI-TOF MS for binding site identification

7.3 Results and Discussions…….113

7.3.1 Pyrolysis identified by MS and affinity differences

7.3.2 Driving force of desolvation

7.3.3 Peptides associated with nanoparticle-protein interaction interface identified by cross-linking and mass spectrometry

7.3.4 Binding sites further confirmed by drug binding tests

7.4 Conclusions……...…….129

Supporting Information……...131

Chapter 8 Conclusions…….……..…..141

References……...…….143

Chapter 1

Introduction

In chemical and biochemical sciences, separating individual components from a complex mixture is a critical step in studying the system. Once individual components are separated and purified, structural and functional study of each specific component can be carried out. By resolving all components, scientists can obtain the relative concentrations of components and how they are affected by external stimuli to the system, propose the relationship between them and further design new experiments to test their hypothesis or predict what would happen under a given condition. With each piece of information obtained, understanding of the system is pushed to an even deeper level. Novel components of interest may need to be separated, identified and characterized along the way.

In order to meet the requirements of real-world problems, separation techniques have been developed and improved considerably. Individual components are usually separated based on differences in their properties, for example, hydrophobicity, molecular weight, charges, et cetera. The term of electrophoresis is from Greek words elecktron: electron and phoresis: carrying. It is a separation method where components are separated from each other under an electric field by differences in charge-to-mass ratio. In 1930s,

Tiselius separated human serum into albumin, α-, β-, and γ-globuIin[1] and was awarded the Nobel Prize in 1948. His pioneering work demonstrated the potential power of electrophoresis. Hjerte`n demonstrated free solution electrophoresis under high electric field strength within a 3 mm-inner diameter (i.d.) capillary in 1967.[2] In 1981, Jorgenson and Lukacs[3] published a pioneering paper on modern capillary electrophoresis, in which a simple theory on dispersion in CE was developed and for the first time a 75 μm i.d. capillary was introduced as a separation channel to demonstrate high separation efficiency with high field strength. Ever since, many important inventions and developments have been made in capillary electrophoresis. At the end of 1980s, commercial CE instrument became available. Intensive development on electrophoresis methodology and instrumentation has resulted in powerful and efficient analytical tools for biomolecule analysis. High-throughput CE separation equipped with laser induced fluorescence detector has played critical role in scientific and commercial genome-wide sequencing. New miniaturized capillary or even micro-chip versions of electromigrational methods have been developed for protein analysis while the traditional 2-D gel electrophoresis method is still most widely applied. Another powerful method, capillary isoelectric focusing with pressurized and pH-driven mobilization, provides efficient separations and on-line sensitive detection of proteins, bacteria and viruses. Electrophoretic microfluidic devices can integrate single-cell injection, cell lysis, separation of its components and fluorescence or mass spectrometry detection. These miniaturized devices also proved the capability of single-molecule detection. Capillary electrophoresis has evolved into one of the most promising tools to analyses and

preparative separations of complex biological samples.[4] This thesis work is focused on methodology development to analyze biomolecule of interest coexisting with large amount of background biomolecules and/or other components in a complex system.

Historically, CE originated from traditional electrophoresis. Therefore, basic theory of CE covers the separation theory of electrophoresis and, more importantly, the theory associated with the capillary features. Under an electric field, charged species will experience Coulomb forces (related to charges of analytes and strength of electric field) and some friction forces from separation media (related to size of particle and viscosity of separation media). The inside wall of a fused-silica capillary will be negatively charged due to the dissociation of –Si–OH into –Si–O^- at most pH conditions. The positive counter-ion layer adjacent to the wall will move toward negative electrode under an electric field, resulting in the bulk flow of liquid toward the electrode like a plug, which is called electroosmotic flow (EOF). At the same time, species with different charges and sizes can be resolved based on their electrophoretic mobility differences (see details on the movement of cations, anions and neutrals discussed in capillary zone electrophoresis section). The plug flow, unlike a parabolic flow which is usually the case for liquid chromatography, provides even flow and very flat flow front and therefore make it possible to achieve extremely high theoretical plate counts in separation. In addition, CE has several other advantages in terms of separation. Some of the advantages include very small sample size, fast separation speeds, various modes of separation and diverse application range (e.g. nucleic acids, peptides, proteins, drugs, chiral compounds). It is

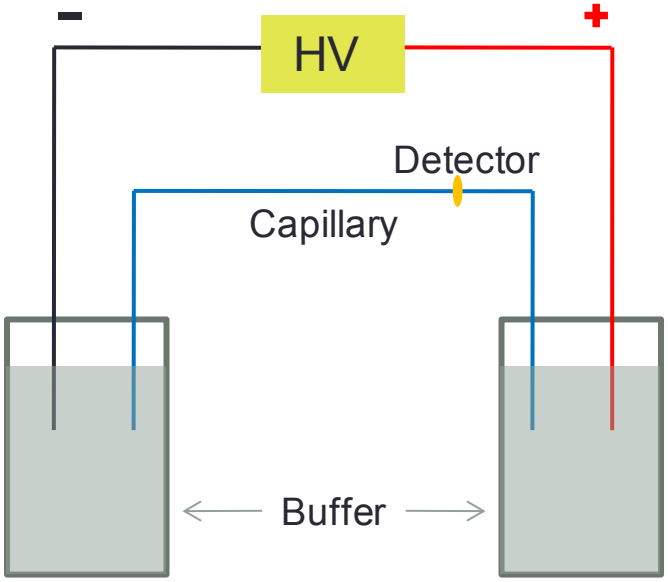
compatible with most of the commercial detection methods (e.g. UV-vis, LIF, microscopic imaging) and hyphenatible with mass spectrometry. The analysis throughput can be enhanced with either a high-throughput CE instrument or a micro-chip CE. It is also a low-cost and low-waste technique. Although CE has its own limitations, such as reproducibility, commercialized instruments have considerably aided in CE reproducibility.

The basic instrumental set up of CE is shown in Figure 1.1. It includes a fused-silica capillary with an optical viewing window, a high-voltage supply, two electrodes, two solution reservoirs and a detector. Commercially available CE instruments usually provide temperature controls on capillary and solution reservoir trays, pressure and electrokinetic injection, automated solution reservoir switching, programmable method development and computer control on all the operations. Several features in recent models of commercial CE instrumentation provide innovating electrophoretic separation solutions. Electrophoretic separation in commercial microfluidic networks of channels and wells is designed for biomolecules and cells analysis. Fractionator based on isoelectric focusing can be incorporated to resolve proteins or peptides by isoelectric point. Seamless integrated with mass spectrometer greatly improves the sensitivity and the accuracy in molecular identification and detection.

There are a couple of widely used modes for CE: capillary zone electrophoresis (CZE), capillary gel electrophoresis (CGE), capillary isoelectric focusing (CIEF), capillary

isotachophoresis (CITP), micellar electrokinetic capillary chromatography (MECC), et cetera. In this thesis, CZE and CGE are major modes that have been adopted. In addition, affinity capillary electrophoresis (ACE), not a mode, but the general term for CE on molecular interaction study, is also a useful tool utilized in this thesis work.

Figure 1.1 Schematic instrumental set-up for CE.



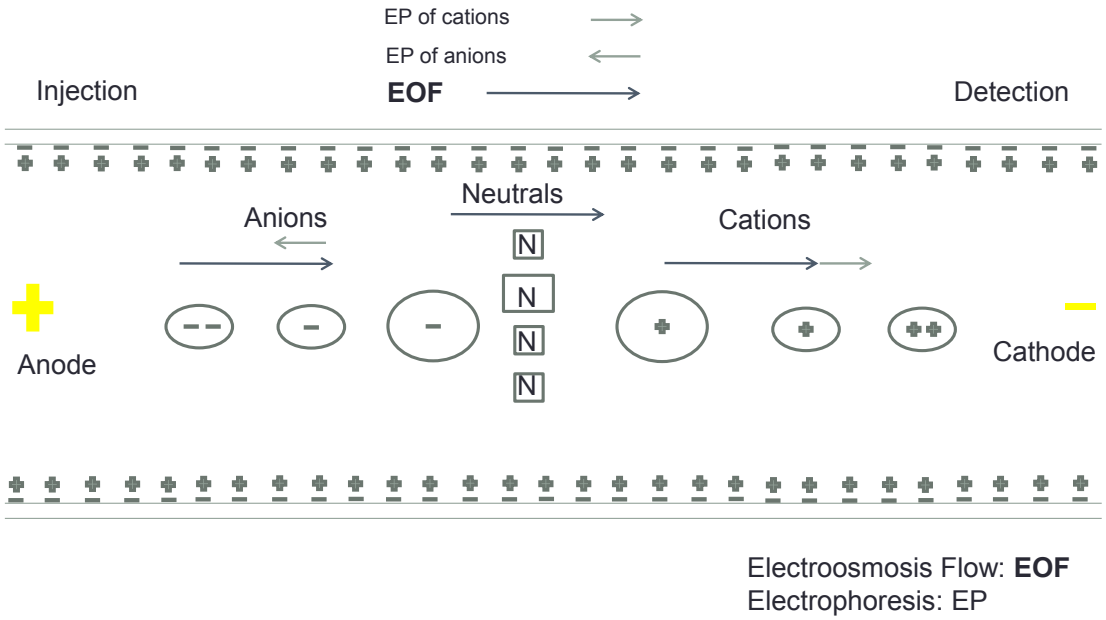
Capillary zone electrophoresis, also called free-solution capillary electrophoresis, is by far the most commonly used CE separation mode due to its simplicity and wide application range. The separation in CZE mode is based on the electrophoretic mobility differences due to different charge to mass ratios of the charged species in an electrophoretic buffer (background electrolytes or running buffer) inside capillary. The EOF generated on the interface between the running buffer and an uncoated fused-silica capillary wall is usually significant, greater than the electrophoretic mobility of injected

ionic analytes. As a result, it takes short time (a few minutes) to bring all the charged analytes passing the optical detection window. In the simplest case, the running buffer maintains a constant pH and ionic strength, which ensures the analytes have stable charges and constant electric field strength inside the capillary. As illustrated in Figure 1.2, in a normal mode (anode on the injection side and cathode on the other side, detection window close to the cathode side) separation, cations are attracted by the cathode under electric field and at the same time the EOF brings everything inside capillary toward cathode in a plug flow. Thus, cations with highest charge-to-mass ratio migrate fastest, followed by cations with lower charge-to-mass ratio. Neutral analytes with a charge-to-mass ratio zero migrate later than all the cations. Anions are repelled by the cathode under electric field and they will be swept toward the cathode by EOF together with all other species. Anions with less charge-to-mass ratio migrate earlier than those with larger ratios. The relationship between electrophoretic mobility (μ_p) and charge-to-mass ratio can be expressed as

$$\mu_p = z/6\pi\eta r$$

where z is the net charge of the analyte, r is the Stokes radius and η is the viscosity of the separation medium. To carry out a successful CZE separation, pH is probably one of the most important conditions to optimize because pH will significantly change ionization status of ionic analytes. Solvation of the ions can also affect the electrophoretic mobility. Hence, solvent selection in CE will ensure good solubility of analytes during seperation and at the same time adjust the electrophoretic mobility.

Figure 1.2 The separation in CZE at normal mode.



Another important concept is effective mobility, which have greatly broadened the application of CE application for biomolecule analysis. It is common that in certain a solution, the analyte is present in a fast dynamic equilibrium. The ensemble of several forms behaves as one entity with certain an effective mobility, for example, the neutral and ionic forms in acid-base equilibria, the free and complexed forms in complexation equilibria. Tuning equilibrium status (e.g. partition equilibria in MECC,[5, 6] host-guest interaction in chiral separation by CE with CD additives[7]) can be used to separate analytes, More interestingly, for interaction equilibria involving biomolecules, such as antibody-antigen interaction, drug-receptor interaction and others, effective mobility shift in affinity CE has been successfully monitored to measure the affinity quantitatively.[8-10]

Most of inorganic ions and small organic ions exhibit different charge-to-mass ratios in aqueous solution. However, there are extremely important biomolecules, e.g. DNA, that have the same charge-to-mass ratio. They can not be effectively separated in free solution CE but capillary gel electrophoresis successfully overcomes the problem. In capillary gel electrophoresis, separation media is either a cross-linked gel or a polymer solution, which plays the role of "molecular sieving". Analytes with similar charge-to-mass ratio, such as DNA and RNA, can be separated mainly by their size. The EOF is generally suppressed by the capillary gel, so the analyte is driven by the electrophoretic mobility. The gel media minimizes analyte diffusion, convection, and prevents sample adsorption to the capillary wall. Thanks to the single-base resolution of commercialized CGE array based DNA sequencers, human genome sequencing, the process of determining the exact order of the 3 billion nucleotides, was successfully carried out by using automated capillary array gel electrophoresis with laser induced fluorescence detection. Currently, the performance of a sequencer equipped with CGE array separation is excellent. Usually ninety-six capillaries are adopted, and in each capillary 1-5 nL of sample is injected. With the ability of reading 166-400 bp/h and average reading length of 650 bp, one round of analysis takes only one to three hours.[11] The term "Gel" in CGE can be cross-linked polymer gel or un-cross-linked polymers for different applications. In this thesis work, un-cross-linked polymer solution was prepared for analyzing short length of oligonucleotide. Polyvinylpyrrolidone (PVP, avg Mw 1,300,000) was adopted to prepare an entangled polymer solution in 1 × TBE buffer with low viscosity for our study. The low viscosity is quite advantageous since without additional hand-held injector, the gel

solution can be easily introduced into and rinsed out from the capillary by the pressure control on the commercial CE instrument, which greatly improved the reproducibility of the separation. Electokinetic injection was employed to introduce charged analytes into capillary. To achieve high efficiency, stacking injection was used based on the viscosity and conductivity differences between the sample solution and the polymer matrix. Desalting is critical before electrokinetic injection if higher sample amount needs to be injected, since ionic species (including oligonucleotides and salts) will be driven into capillary be voltage and only when the salt amount is minimized, can the injection efficiency for oligonucleotide be maximized. Negative separation mode (cathode on the injection side and anode on the other side, detection window close to the anode side) was chosen for oligonucleotides detection. In this mode, negatively charged oligonucleotides were attracted by anode (close to the detection window) under electric field. Laser induced fluorescence detection was adopted by adding intercalating dye SYBR GREEN in both gel solution and running buffer.

Within the past 20 years, CE has been successfully utilized in a wide range of applications. It has been adopted for pharmaceutical analysis, food and beverage analysis, forensic purposes, molecular diagnosis, plant and agriculture studies, environmental studies, et cetera. The analytes can be analyzed by CE include small molecules[12] (i.e. basic drug molecules, chiral compounds, metal ions and inorganic anions, amino acids), large molecules (i.e. DNA, RNA, peptides and proteins) and particular analytes (i.e.

inorganic particle, lipoprotein particle, liposomes and microsomes, viruses).[13] In terms of biomolecule analysis, nucleic acids, proteins, carbonhydrates, lipids can all be analyzed by CE.[14] In recent years, a lot advances and development on CE have been made for biomolecue-analysis.

Novel solutions to problems related to biomolecule analysis have been found using CE. There are many interesting biomolecule associated problems in research. We will focus on a few problems related to this thesis work. In the field of single-cell nucleic acid analysis, for instance, CE was adopted as an enabling separating tool and utilized in versatile forms for various purposes, such as cell lysis, nucleic acid amplification, et cetera. Cells, as a functional basic unit of life, attract great attention from biologists, pathologists, toxicologists, pharmacologists and medicinal chemists. One of a few cells significantly different from its or their neighbors under certain condition or at some specific stage can be beneficial or more commonly harmful for the existing living organism. For instance, bacteria cells have different resistance to antibiotics which could be attributed to accidental gene mutations occurred in few bacteria strains. Such difference is the basis for the selection of bacteria strain with the capability to survive the antibiotics. Stem cells are another group of cells that show significant variations from cell to cell, each having the ability of renewing themselves through mitotic cell division and differentiating into a diverse range of specialized cell types. What controls the cell development at each growing stage? What determines the final cell phenotype? Only with advanced development in techniques analyzing gene mutation and expression at the

single-cell level may all those puzzles be solved. Enabling techniques for single-cell analysis are also beneficial to investigations on cells with extraordinary complexity, such as mammalian neurons and tumor cells,[15] and to studies dealing with limited availability of homogeneous cell populations, like stem cells. Unfortunately, classic analytical methods only report the average composition of a number of cells due to limited sensitivity and sample handling ability. In the past ten years, researchers put efforts towards developing novel assays toward genes and gene expression at the single cell level based on the analytical devices (i.e. CE, microfluidic chips) with small volume and high sensitivity in detection (i.e. Laser-induced fluorescence, intense CCD camera imaging). Capillary electrophoresis-based gene and gene expression analysis studies demonstrated the basis of constructing affordable and applicable assay platforms. In these platforms, conventional gene analysis assays were performed in miniaturized devices with high degree of automation,[16, 17] and several challenges were addressed, including how to integrate and simplify the processes of cell introduction,[18] cell lysis,[16, 19] protein removing and gene amplification, how to modify the enzymatic reactions for adaptation to the capillary column reactor,[17, 20, 21] and how to extract as much information as needed from one single cell.

Nanotechnology is another field of interest. Compared to bulk materials, nanomaterials showed intrinsic unique mechanical, electric and optical properties due to their nanometer-scale size effect. From “bulk” to “nano”, a lot of material features change. For example, the surface to volume ration increases significantly, specific surface

energies of nanomaterials are higher than the bulk, and the size below 100 nm is small enough to enter living systems. Many revolutionary discoveries and inventions are expected from nanomaterials,[22-24] such as next-generation computer processors, novel fuel-cells, bio-sensing, bio-imaging tools, drug-delivery systems, et cetera. In order to take full use of nanomaterial properties for specifically designed usages, nanomaterials have to be well-characterized, both qualitatively and quantitatively. A lot of techniques have been used on nanomaterial characterization but challenges still exist.[25] Several microscopy techniques, including atomic force microscopy (AFM), transmission electronmicroscopy (TEM) and scanning electron microscopy (SEM), are used for morphology observation. Dynamical light scattering based instruments are utilized to measure hydrodynamic sizes and zeta potentials. X-ray diffraction (XRD) is useful for crystal structure analysis. Classic spectrometry techniques, including UV-vis, IR, Raman, provide functional group information for nanomaterials. The above mentioned techniques are very familiar to nanomaterial synthesis chemists because they need to figure out what kind of nanomaterials they are synthesizing. However, more quantitative analytical methods are less commonly used. Inductively coupled plasma-atomic emission spectroscopy (ICP-AES) and ICP-mass spectrometry[26] have been used to quantitatively measure element composition in nanomaterials. Separation techniques are also important for nanomaterial analysis. However, these techniques have several difficulties that need to be overcome before they can be regularly used. Since nanomaterials may clog the separation channel of a chromatographic column, an open channel separation, such as CE, would be beneficial. So far, CE has been successfully used for nanoparticle

characterization and bioconjugation on nanoparticles.[27-29] For the applications in biomedical fields, nanomaterials have more opportunities to be exposed to biomolecules. When engineered nanomaterials enter the circulatory system, they will immediately interact with protein in the bloodstream, giving the nanomaterial new surface features. What a cell sees is the protein corona coating the nanomaterials.[30] In addition, on the market, there are more and more consumer products (i.e. sunscreens, painting products and many more) available to the consumer that contain these nanomaterials. There are also concerns from environmental contamination of nanomaterials. Both intentional and accidental exposures to nanomaterials have raised concerns about the nanotoxicity of these materials. Capillary electrophoresis separation can be done in an open tubular channel. It is a technique widely used for bioanalysis purposes. It is also a technique useful for nanomaterial analysis. To study the system containing both biomolecules and nanomaterial, CE would be a good choice. In this thesis work, we took advantages of CE and developed methods to probe protein and nanoparticle interaction (see Chapter 5-7).

On the other hand, the technique itself, with some modification, or coupled with other techniques, is becoming a powerful separation-based analysis platform for biomolecule analysis. Nearly all electrophoretic separation techniques have been reviewed by experts and specialized reviews and even special review issue[31] can be found. Methodology development is enabling this classical separation tool to handle novel tasks When studying nucleic acids, it is important to balance sensitivity and specificity. For protein related studies, the separation condition has to be well selected to avoid non-specific

adsorption to the capillary wall. In addition, for binding assays, it would be ideal to carry out the separation in buffers close to physiological conditions, and no extra disturbance to the binding system. To solve those problems, methodology development on new additives, new gel recipes, new capillary wall coating, new integrated design, CE-MS and chip-based CE have improved the performance of CE for various purposes. Additives in running buffer are used to obtain better separation or avoid non-specific interaction. CTAB/chloride (CTAB/C), a cationic surfactant, has been used as buffer additive for CE of proteins.[32-35] By using CTAB, both capillary wall and proteins have positive charges, thus the proteins may be repelled from the capillary wall. In addition, CTAB interacts with proteins in a quite different manner from SDS: the stoichiometry of SDS bound to proteins is relatively uniform, i.e. one SDS molecule interacts with two amino acid residues at SDS concentration above the CMC [36]; whereas CTAB interacts to different degrees with different proteins, which may enlarge the differences in mass-to-charge ratio between proteins [32, 34] and thereby facilitate the separation.[37] Well studied uncross-linked polymer, including linear polyacrylamide,[38] hydroxyethyl cellulose,[39, 40] and their derivatives,[40, 41] have been used for separation of DNA, protein, sugar isomers, low-molecular compounds, *etc.*. in traditional CE. With the development of microchip-base electrophoresis, some new gel recipes showed their advantages. For example, a novel DNA separation matrix, cholesterol-bearing pullulan (CHP) nanogels, for microchip electrophoresis was reported last year.[42] The solution of the CHP showed a unique phase transition around 30 mg⁄mL and formed gel phase over this critical concentration. This gel phase consists of the weak hydrophobic interactions between the cholesterols could

be easily deformed by external forces, and thus, loading process of the CHP nanogels into microchannels became easier. The high concentration of the CHP nanogels provided excellent resolutions especially for small DNA fragments from 100 to 1500 bp. Fast (within 170 s) and excellent separation of DNA restriction fragments ranging in size from 72 to 1353 base pairs (bp) is achieved in a 30 mm length channel of polymethylmethacrylate (PMMA) microchips electrophoresis at an electric field strength of 300 V/cm, by introducing 8% mannitol, 8% glucose or 10% glycerol additives into a 2% HPMC-50 / 1 × Trisborate-EDTA (TBE) solution. The low-viscosity (40 cP) matrix formulation enhanced by polyhydroxy compounds additives provides both coating of the microchannels and separation of DNA in one step.[43] Capillary wall coating, non-covalent[44, 45] or covalent coating[46], is generally to alter surface charge status for different purposes, mainly aiming at avoiding analyte adsorption by suppressing EOF. Integration or coupling with other techniques has powered CE up for more efficient analysis. For example, a micro-solid-phase extraction (μSPE) device containing only nanograms of silica resin was demonstrated by Tian et al.to be effective for the adsorption and desorption of DNA in the picogram–nanogram mass range for a CE-LIF system.[47] Kato et al. reported an integrated system including on-line protein digestion, peptide separation, and protein identification using pepsin-coated photopolymerized sol-gel columns and capillary electrophoresis/mass spectrometry. The miniaturized pepsin reactor was prepared inside a fused-silica capillary (i.d. 75 μm) by coating a pepsin-containing gel on a photopolymerized porous silica monolith (PSG). The immobilized pepsin-digested peptides and proteins, and the resulting mixture of peptide fragments,

could be directly separated in the portion of the capillary where no PSG monolith exists. The on-line digestion of insulin chain beta and lysozyme provides identification of the proteolytic peptides. Recovery was achieved for 100% of the insulin chain beta amino acid sequence and 73% of the lysozyme amino acid sequence.[48]

In the past five years, I focused on developing CE-based methodology for biomolecule analysis, mainly on two topics: nucleic acid sensing and nano-bio interface probing. More detailed backgrounds for those two research topics will be discussed respectively in Chapter 2 and Chapter 5.

Our work has explored CE applications on separating and analyzing interested small amount of biomolecules co-existing with large amount of backgrounds; and also probing the supermolecule assemblies composed of multi-components, such as proteins, nanoparticles and drugs. The resolving power of CGE in part I enabled us to analyze the reaction mixture containing different lengths of nucleic acids when RCA was adopted to enhanced the sensitivity. The RCA-CE method has adequate sensitivity (LOD 1.6 fmol) to detect DNA materials extracted from several hundred cells if the amplification is performed on-line. The stand-alone RCA-CE method, with a further decreased detection limit by 10-fold, can be applied to detect small RNA extracted from a few cells. Our work on nucleic acid sensing is one important step towards single cell level detection using isothermal amplification. We expect that in the future, a micro-chip integrating cell sorting, nucleic acid extraction, RCA, electrophoresis separation and online real-time

detection would be capable to detect nucleic acid of interest at single cell level. In part II, to probe the interaction in a complex system, especially when the components appeared to be different groups of molecules, including large biomolecules, inorganic nanoparticles with polymeric ligands, and small drug molecules, a flexible separation platform of open tubular channels imposing minimized disturbance to the complex system was demonstrated and applied to quantify the affinity and monitor the competition of binding. Quantitative affinity measurements, using CZE and ACE, are easy to carry out and only require very small amount of samples. Thermodynamics studies were demonstrated by altering the temperature. We isolated surface ligand from nanoparticle and characterized them by MS. This novel strategy is greatly needed since the information at the molecular level provided by MS would be quite beneficial. Our findings proved that small changes on the synthesis procedures might generate different ligand features and hence distinct binding behaviors. Cross-linking coupled with MS was for the first time adopted for binding site identification between nanoparticle and protein. Until now, complexes involving known identities of interaction parties can be probed and mechanism was illustrated based on our experiments on a few proteins and nanoparticle pairs. In order to obtain full and deep understanding of the interaction, more pairs of interaction parties should be tested and physicochemical properties can be altered one by one, and more information should be collected by applying other techniques to characterize interaction parties before, during and after the interaction. The long term goal of the research is to obtain the guiding rules for the interaction based on systematical experiments and

thorough theoretical explanation. This will be greatly beneficial for better bionanomaterial designing and less unwanted nanotoxicity.

In summary, CE is way more than a simple separation in present days. The trends in CE biomolecule analysis are towards broader application range, better separation efficiency, and higher throughput. Highly integrated with other sample preparations and detection techniques, and precisely controlled by computer programs are necessary for automated biomolecule analysis. We've seen a few milestones along the way so far. They are capillary array separation format, online laser-induced fluorescence detection, coupled to mass spectrometry, multi-dimension separation, miniaturized on chip, incorporation of immunoassay concept, et cetera. In biological research field, new research topics will keep on bringing up interest to new analytes. More importantly, platforms aiming at sensitive and fast analysis with minimum sample preparation need to developed for many known analytes, especially in early diagnosis for some diseases. CE has been proven as a state-of-the-art technique for biomolecule analysis. Advanced methodology development and frontier instrumental design will further power up CE to approach the ultimate qualitative and quantitative analysis goals for biomolecule analysis in complex sample matrixes.

Chapter 2

Amplification-based nucleic acid sensing

Nucleic acids are essential biomolecules for life, and include DNA and RNA. In 1871, nucleic acids were for the first time discovered by Friedrich Miescher.[49] Scientific studies on nucleic acids are a major part of molecular biology and medical research. Based on the understanding of nucleic acids, biotechnology, pharmaceutical industries and forensic sciences developed to a great degree. The central dogma of molecular biology[50] states about the normal flow of biological information: DNA can be replicated or transcribed into mRNA, and proteins can be synthesized using the information in mRNA as a template (translation). The uncoding process passes the core genetic information, coded in DNA, to the next generation accurately. Knowing the exact copy numbers of specific DNA or RNA strand, or the mutations occurring, are beneficial for all fields utilizing molecular biology information, especially in a fast, affordable and accurate way. Unfortunately, acquiring this information is difficult when limited amounts of sample are available, such as in forensic sciences and clinical diagnosis. Therefore, scientists have developed many nucleic acid sensing platforms to meet these requirements of the real-world problems. In general, a nucleic acid sensor contains a biological element where target nucleic acid can be specifically recognized, mostly by sequence complementary hybridization, or some other methods, such as aptamer recognition; it also contains a

transducer where signals can be generated and recorded, where it could be realized by electrochemistry,[51] optical labels (i.e. fluorophore labels[52, 53]), or other readouts without any labels (i.e. surface plasmon resonance (SPR);[54] microgravimetric balance[40], a field-effect transistor device [55]); another important part for a nucleic acid sensor could be designed to amply either the target amount,[56] or the readout signals.[53] Separation in a broad definition, such as washing, is in many cases used to remove non-specific nucleic acid strands. More specific separation techniques, such as CE,[57] magnetic pull-down,[58] and microfluidic separation,[59] are also useful for sensing target nucleic acid in presence of background strands with improved signal to noise ratio. In this thesis work, we mainly utilized CE as a robust tool for multi-target nucleic acids sensing with good high-throughput compatibility.

Amplification is a crucial step for nucleic acid sensing because it will greatly improve the sensitivity. Here we will focus on some biological reactions for nucleic acid amplification purpose. Polymerase chain reaction (PCR) is a molecular biological reaction catalyzed by DNA polymerase in which single or a few copies of a piece of DNA can be amplified by several orders of magnitude. Most PCR requires a heat-stable DNA polymerase, such as Taq polymerase, which is good for amplification reactions with thermal cycling (repeated heating and cooling for DNA melting and enzymatic replication of the DNA). An automated thermal cycler is required to accurately control the programmed cycles on temperature. Primes are designed to fully complementary to target DNA region. The length of prime affects the selectivity of the PCR. Usually a primer slightly longer than

17nt is adopted so that it will target specific DNA piece in a genome-wide pool. The widely accepted quantitative PCR is real-time PCR, in which two common methods for detection of products are employed. One is that non-specific fluorescent dyes intercalate with double-stranded DNA, and the other is sequence-specific DNA probes consisting of fluorescence-labels permits detection only after hybridization of the probe with its complementary DNA target. To amplify a RNA target, reverse transcription polymerase chain reaction (RT-PCR) is needed. The polymerase is called a reverse transcriptase, or a RNA-dependant DNA polymerase, which will utilize a RNA template to reverse transcribe into its DNA complement (cDNA) strand and the cDNA strand is then amplified by traditional or real-time PCR.

Both PCR and RT-PCR require well controlled thermal cycling. Those techniques can improve the detection limit greatly. However, for short stand DNA or RNA targets, PCR and RT-PCR exhibit inherent limitations due to primer design. Short DNA strands are usually generated during the process of gene fragmentation. Efficient alignment of short DNA strands is needed to read the full genome. Artificial short DNA strands are widely used on microarray as capture probes or detection probes. In comparison, with more biological effects, short RNA strands naturally exist in living cells playing very important regulatory roles. Non-coding, small (17-25 nt) RNAs are a big family of RNA molecules that do not encode for proteins but carry out their highly specific regulation of gene expression through the RNA-mediated silencing mechanism in multicellular organisms like plants and animals.[60-62] Several small RNA classes have been discovered and linked

to diverse biological processes. For example, microRNAs (miRNAs) play important roles in cell development, proliferation, and apoptosis; small interfering RNAs (siRNAs) are involved in pathogen defense[63, 64] and stress response[65, 66] in plants and animals. Small RNAs have also been found to be key regulators of quorum sensing [67, 68] and metabolism[69] in bacteria. Moreover, recent research has demonstrated that the regulatory roles of small RNAs could be expanded to disease initiation and development,[70-75] as well as stem cell maintenance and differentiation.[76] Despite small RNA's significance in biological processes, their underlying molecular and cellular mechanisms are not fully understood. Successful exploration of novel small RNA species and their functions vastly depends on high-throughput analysis of the expression of small RNAs during functional studies, which calls for sensitive, simple, rapid, and cost-effective detection assays.

Rolling circle amplification (RCA), an isothermal DNA replication technique, has been proved very useful for the detection of target nucleic acids and proteins.[77, 78] In RCA, a DNA polymerase with strand displacement activity amplifies a circular template using a forward primer. The resulted product is a long single-stranded DNA molecule that contains thousands of repeats of the complementary sequence to the template, meaning that thousands of detection sites are generated from each target molecule.[79] The circular template for RCA can be formed from a linear ssDNA, the padlock probe. The 5' and 3' termini of the padlock probe first hybridize precisely onto the target and then are joined by a DNA ligase.[80] RCA offers several advantages over other amplification technologies. The linear amplification process of RCA allows better quantification compared to the

exponential amplification process in regular PCR/RT-PCR. The stringent requirement of ligation on strand matching increases the specificity of RCA in DNA detection. The isothermal reaction condition eliminates the requirement for a temperature cycler and makes RCA readily adaptable to routine clinical use with less issues concerning quality control of the instrument. Furthermore, the amplification signal can be confined locally if the amplification primer is immobilized onto a solid support. Because the DNA polymerase acts equally on circular probes with different sequences, the amplification is independent of strand sequences, simplifying the design of multiplexed assays. All these unique properties of RCA facilitate its applications in different research and molecular diagnosis areas like in situ detection, microarray, immunoassay, single nucleotide polymorphism (SNP), et cetera.

In Chapter 3, we developed a novel ssDNA sensing method by combining RCA and CE-LIF. In this work, target ssDNA strand was specifically recognized by perfect hybridization with two ends of a linear padlock probe which would be nicked together by ligation reaction catalyzed by ligase. Then, the RCA reaction generated elongated products with repeating sequence complimentary to the circular probe. The elongated ssDNA products would then be digested into short ssDNA sequence since we incorporated one endonuclease reaction site in the designed linear padlock probe. In this way, we solved the problem that elongated long ssDNA stands from RCA are difficult to be introduced into a capillary for quantitative analysis. Those short ssDNAs were ready for separation and detection in CE-LIF system quantitatively. Multiplex target sensing

was demonstrated with two target ssDNA strands and two specifically designed linear padlock probes.

In Chapter 4, we further expanded the similar strategies to small RNA sensing. In order to enhance the overall reaction efficiency and simplify the procedure, RCA was not preceded with ligation, and a preformed circular probe was employed as the template for the target small RNA-primed isothermal amplification. The long RCA product was digested and analyzed by CE. Two DNA polymerases, the *Phi29* and *Bst*, were compared for their detection performance. *Bst* is superior in the aspects of specificity, procedure simplicity, and reproducibility, while *Phi29* leads to a 5-fold lower detection limit and is able to detect as low as 35 amol of the target small RNA. Coamplification of an internal standard with the target and employment of the RNase A digestion step allow accurate and reproducible quantification of low amounts of small RNA targets spiked into hundreds of nanograms of the plant total RNA extract with a recovery below 110% using either enzyme. Our assay can be adapted to a capillary array system for high-throughput screening of small RNA expression in biological samples. Also, the one-step isothermal process has the potential to conveniently amplify a very limited amount of the RNA samples, e.g., RNA extracted from only a few cells, inside the capillary column or on a microchip.

Chapter 3

Combining rolling circle amplification with CE-LIF for sensitive DNA detection

3.1 Introduction

RCA is an isothermal amplification technique with great potentials to be combined with CE for nucleic acid detection. Because ligation is very sensitive to base-pair mismatch between the padlock probe and the target, ligation of the padlock probe followed by RCA can be used to detect SNP.[81, 82] Mutant strands mixed with excess wild-type alleles at a ratio of 1:10,000 were detected combining PCR for target amplification and RCA for SNP discrimination. [83] Most frequently, RCA was employed to detect nucleic acids. RCA resulted in around 8,000-fold signal enhancement over simple hybridization on a DNA microarray as demonstrated by Nallur et al..[84] A few copies of DNA extracted from a bacterial pathogen, Vibrio cholerae, were detected by counting individual amplification products under a confocal fluorescence microscope after circle-to-circle amplification (C2CA), a cascade RCA technique.[85] A miRNA detection system developed by Kjems et al. amplified several specific miRNAs from a few nanograms of total RNA by RCA.[86] The products were transferred to a membrane and labeled with radioisotopes for detection. The padlock hybridization enabled unambiguous

discrimination of the closely related miRNAs.[86] On the other hand, RCA was applied to detect proteins as well. The RCA primer can be linked covalently to the reporter antibody and RCA can improve the sensitivity of the immunoassays hundreds or even thousands of times.[78] For example, RCA facilitated the multiplexed measurement of cytokines on microarrays with femtomolar sensitivity. [47]

In the RCA-based assays, target quantification is done through the quantification of the RCA products. Different techniques have been utilized for this purpose. For amplifications performed on solid surfaces like the glass arrays, the RCA products hybridized to multiple fluorescent, complementary oligonucleotide probes, and the fluorescence was measured by a conventional microarray scanning device.[47, 82, 84] For solution-based reactions, a confocal microscope or a flow cytometer was used to count individual RCA products, because they generated local enrichment of the DNA binding fluorophores and induced distinguishable fluorescence difference from the background.[83, 85, 87] A slot-blot system was employed for miRNA detection and quantification after RCA.[86] These detection schemes usually require the usage of advanced laboratory equipments and complicated data acquisition techniques. Due to the wide application range of RCA, it is still in demand to develop more simple and rapid methods for RCA.

Because RCA products are large, megabase fragments and fold into micrometer-sized random coils in solution, it is not practical to analyze the products directly using gel electrophoresis.[88] Pulsed-field gel electrophoresis could be a solution, but smear bands

may be produced due to the various fragment sizes generated in the one-primer amplification process, making it difficult to perform quantification. Compared to slab gel electrophoresis, CE is simpler, faster, consumes much smaller amount of samples, and offers higher separation efficiency. CE can separate DNA molecules with different sizes or even different conformations. CE-LIF with intercalating dyes in both the running buffer and the separation matrix offers effortless and sensitive detection of DNA fragments, no chemically modified detection probes needed. However, to our knowledge there has been no attempt in applying CE to analyze the RCA products so far. Hence, in this study we explored the possibility of using CE to detect and quantify synthetic DNA targets via RCA. We proved that CE was a simple and sensitive detection platform for RCA, and it was possible to use the RCA-CE assay to detect multiple targets within one sample. The duplexed detection could be used for accurate relative quantification of DNA or RNA targets in biological samples.

3.2 Experimental

3.2.1 Reagents

Polyvinylpyrrolidone (PVP, average molecular weight of 1,300,000), Tris, boric acid, disodium ethylenediamine tetraacetate (EDTA), hydrochloric acid (HCl), and methanol were purchased from Fisher Scientific (Fairlawn, NJ, USA). SYBR® Green II RNA gel stain (10,000 × concentrate in DMSO) was obtained from Invitrogen (Carlsbad, CA, USA). All solutions were prepared in deionized water (18 MΩ) from a Milli·Q™ water

purification system (Millipore, Billerica, MA, USA). Oligonucleotides and the ssDNA ladder (20 – 100 nt) were from Integrated DNA technologies (Coralville, IA, USA). RepliPHI™ *Phi29* DNA polymerase and mixture of deoxyribonucleotides (dNTPs) were purchased from Epicentre (Madison, WI, USA). *HhaI* restriction enzyme and *E. coli* DNA ligase were from Promega (Madison, WI, USA) and Takara (Shiga, Japan), respectively. Magnesium chloride hexahydrate ($MgCl_2$), albumin from bovine serum (BSA), and β-nicotinamide adenine dinucleotide hydrate (NAD^+) were purchased from Sigma-Aldrich (St. Lousi, MO, USA). CentriSpin 20 columns were from Princeton Separations (Adelphia, NJ, USA).

3.2.2 Instrumentation

All capillary electrophoresis experiments were performed in a P/ACE™ MDQ Glycoprotein Capillary Electrophoresis System equipped with a 488 nm laser (Beckman Coulter, Fullerton, CA, USA). Sieving matrix for DNA separation was 2% or 4% PVP solutions prepared in 1 × TBE buffer and stained with 1 × SYBR Green. The 50-cm fused-silica capillary (75 μm i.d., 365 μm o.d., Polymicro Technologies, Phoenix, AZ, USA) with an effective length of 40 cm was rinsed at 30 psi for 3 min with 0.1 M HCl, deionized water, methanol and PVP solution sequentially prior to injection. Injections were either done at -5 kV for 5 seconds (normal injection) or at -2 kV for 60 seconds (stacking injection). All CE separations were done at -15 kV in 1 × TBE with 1 × SYBR Green. Peak area calculation was done by the 32 Karat software provided with the CE instrument.

3.2.3 RCA templates, probes, replication primers, and reaction conditions

Two synthetic oligonucleotides served as the arbitrary targets, and were detected by the RCA-CE assay using two padlock probes and one amplification primer in the present study. The sequences of the reaction substrates can be found in Table 3.1. Target 1 contained the sequence on the human K-ras gene with a G12A mutation, and target 2 was derived from the human TP53 gene with an R273H mutation. [89, 90] Even though these two targets were originally designed for detection of DNA point mutations, the current study was dedicated to the detection of specific DNA targets instead of SNP. Probe 1 was complimentary to target 1 and probe 2 was to target 2. Firstly, a 40-μL reaction mixture in solution A (30 mM Tris-HCl (pH 7.8), 0.1 M KCl, 0.2 mM NAD+, 4 mM $MgCl_2$), which contained the target oligonucleotide and the padlock probe, was heated up to 65-70 °C and then incubated in a 45 °C water bath (Isotemp® 2150-B5, Fisher Scientific) for 1.5 hrs. No target DNA was added to the blank reaction mixture. Then, 2.26 μL 1.2 U/ μL E. coli DNA ligase and 1 μL 2% BSA were added to each reaction mixture. Incubation in a 37 °C water bath for 15 min was required for ligation. Secondly, RCA was carried out with the addition of 1.7 μL 10 μM primer solution, 1.6 μL 0.2 M MgCl2, 6.4 μL 25 mM dNTPs, 6.4 μL 50 mM Tris-HCl (pH 7.5), and 2 μL 100 U/μL *Phi29* DNA polymerase to each reaction mixture followed by incubation at 37 °C for 45 min. A denaturing step at 65-70 °C for 15 min was necessary before digestion. Thirdly, 0.5 μL 10 μg/μL acetylated BSA and 1.3 μL 10 U/μL *HhaI* were added to perform a 2-hr digestion at 37 °C. Reaction mixtures and blanks were denatured at 65-70 °C for 15 min

and then cleaned-up by spin columns to remove salts, dNTPs and other low molecular weight impurities.

Table 3.1. Oligonucleotides used in this study[a)]

Replication Primer	5'-TGC GCT ATC TTC A-3'
Probe 1	5'-p T GGC GTA GGC AAG ATA GAA TGA AGA TAG CGC ATC GTA GGA CTT ATT TCG TAG GAC TTA GGT AGT TGG AGC TGT-3'
Probe 2	5'-p TGT TTG TGC CTG TCC TAG AAT GAA GAT AGC GCA TGA GGT GTT ACA GCT TTG AGG TGC A-3'
Target 1	5'- TCT TGC CTA CGC CAA CAG CTC CAA CTA CC-3'
Target 2	5'- GG ACA GGC ACA AAC ATG CAC CTC AAA GCT GT -3'

a) Target 1 and probe 1 used in this paper were designed according to ref. [14] with some modifications.

3.3. Results and discussion

3.3.1 Initial investigation of the RCA reaction with CE

The first step in our investigation was to explore the possibility of using CE to analyze the RCA products directly. Padlock probe 1 hybridized onto target 1 and formed a circular probe by the *E. Coli* ligase, which was then amplified by the replication primer and the *Phi29* polymerase. Because the amplification is linear, the product amount

should be proportional to that of the target. Previous studies have confirmed that RCA generates DNA fragments with very high molecular weights which can not be separated in polyacrylamide gels under traditional electrophoresis conditions.[79, 88, 91, 92] Based on the biased reptation model that depicts the electrophoretic migration of DNA in a polymer network, as the DNA coil becomes more elongated than 20,000 base pairs, the size dependence of the electrophoretic mobility μ disappears.[93] Beyond this limit, pulsed-field techniques must be used for effective size separation of the ultra-large DNA molecules. Another factor that prevents direct gel electrophoretic separation of the RCA products probably lies in their large gyration radius. Because the elongated DNA fragment is single-stranded, it forms a random coil in free solution. It was once estimated that the gyration radius of a RCA product containing 1,000 repeats of a 93-nt template was 775 nm.[87] Once the product was hybridized to the fluorescently labeled oligonucleotide probes, the diameter of the random coil could go up to 1 μm.[85] Such a large gyration radius would cause great difficulties for the RCA product to enter the gel. Due to the same reasons, CGE or CE with entangled polymer solutions would not be feasible, either.

We proved this hypothesis by injecting the amplification product into a capillary filled with 1% PVP solution. No peak showed up within 60 min except the background peaks from the padlock probe (73 nt) and the amplification primer (13 nt) (data not shown). On the other hand, if the same reaction mixture was analyzed in an open capillary coated with 0.05% polyethylene oxide (8,000 kDa molecular mass), the electropherogram

showed multiple narrow peaks (spikes), indicating the presence of sub-micron- and even micron-sized large DNA conglomerates with different size-to-charge ratios (Data not shown).[94] The spikes were irreproducible in both peak height and migration time, which could be attributed to the irregular shape and size of the RCA products and the low data acquisition rate (4 Hz) of the commercial CE system. The high electric field may introduce further deformation of the random coils and promote entanglement among the DNA coils, increasing their size and shape variations. Another contribution to the size variation is from the reaction itself, which does not have a mechanism to generate DNA fragments with defined fragment lengths. The multiple and irreproducible spikes are not useful at all in target DNA quantification via RCA, and a different approach has to be taken.

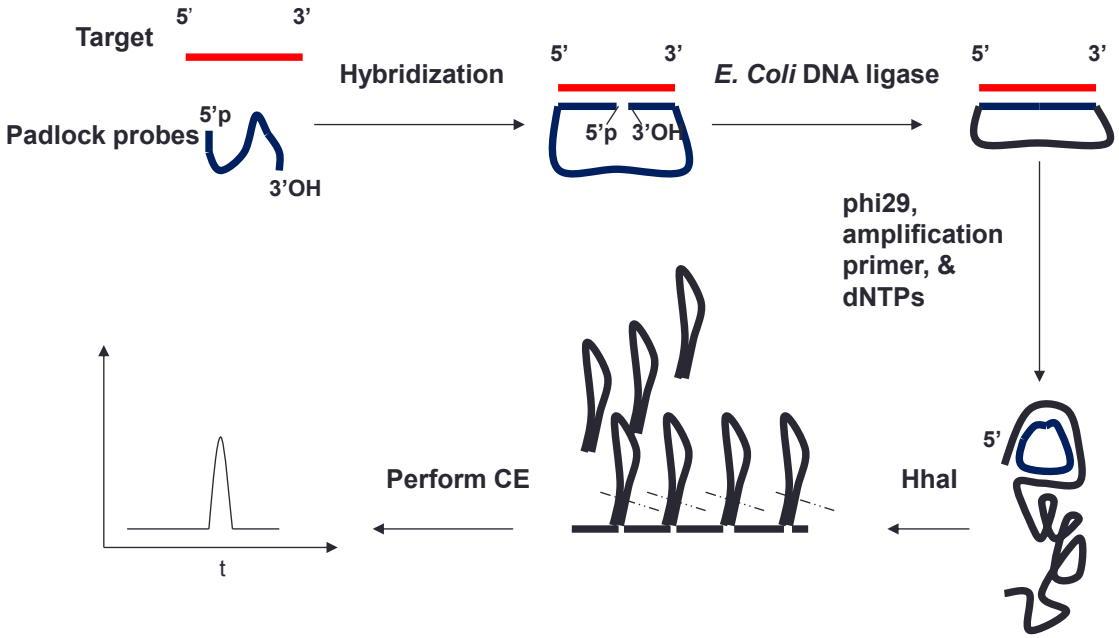
3.3.2 Enzyme digestion of the RCA product

Since the RCA product is actually a concatemer with repeated sequences arranged end to end, it can be digested into identical fragments by restriction enzymes if we incorporate a digestion site to the template sequence. An oligonucleotide complementary to the RCA product is added to form a double-stranded portion for restriction enzyme digestion. The much smaller monomer can then be analyzed easily by CE. The monomerization of RCA products has been successfully employed in C2CA to obtain higher amplification folds by repeated circularization and polymerization.[92, 95] To increase digestion efficiency and simplify the procedure, a sequence of 5'-GCG^C-3' that can be cleaved by *HhaI* was

introduced to both the padlock probes and the replication primer. *HhaI* not only works within the double-stranded region, but also cuts the single-stranded region via the transiently formed double-stranded hairpin structures at a relatively fast reaction speed compared to other endonucleases like *CfoI*.[96] We found out that incubating the reaction mixture at an elevated temperature like 65-70 °C prior to enzyme digestion was necessary to obtain optimal reaction yield. This denaturing step may loosen up the coiling structure of the single-stranded product, expose more binding sites, and consequently allow better attachment of the replication primer and the digestion enzyme.

The schematic diagram of the RCA-CE assay was displayed in Figure 3.1, and the results from enzyme digestion of the RCA products were shown in Figure 3.2.

Figure 3.1. Schematic illustration of the RCA-CE assay for ssDNA sensing



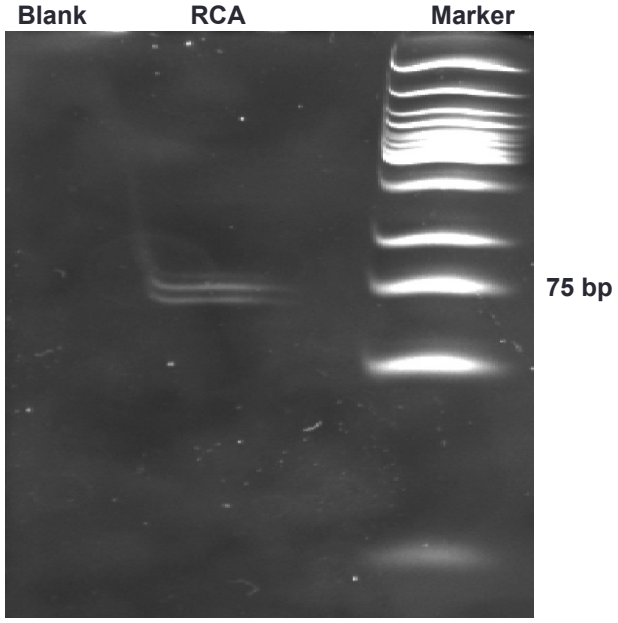
HhaI digestion was performed after rolling circle amplification of the target oligonucleotide. Then the reaction mixture was first cleaned up by phenol extraction and ethanol precipitation, and then analyzed on the 20% denatured polyacrylamide gel (Figure 3.2 a). It can be seen that the product has a fragment size similar to that of the padlock probe (73 nt). The additional product band may be a ghost band because it did not show up in CE. No linear padlock probe was seen in the trace for blank reaction. Nevertheless, this result demonstrated that the enzyme digestion step resulted in a much smaller reaction product suitable for CE analysis.

Next, the reaction mixture was separated by CE. In order to keep the whole assay simple, we performed all reactions in one tube. Reaction substrates were simply mixed and enzymes were added sequentially. No wash procedure was involved, and no extra effort except simple desalting was taken to purify the final product. The SYBR Green II RNA gel stain was used to label the single-stranded oligonucleotides so that they could be detected by LIF. The capillary electrophoresis was done under a native condition, because we found that the denatured condition of 7 M urea lowered the fluorescence intensity in detection. This phenomenon indicates that the ssDNA product may contain some double-helix structures along the molecule which bind better to the intercalating dyes. Therefore, more sensitive intercalating dyes for dsDNA detection, such as the Yo-Pro, SYBR Gold, and SYBR Green I, can be tested in the future to enhance the assay sensitivity. Since the reaction substrates and intermediates (padlock probe, replication primer, circular probe, products from enzyme digestion of the padlock probe and the

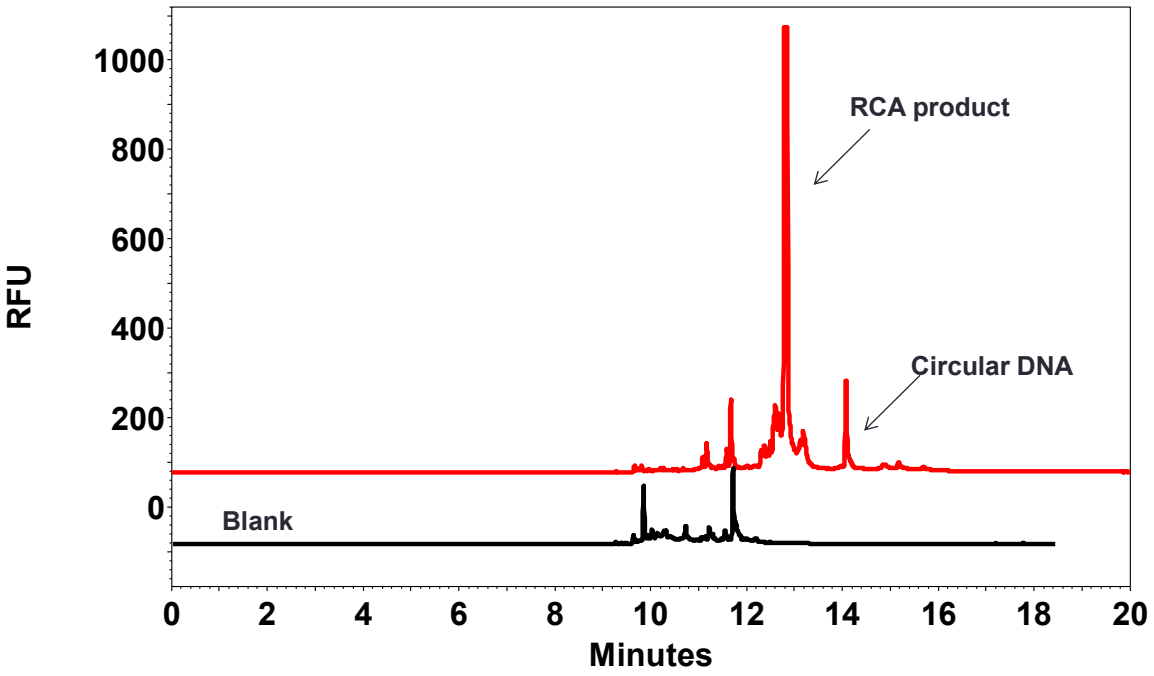
primer) were co-injected into the capillary with the final product, we optimized the CE conditions to resolve the final product from the background oligonucleotides. Different PVP concentrations and running voltages were compared, and the 4% PVP solution and the running voltage of -15 kV were chosen. The electropherograms of the positive and blank reactions were shown in Figure 3.2 b. The residue circular probe was eluted later than the digested RCA product in CE. Surprisingly, if we spiked the padlock probe into the reaction mixture, the digestion product migrated slower than the padlock probe under our native running condition. We suspected the conformation of the digested RCA product was different from that of the original padlock probe. CE is well known for its capability to separate ssDNA with different conformations in native running conditions.[97] In addition, by monitoring the products from every step of the whole process using CE, we found out that most of the padlock probes were digested by *HhaI* if co-incubated with excess amount of the replication primer. Both phenomena indicated that the padlock probe imposed no interference to the analysis of the final product. The background peaks were resulted from residue reaction substrates, enzyme digestion of the replication primer and the linear padlock probe, and other reaction intermediates, which were well separated from the digested RCA product (Figure 3.2 b). The separation was rapid, taking less than 15 minutes after the enzymatic reaction.

Figure 3.2 (a) Size confirmation of the digestion product by gel electrophoresis. Blank, blank reaction without any target DNA; RCA, positive reaction with 80-fmol target 1; Marker, low-molecular-weight DNA ladder (25–766 bp; New England Biolabs, MA, USA). Gel electrophoresis conditions: 20% polyacrylamide gel with a size of 10 cm × 10 cm, 1×TBE, 200 V, stained with ethidium bromide. (b) Electropherograms of digestion products from blank and positive reactions. Separation conditions: uncoated fused-silica capillary (total length 50.0 cm, effective length 40.0 cm, 75 mm id); temperature, 25°C; separation at -15 kV; injection at 25 kV for 5 s; sieving matrix: 4% PVP in 1×TBE, with 1×SYBR Green II RNA gel stain; LIF excitation at 488 nm.

(a)



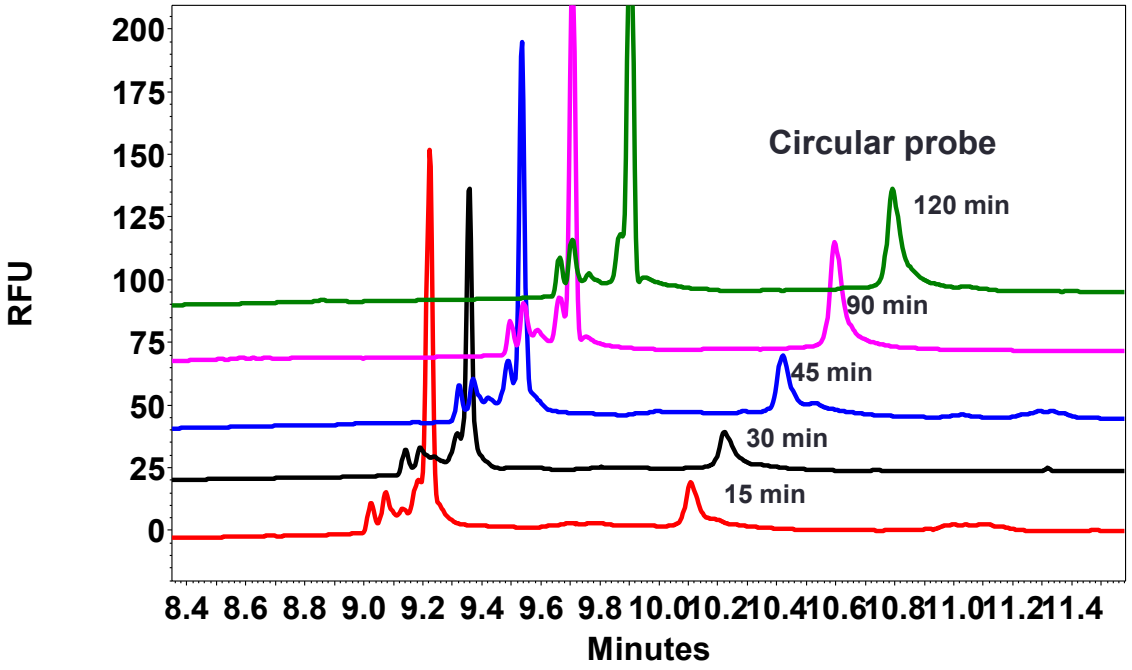
(b)



3.3.3 Reaction optimization

Once we confirmed that CE could be used to monitor the RCA product, we carried out investigations on the reaction conditions to optimize the RCA-CE assay. We first tested the padlock probe circularization conditions because it determined the successful linear amplification of target DNA. The circular probe was eluted later than the linear padlock probe in CE when using 2% PVP as the sieving matrix (Figure 3.3). The peak area of the circular DNA can be used as an indicator for the reaction yield. Figure 3.3 superimposed the electropherograms of ligation products generated with different hybridization duration. It can be seen that, the reaction yield increased with the hybridization duration, but the augmentation leveled off once the duration was longer

Figure 3.3 Electropherograms of circular DNA formed by ligation with different hybridization durations. Traces moved to increase visual clarity. Separation conditions as in Figure 3.2 b, except that PVP concentration was 2%.



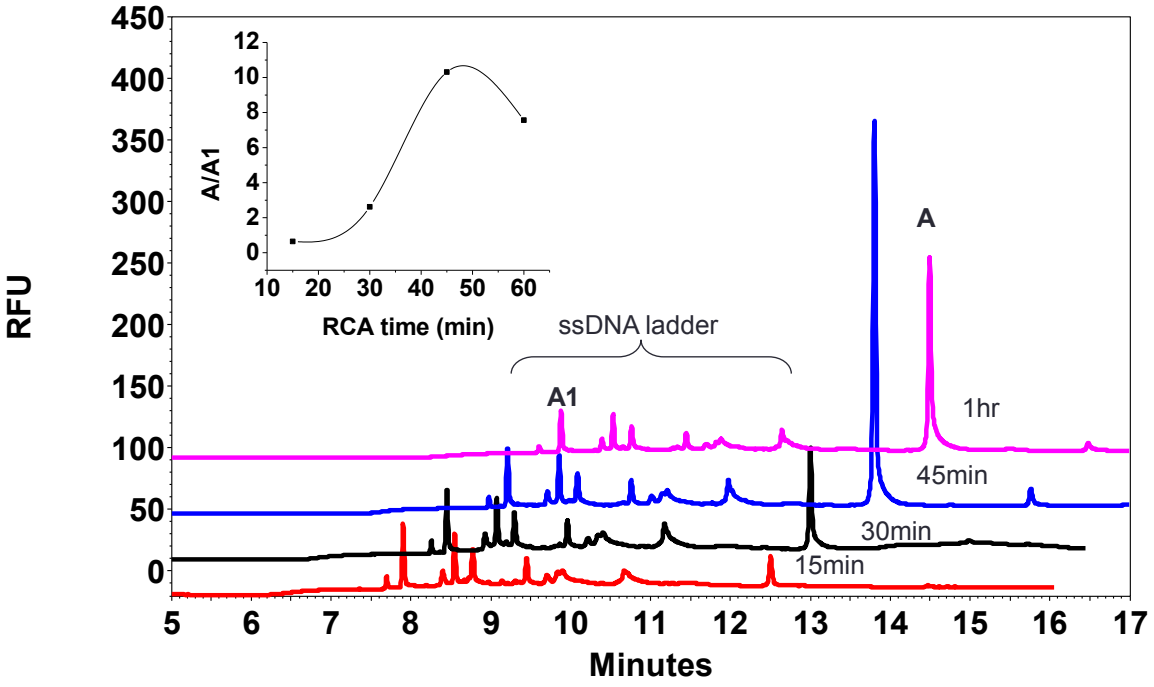
than 1.5 hours. The long hybridization time ensures that more target molecules can anneal to the padlock probes to obtain higher reaction yields. Other reaction conditions like the initial concentration of the padlock probe and the ligation duration were also investigated using the same strategy. Higher concentration of padlock probe did not increase the yield of circularization once the concentration ratio of the padlock probe to

the target was larger than 1. Ligation was very efficient if enough time was given for hybridization, taking only fifteen minutes to reach the optimal yield.

Different RCA durations were compared as well and the results were shown in Figure 3.4. The digested RCA product was co-injected with a ssDNA ladder (20 – 100 nt with a 10-nt increment), and the product peak area (A) was normalized against that of the first peak of the ladder (A1) to eliminate random variations in different CE runs. Optimal RCA duration was found to be at 45 min from the plot of normalized peak area (A/A1) vs. RCA duration (inserted graph in Figure 3.4). Longer RCA duration than 45-min actually decreased the product signal. We suspected that as the RCA product grew too long and formed a very compact random coil, some of the digestion sites might be embedded too deep inside the coil and become inaccessible to the digestion enzyme. The phenomenon that the supercoiled DNA was a poor substrate for primer and enzyme binding was also observed in using real-time PCR for mitochondrial DNA quantification.[98]

The co-injection with a ssDNA ladder allowed us to study the reproducibility of the CE runs. The relative standard deviations of peak areas and migration times of each ladder fragment within these four injections were calculated to be between 1% and 3%, respectively, which confirmed the practicability of using migration time and peak area to identify and quantify the RCA product.

Figure 3.4 Overlaid electropherograms of digested RCA products with different RCA durations. Separation conditions as in Figure 3.2 b. Inserted: plot of normalized peak area ratio (A/A1) vs. RCA time.



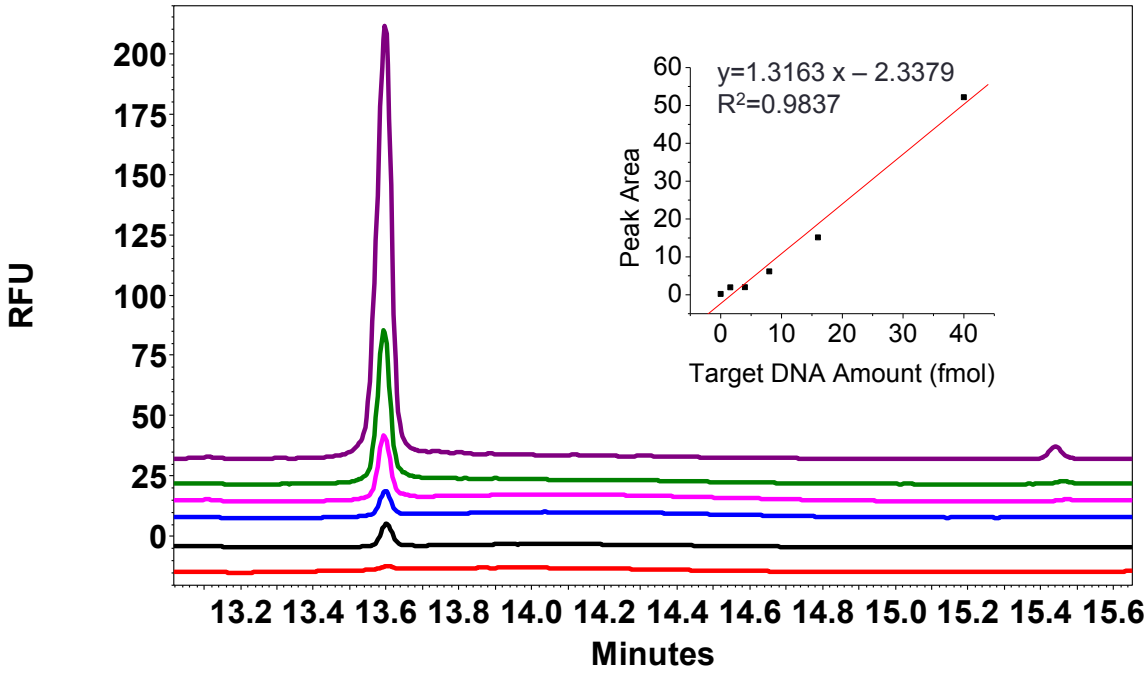
3.3.4 Target quantification and duplexed sensing

Next we applied this RCA-CE assay to detect and quantify the artificial DNA targets. We performed reactions with different amounts of target 1 (40, 16, 8, 4, 1.6, and 0 fmol in 40 μL reaction mixtures) and analyzed the products by CE using 4% PVP solution stained with SYBR Green as the sieving matrix. The injection was done at -2 kV for 60 s

to increase the injected amount. Our preliminary investigation found that such a stacking injection could enhance the product signal by 40 folds under current experimental conditions. The product peak from the reaction with 1.6 fmol target was clearly distinguishable from the background. The electropherograms and the titration curve of target amount vs. peak area are displayed in Figure 3.5. Since CE consumes very small amount of sample for each analysis, we can further minimize the total reaction volume or use SPE columns to reduce the final product volume during sample clean-up. Either way should result in even lower detection limit of the RCA-CE assay. A relatively narrow dynamic range of two orders of magnitudes was obtained in our study because higher target amount than 80 fmol would saturate the detector in our commercial CE instrument using the stacking injection.

Till now, we demonstrated that the RCA-CE assay could be used to detect low amount of target oligonucleotides, but the quantification was entirely relied on one single peak from the digested RCA product. It is not a reliable quantification method because many variations would arise during the whole process. For instance, slight fluctuation in the reaction conditions, like the incubation temperature and the concentrations of the starting materials, may be amplified during reaction and introduce big errors to the final quantification. The running and dye staining conditions of CE may vary from run to run as well, leading to irreproducible peak intensities.

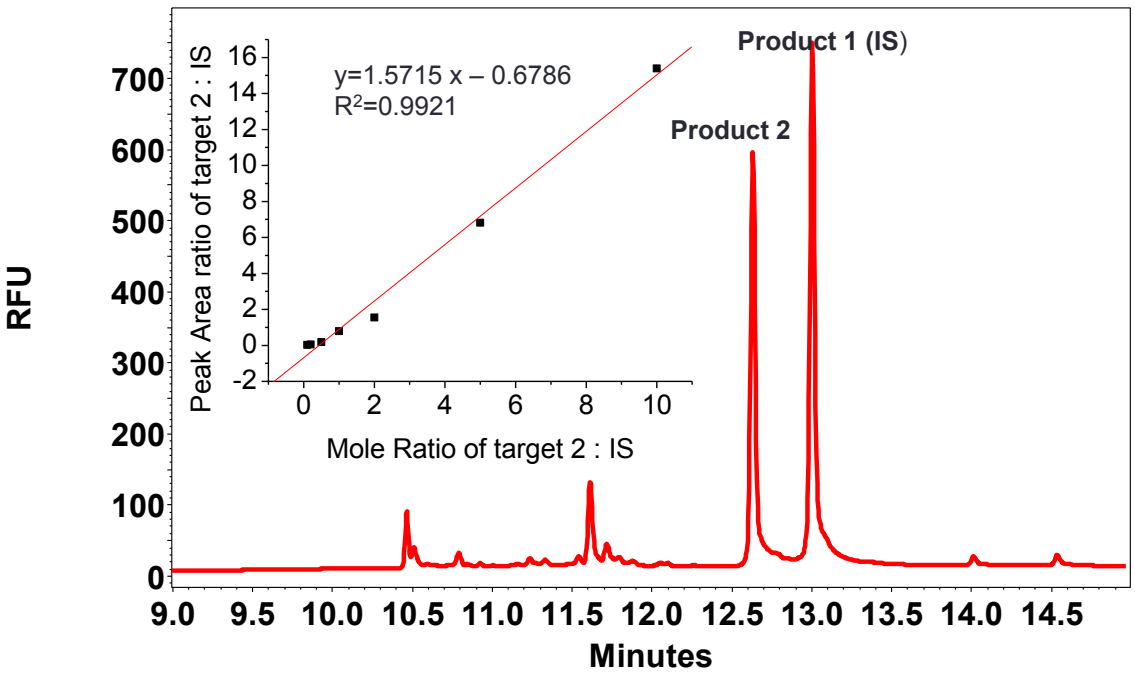
Figure 3.5 Electropherograms of reaction products from different amounts of target 1. From top to bottom, reaction containing 40, 16, 8, 4, 1.6, 0 fmol target 1. Inserted: the plot of product peak area (original reading from the 32 Karat software divided by 10^8) vs. target amount. Separation conditions as in Figure 3.2 b, except that injections were done at -2 kV for 60 s.



To improve the accuracy of target quantification, duplexed detection of two DNA targets was tested in our study, one of the targets being viewed as the internal standard (IS). A second padlock probe (probe 2) was designed with a shorter fragment length than probe 1, and used to amplify target 2 in this demonstration. Since the enzyme digestion product has a fragment size similar to the padlock probe, the products from these two targets can be separated quite well by CE. The internal standard (target 1 in this case) and the target

(target 2) are amplified simultaneously in one reaction tube and the resulted products are analyzed together in one capillary. Therefore, the peak area ratio should accurately reflect the quantity ratio of the starting materials. In this way, we can normalize the signal intensity obtained from the target to that of the IS and improve the quantification accuracy. Such a normalization concept has been applied widely in microarray analysis.[99] Figure 3.6 displays the electropherogram from the amplification of both target 2 and IS mixed at a ratio of 1:1. Other mole ratios (target 2/ IS) of 1:10, 1:5, 1:2, 2:1, 5:1, and 10:1 were also tested, keeping the amount of IS constant. The product peak area ratio (product 2/IS) was plotted against the target ratio, which showed a good linearity of $R^2 = 0.9921$ (Figure 3.5).

Figure 3.6 Electropherogram of reaction with target 2 and IS at a mole ratio of 1:1. Inserted: plot of peak area ratio of product 2/IS vs. target mole ratio of target 2/IS.



However, the function between the peak area ratio and the target ratio in Figure 3.6 is not an identity function. The plot has an overall slope larger than 1. It indicates that the reaction kinetics is different for the two padlock probes. The longer probe (probe 1, 73 nt) seemed to have a faster reaction rate than the shorter probe (probe 2, 58 nt), because the peak area ratio of product 2: product 1 was smaller than 1 when the two targets were mixed at a mole ratio of 1:1. Since the amplification procedure is sequence independent, the kinetics difference should be from the ligation reaction. The shorter probe may need to overcome higher free energy barrier in folding because of its short strand length. The ligation kinetics may also be concentration dependent. As the concentration of target 2 increased in the reaction mixture, the product peak area ratio became larger than the target mole ratio. Such a deviation from the true value should not affect the relative quantification because the relationship between the peak area ratio and the target mole ratio is linear. A pre-circularized probe instead of a padlock probe can be used in the amplification reaction to reduce the difference brought in by the ligation reaction. Anyhow, simultaneous detection of both the DNA target and the IS eliminates the variations caused by random differences in the reaction or analysis procedure and improves the quantification accuracy. Therefore, expression levels of genes or small RNAs can be assessed correctly using our assay if an internal standard that has a constant concentration level could be found.

3.4. Conclusions

In this chapter, we demonstrated that RCA-CE assay is a fast and effective technique for sensitive detection of target nucleic acids. Because the RCA products have very large and different fragment sizes not suitable for direct electrophoretic separation, a specific sequence is introduced into the padlock probe for restriction enzyme digestion of the products. The digested fragments are subject to CE separation using 4% PVP solution as the sieving matrix under native running condition. The RCA-CE assay is a low cost and simple technique for detection of target nucleic acids. The separation process takes less than 15 min; no fluorescent dye- or radioisotope-labeled probes are needed; no sophisticated instruments are involved. A detection limit of a few femtomole was achieved after simple desalting of the final product in our study. Decreasing the reaction volume and removing the reaction substrates after RCA should be able to improve the detection limit further. Simultaneous detection of multiple targets was also demonstrated for more accurate target quantification. We co-amplified the target with an internal standard and the relative quantity of the target to the IS was achieved. More targets can be detected simultaneously with the RCA-CE assay because RCA is independent of the template sequence. This is one big advantage of using CE as the detection method for RCA compared to other real-time detection techniques with molecular beacons.[100, 101] Multiple padlock probes with one or more nucleotides difference in length can be designed for different targets and the products can be well resolved with CE's high separation efficiency. Additionally, the single column RCA-CE assay can be easily adapted to a capillary array system to enhance the sample throughput hundreds of times.

Short, single-stranded oligonucleotides like small RNAs that are hard to be analyzed with real-time or regular PCR due to their small strand sizes can be amplified and detected with our RCA-CE assay, because RCA can extend the small RNAs directly from their 5' end upon hybridization to the circular probe and does not require any amplification primers. For other types of nucleic acids, the reaction process can certainly be modified to be compatible with different targets, and this assay should be able to detect SNP or proteins (via immuno-RCA or aptamer) like other RCA techniques. The isothermal reaction condition makes it simple in designing an on-column or on-chip reactor to minimize the reaction volume, integrate the analysis procedure, and enhance the assay sensitivity. High-throughput screening of small RNA expression in biological samples using this RCA-CE assay is under development in our lab.

Chapter 4

Stand-alone rolling circle amplification combined with capillary electrophoresis for specific detection of small RNA

4.1 Introduction

Non-coding small RNAs play diverse, important biological roles through gene expression regulation. However, their low expression levels make it difficult to identify new small RNA species and study their functions, calling for the development of detection schemes with higher simplicity, sensitivity, and specificity.

The gold standard in small RNA detection is Northern blotting, [102, 103] which is straightforward and quantitative, but with low sensitivity. Around 50-100 μg total RNA extract is often needed for the detection and the low molecular weight RNA should be concentrated from the total RNA extract by gel electrophoresis to enhance the abundance of small RNA in the sample. [104] Microarray-based assays are particularly attractive because of their high analysis throughput. [104] Like in Northern blotting, stable radioisotope labeling is needed to reveal the low abundant small RNA, imposing

potential hazards to the environment and the operator. Locked nucleic acids (LNA) were employed to hybridize to small RNA with improved affinity in microarray, along with sophisticated detection schemes like nanoparticle-amplified surface plasmon resonance imaging and dual-color single-molecule fluorescence microscopy.[105-108] On the other hand, signal amplification strategies employing biotin-labeled dATP, [109] monoclonal antibody specific to the DNA/RNA hybrid,[110] horseradish peroxidase, [111] or Renilla Luciferase [112] were developed to detect femtomole small RNA in biological samples.

To further reduce the detection limit, the small RNA can be amplified by PCR before detection, but the primer design is challenging due to the short length of small RNAs.[53, 86] An alternative amplification scheme, the rolling circle amplification (RCA), has also been applied to detect a few picograms of miRNA using the blotting technique with radioisotope labeling. [86, 113] RCA generates long ssDNAs with tandem sequence isothermally using random primers, a DNA polymerase having exceptional strand displacement ability and great processivity, and a circular amplification template formed by joining the 5'-PO_4 and 3'-OH ends of a linear padlock probe using the target nucleic acid as the ligation template.[114] DNA can be amplified 10,000-fold in a few hours with RCA.[115] The ligation-RCA combination has been widely applied to detect DNA targets or adapted in immuno-sorbent assays for signal amplification.[116, 117] However, its application in small RNA detection is limited by the low ligation efficiency and slow reaction kinetics in RNA-templated DNA nick joining.[118-120]

Actually, small RNA molecules can serve as the primer for RCA and initiate the polymerization from their free 3'-OH ends. Herein, we reported a stand-alone RCA assay that was coupled with capillary electrophoresis for sensitive and specific detection of small RNA in total RNA extracts. The stand-alone RCA employed no ligation for sequence recognition and directly amplified the small RNA molecules using a preformed circular probe.[59, 121] The long amplification products were digested into small oligonucleotides and analyzed by capillary electrophoresis (CE) with intercalating dyes in the running buffer.[122] We compared the performance of two DNA polymerases: the mesophilic *Phi*29 and the thermophilic *Bst* (large fragment), both leading to rapid and sensitive detection of small RNA with different degrees of specificity. Furthermore, we demonstrated that the assay could accurately quantify the target small RNA spiked in the plant total RNA extract after the background RNA was removed by RNase digestion. This stand-alone RCA-CE method is simple, sensitive, and provides sufficient specificity in target recognition. Moreover, its throughput can be improved by using a capillary array system for product analysis.

4.2 Experimental

4.2.1 Reagents and Materials

Circligase™ ssDNA ligase kit and RepliPHI™ *Phi29* DNA polymerase kit were purchased from Epicentre (Madison, WI). *Bst* DNA polymerase (large fragment), T4 DNA ligase, T4 RNA ligase 2, and deoxynucleotide solution mix (dNTPs) were from New England Biolabs (Ipswich, MA). *Hha I* restriction enzyme was from Promega

(Madison, WI), and *Exo I*, *Exo III* and RNase A (DNase and protease-free) were from Fermantas (Glen Burnie, MD). The target and internal standard small RNA and other oligonucleotides were from Integrated DNA technologies (Coralville, IA). The target strand, nat-siRNAATGB2, was a 22-mer pathogen-inducible siRNA discovered in plants.[123] Its sequence is listed in Table 4.1 along with the artificial internal standard and all other oligonucleotides employed in the present study. The nuclease-free water from Sigma-Aldrich (St. Louis, MO) was used to prepare the standard oligonucleotide solutions as well as all the reaction mixtures. The total RNA extracts from *Arabidopsis thaliana* were kindly provided by Dr. Hailing Jin in Department of Pathology of UCR. The phenol-chloroform extraction buffer was prepared from the saturated phenol, the biological grade chloroform and the iso-amyl alcohol (Fisher, Fairlawn, NJ) at a ratio of 25:24:1. Biospin 6 columns were from Biorad (Hercules, CA) and Illustra MicroSpin™ G-25 columns were from GE healthcare (Piscataway, NJ). Polyvinylpyrrolidone (average M.W. 1,300,000), Tris, boric acid, disodium ethylenediamine tetraacetate (EDTA), hydrochloric acid (HCl), methanol and sodium chloride (NaCl) were purchased from Fisher Scientific (Fairlawn, NJ). The SYBR Green II RNA gel stain (10,000 × concentrate in DMSO) used in CE analysis and the SYBR Gold (10,000 × concentrate in DMSO) gel stain for polyacrylamide gel electrophoresis (PAGE) were from Invitrogen (Carlsbad, CA). Deionized water from a Milli·Q ™ water purification system (Millipore, MA) was used to prepare the wash and running solutions for CE.

Table 4.1. Oligonucleotides used in this study

nat-siRNAATGB2	5'-p-rArCrUrCrArArGrGrUrGrCrArGrCrUrGrGrArGrGrArA-3'
IS RNA	5'-p-rArArArArCrGrArCrUrCrUrCrGrGrCrArArCrGrGrA-3'
Linear padlock probe for nat-siRNAATGB2	5'- p-GCACCTTGAGTAAACAAAGAACATGCGCAGTAAACAAATAAACAAAATTCCTCCAGCT-3'
Linear padlock probe for IS RNA	5'-p-AGAGTCGTTTTAAGATTCAATCAACATGCGCAGTAATTACAAAAAAGAAAATCAAAGAACAAAATCCGTTGCCG-3'
Digestion primer	5'-ACATGCGCAGTA -3'
DNA version of siRNA	5'-p-ACTCAAGGTGCAGCTGGAGGAA-3'

Note: The letter "r" indicates "ribose nucleotide".

4.2.2 CE Conditions

A P/ACE™ MDQ Glycoprotein Capillary Electrophoresis System equipped with a 488 nm laser (Beckman Coulter, Fullerton, CA) was used for all CE runs. The sieving matrix contained 4% PVP and 1 × SYBR Green II dye in 1 x TBE which was also the running buffer. Prior to injection, the 50-cm fused-silica capillary (75 μm i.d., 365 μm o.d., Polymicro Technologies, Phoenix, AZ) with an effective length of 40 cm was rinsed

sequentially with 0.1 M HCl, deionized water, methanol, and the PVP solution at 30 psi for 3 min. Sample injection was carried out at -2 kV for 90 seconds, and the separation voltage was -15 kV.

4.2.3 Circular probe generation

The circular probes were synthesized from the linear ssDNAs padlock probes through ligation catalyzed by the Circligase™ ssDNA ligase. Two individual circular probes were generated, one for the target small RNA and the other for a 21-mer ssRNA internal standard (IS). Circligation was completed at 60 °C (water bath) for 45 min. The reaction mixture contained 100 pmol linear padlock probe and 100 U Circligase in the 1 × reaction buffer provided by the manufacturer. After the deactivation of the Circligase at 80 °C for 10 min, the exonucleases, 20 U *Exo I* and 100 U *Exo III*, were applied to digest the residue linear DNA at 37 °C for 50 min. The enzymes were then removed by phenol-chloroform extraction, and the circularization products were desalted with the Biospin 6 column. The purity of the resulted circular probes was verified by denatured PAGE gel electrophoresis, and stored at -20 °C at the stock solution with an estimated concentration of 1 μM.

4.2.4 Comparison of ligation efficiency

The ligations were performed in the ligase buffers supplied with the corresponding enzymes by the manufacturer to ensure the highest enzyme activity. One microliter of the

target small RNA or its DNA counterpart at a concentration of 50 μM was mixed with 1.5 μL 100 μM linear padlock probe and 5 μL 10 × reaction buffer. The final volume was brought up to 50 μL. The mixture was denatured at 65 °C for 10 min and incubated at 45 °C for 1 hr to hybridize the small RNA and the padlock probe. Then, the T4 DNA ligase (200 cohesive end units) or the T4 RNA ligase 2 (5 U) was added at the extremely excessive level to drive the complete circulation of all the linear probes. The circular products were then cleaned up by the phenol-chloroform extraction and desalted by the Microspin G-25 column before being separated with the 20% denaturing polyacrylamide gel. The gel was then stained with SYBR Gold and the gel image was taken with the Typhoon Fluorescence Imager.

4.2.5 Stand-alone rolling circle amplification, restriction enzyme digestion and sample clean-up

RCA was carried out in the stand-alone format without ligation using the procedure described below. The reaction volume was kept at 10 μL to minimize sample consumption and reduce the influence of the RCA buffer on the following *Hha I* digestion, because the two reactions were performed at different optimal pH values. For amplifications with *Bst* or *Phi*29 as the polymerase, the corresponding enzyme reaction buffer provided by the manufacturer was used. Two circular probes were used in each reaction, one for the target siRNA and the other for the IS RNA. To the 10-μL 1× reaction buffer, 1 μL of each of the circular probes diluted 100-fold from the stock was mixed with 5 nmol dNTPs, 2 U *Bst* or 25 U *Phi*29 DNA polymerase, 5 fmol IS RNA, and

different amounts of the target small RNA. The target nat-siRNAATGB2 was added at 5, 2.5, 1, 0.5, or 0.25 fmol to obtain the standard calibration curve. Alternatively, 5, 2.5, 1, 0.5, or 0.25 fmol of the target siRNA was spiked into 117 ng total RNA extracts to test the capability of our assay in accurately detecting low amount of small RNA in biological samples. The blank reactions contained only the IS RNA but no target siRNA. Nuclease-free mineral oil was added on top of the reaction mixture to prevent evaporation.

In the case of *Phi*29, the target was first hybridized to the circular probe through 10-min incubation at 65-70 °C. Then the mixture was cooled to room temperature and the polymerase was added to initiate the RCA that lasted for 1.5 h. Then, *Phi*29 was deactivated at 70 °C for 10 minutes. The reaction mixture, to which 4 μL 10 × Buffer C, 4 pmol digestion primer, and 4 μg acetylated BSA were added, was equilibrated at 75 °C for 15 min and at 45 °C for another 15 min to hybridize the primer onto the RCA product, Finally, the mixture was cooled down to 37 ˚C and the restriction enzyme digestion in a water bath of 37 ˚C was initiated by the addition of 11 U *Hha I*. In this step, the final volume reached 40 μL. If *Bst* was used, no target hybridization was required and the amplification started immediately by putting the reaction mixture into a water bath of 65 ˚C. After 1.5-hr RCA, the reaction temperature was dropped to 37 °C and the digestion started upon the addition of the 1 × buffer C, the digestion primer, the acetylated BSA, and the *Hha I*. The procedure following the digestion step was the same for both

enzymes: *Hha I* was deactivated at 80 ˚C for 20 min and the reaction products were desalted by the Microspin G-25 column before being stored at - 20 ˚C.

For reactions containing plant total RNA extracts, RNase digestion was needed before the desalting step, in which 3.9 μg DNase-free RNase was added to the reaction mixture to digest the background RNAs via 30-min incubation at 37 ˚C. The RNase A was removed by phenol-chloroform extraction. Additionally, to eliminate the secondary structures formed by the single-stranded products, before CE injection, 10 μL of the cleaned reaction mixture were dried in a speed-vac; the pellet was dissolved in 10 μL mixture of formamide and 8 M urea at 1:1 ratio, boiled in water for three minutes, and kept in the ice-water bath.

4.3 Results and discussions

4.3.1 Design of the detection scheme

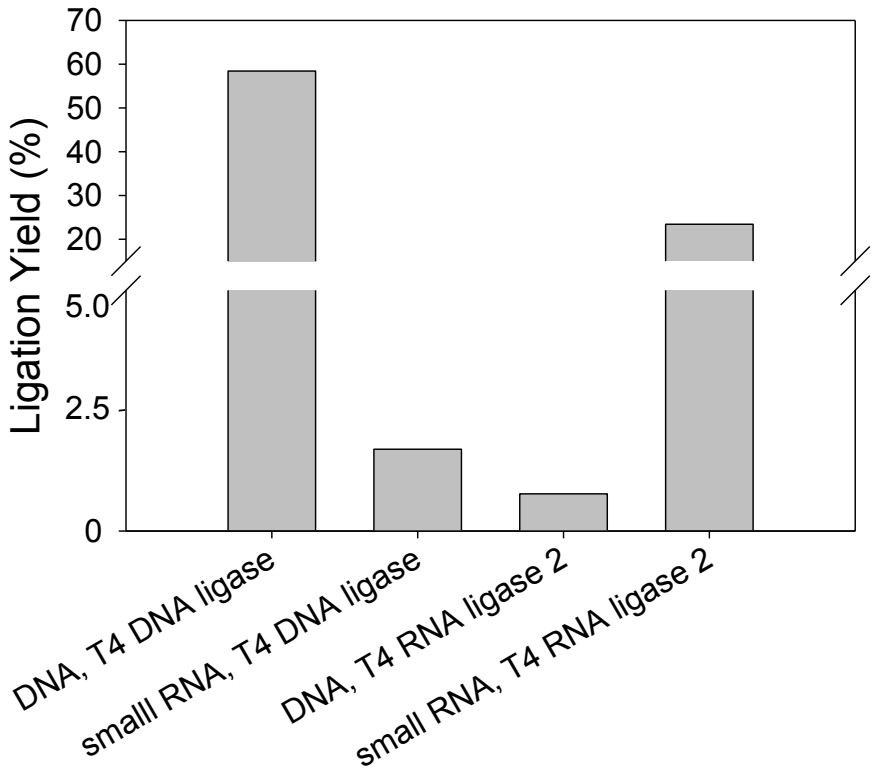
Normally a ligation is preceded to generate a circular template from a linear, padlock probe, the 3' and 5' ends of which can be juxtaposed by the precise hybridization to a target DNA (or RNA) sequence. Because DNA ligases hardly join terminally mismatched oligonucleotides, ligation brings RCA sufficient specificity in target recognition. However, such a combination may be problematic in RNA detection because the RNA-templated DNA ligation has very low reaction efficiency.[119, 120] It is believed the transient complex formed between the DNA ligase and substrates containing RNA or vice versa

may be so unstable that the enzyme would be prematurely released before the nick closure and fail the ligation.[119]

We compared the performance of two most common ligases, the T4 DNA ligase and the T4 RNA ligase 2, on joining the 5'-PO_4 and 3'-OH ends of the same linear padlock DNA probe using the small RNA of nat-siRNAATGB2 or its DNA version as the templates. Two-hundred units of the T4 DNA ligase, enough to catalyze the ligation of 13 μM 5' DNA termini, or 5 units of the T4 RNA ligase 2, enough to join two RNA strands at 7.5 μM, were added to the reaction to catalyze the linkage of 3 μM padlock probe on 1 μM RNA or DNA template. Therefore, both ligases were provided in 2.5- to 4-fold molar excess over the linear probes. Each ligase worked under its optimal buffer condition. The products of 1-hr ligation were separated by PAGE, and the gel image (Supporting Information Figure S 4.1) was analyzed by ImageQuant (Version 5.2). The reaction yields were shown in Figure 4.1. As expected, the cross combinations of T4 DNA ligase with the RNA template and T4 RNA ligase 2 with the DNA substrates had poor yields, both below 2.5%. When supplied with the right type of template, the DNA version of the target small RNA, T4 DNA ligase achieved the highest ligation yield of 58.4 %. T4 RNA ligase 2 showed better tolerance with RNA in the substrate structure than the DNA ligase,[120] and resulted in a ligation yield of 23.4%. Higher yields are possible with both ligases by optimizing the reaction buffer composition, for example, lowering the concentration of the co-substrate ATP and increasing the ligase and salt concentration.[119, 120] However, the revised ligation condition may affect the subsequent RCA reaction due

to the high protein and salt content. Longer ligation time may help to improve the yield, but the duration of overall assay would also be extended.

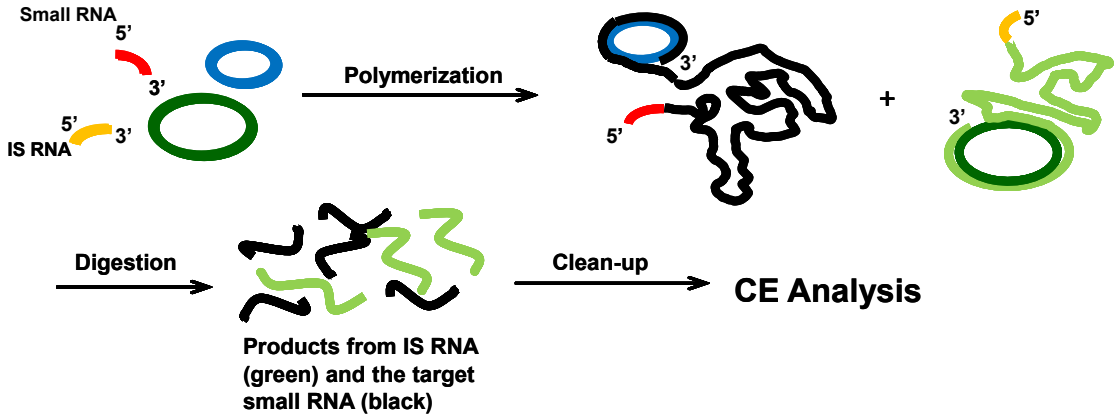
Figure 4.1 Comparison of the ligation yields calculated from the PAGE band intensity of the circular probe relative to the sum of circular and linear probes.



The low reaction efficiency in RNA-templated ligation would definitely diminish the sensitivity in small RNA detection if the traditional ligation-based RCA design was employed. Therefore, we eliminated the ligation step in our scheme and amplified the small RNA by continuously extending its 3' end on the pre-formed circular templates

with RCA. Since we have demonstrated in our previous study that capillary electrophoresis (CE) is a simple and low-cost detection platform for the RCA product,[122] we continued to use CE in the current design. The schematic illustration of the entire stand-alone RCA-CE assay was shown in Figure 4.2. A pre-formed circular probe is mixed with the target small RNA and the internal standard (IS), which is an RNA molecule with comparable length (21-nt) to the target RNA, and RCA is initiated upon the addition of the polymerase. The amplified products are digested by the restriction endonuclease *HhaI* and analyzed by CE. The internal standard is used to correct variations brought in from solution handling and CE injection and thus improve the quantification accuracy.

Figure 4.2. Schematic presentation of the stand-alone RCA-CE assay for small RNA sensing



Since the current design of stand-alone RCA removes the ligation step, complementary hybridization of the small RNA onto the circular template becomes the only control over the specific recognition of the target sequence. To obtain satisfied specificity, higher reaction temperature should be used to disable the hybrids formed between the non-specific small RNA molecules and the circular probe. Several commercially available polymerases with strand displacement activity, a pre-requisite for RCA polymerase, were considered (Supporting Information Table S 4.1). *Phi*29 is the most common polymerase employed in RCA because its high strand displacement activity comes with high reaction yield and thus high detection sensitivity. It operates at 37 °C, which may not be stringent enough for the mismatches between small RNA and circular template. The 9°N_m and $Vent_{R^®}$ DNA polymerases are active at 72-75 °C, a temperature range high enough to denature even the perfectly matched double-stranded small RNA. On the other hand, *Bst* DNA polymerase (large fragment) has a moderately elevated operation temperature of 65 °C. Moreover, it has similar strand displacement capability and specific activity as *Phi*29. Therefore, in the following studies we compared the performance of *Phi*29, and *Bst* in detection of small RNA targets by our stand-alone RCA-CE assay.

4.3.2 Specificity study

We first investigated the specificity of the stand-alone RCA-CE assay using the polymerases of *Phi29* and *Bst*. The wild-type nat-siRNAATGB2 and three arbitrary mutations were employed as the targets. Mut1 has a single-nucleotide mutation on the small RNA at the complementary position to the 3'-OH end of the linear padlock probe.

This design is to facilitate the specificity comparison with ligation, which is most sensitive to the base-pair mismatch at the ligation junction. The other two contain two mutated nucleotides, which hybridize to positions either distributed on the 5'- and 3'- arms of the padlock probes (Mut2), or located only on the 3'- arm (Mut3). Their sequences and melting temperatures calculated with the DINAMelt Server on the corresponding DNA sequences were shown in Figure 4.3 a. Ligation-RCA on the DNA version of the target using T4 DNA ligase was also included as the "gold" standard, which was performed with the procedure reported in our previous work.[122] Five femtomole targets were used to ensure clear detection of the products. The RCA products were analyzed by CE and dynamically stained by the intercalating dye of SYBR Green II. Within each set of reactions, the product peak areas from the mutated targets were normalized against that from the wild-type strand and the obtained relative RCA yields were plotted in Figure 4.3 b, from which we observed various degrees of discrimination over the mutated strands in all three sets of reactions. As expected, the DNA-templated ligation-RCA led to the best specificity with relative yields of 1% and 0.5% from the DNA version of Mut1 and Mut2, respectively. Unfortunately because of its low efficiency with RNA as the ligation template, it could not be employed for detection of small RNA. The RNA-primed stand-alone RCA with *Phi29* displayed the worst loyalty to the target sequence, generating relative yield of 55% for Mut1, 19% for Mut2, and 25% for Mut3. Even though there were still some products detected from Mut1 and Mut2 with the RNA-primed RCA using *Bst*, the relative yields of 27% and 1.7%,

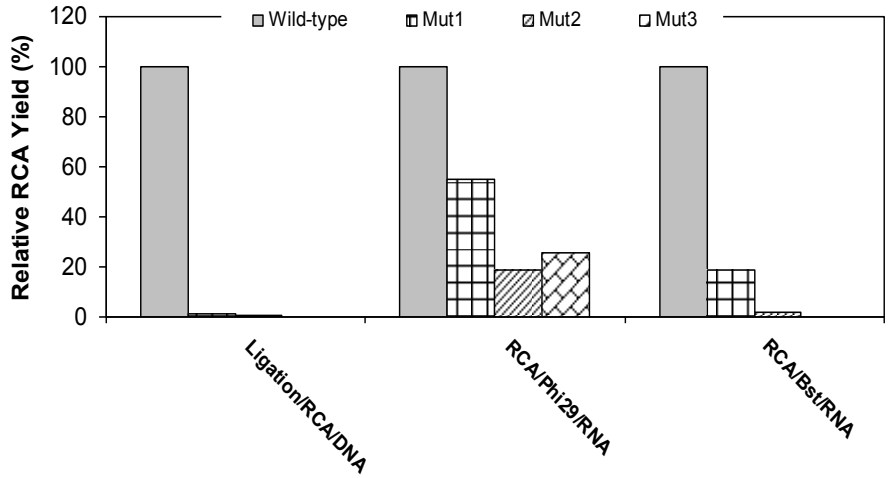
respectively, were much lower than those from the *Phi29*-mediated amplification, and no product from Mut3 was detected.

Figure 4.3 (a) Sequence of the wild-type small RNA target of natsiRNAATGB2 and the types and positions of the point mutations in the mutated strands. (b) Comparison of the relative RCA yields on different targets using ligation-RCA and stand-alone RCA with *Phi*29 or *Bst* DNA polymerase.

(a)

Wild-type small RNA:	5'-ACUCAAGGUGCAGCUGGAGGAA -3' (T_m = 69.3 °C)
Mut1:	**A → U** (T_m = 64.8 °C)
Mut2:	**G → A, G → C** (T_m = 51.5 °C)
Mut3:	**G → C, C → A** (T_m = 55.0 °C)

(b)



The specificity differences of *Phi29* and *Bst* should be originated from their operating temperatures. All of the three mutated strands have melting temperatures (T_m, calculated from double-stranded DNA with the same sequences as the small RNA and the mutants) above 50 °C, higher than the operation temperature of *Phi*29, thus the mismatched hybridization could remain stable and were falsely amplified. Higher amplification temperature up to 40 °C for *Phi*29 can be used to enhance the specificity, but an activity loss of 20% for the enzyme was observed at a higher temperature of 42 °C.[124] By contrast, *Bst* operates at 65 °C, higher than the T_m of Mut2 and Mut3, and thus generated very few or not-detectible products from these two mutations. The Mut1 has a T_m of 64.8 °C and a significant portion of it could remain bound to the circular template and amplified by *Bst*.

Based on different specificity requirements, different enzymes can be selected in our stand-alone-RCA-CE assay for small RNA detection. Since *Bst* has better accuracy in sequence recognition than *Phi*29, it is suitable in discovering new small RNA molecules and studying the relationship between the functions and the structures of small RNA molecules, in which capability to discriminate even single-nucleotide mutation is essential. So far few small RNA families having members with only one or two nucleotides difference in their sequences, like the *let*-7 small RNA family, were discovered, and the *Bst*-based stand-alone RCA-CE should be useful in detecting the various expression of each family member in different organisms, which could be related to their different functions in regulation of cellular processes.[125, 126] Alternatively, most of the discovered small RNAs, especially the miRNAs, differ by four or more nucleotide

bases, and *Phi*29 should have sufficient specificity in the detection of the known small RNAs in biological samples.[127] The mild amplification temperature and the high reaction yield, as revealed in the following study, of *Phi29* can compensate for its lack of specificity over 1- or 2-point mutation in these applications.

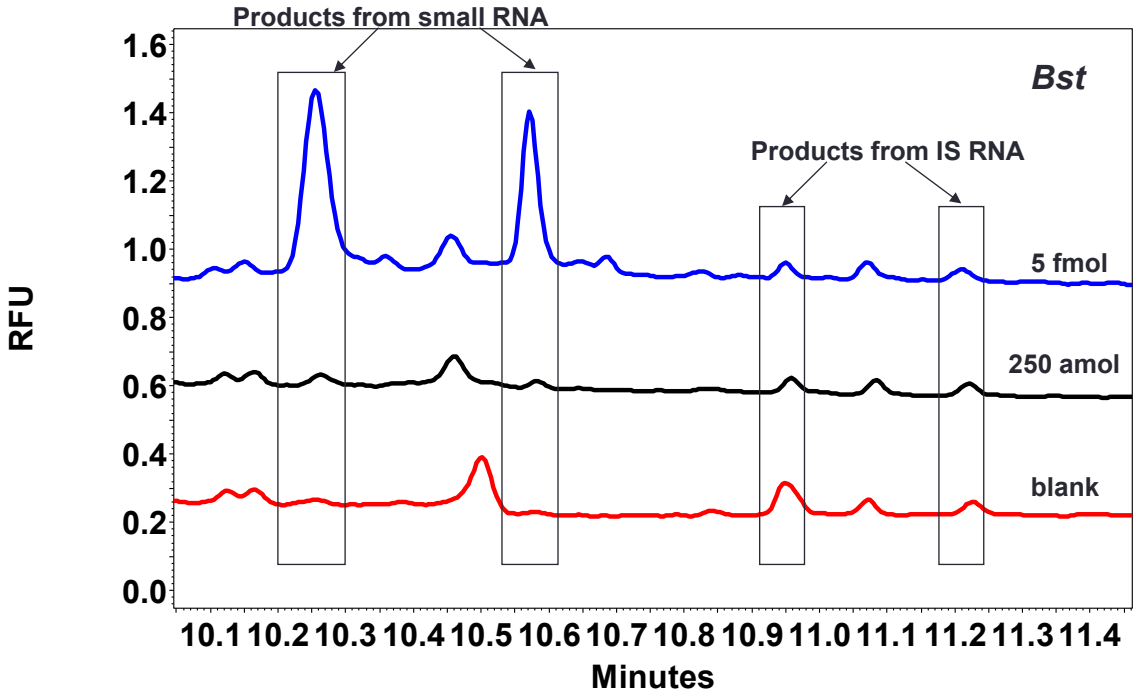
4.3.3 Standard calibration curve

Next, we went on to test the linearity range and detection limit of the stand-alone RCA-CE assay. Standard reaction mixtures contained 5, 2.5 (*Bst* only), 1, 0.5, 0.25, 0.05 (*Phi*29 only) and 0 fmol of the small RNA target and 5 fmol of the IS RNA. The electropherograms from target amounts of 5, 0.25, and 0 fmol were displayed in Figure 4.4, with Figure 4.4a dedicated to *Bst* and 4.4b to *Phi29*. In the case of *Bst*, we detected multiple peaks in the CE traces for both the target and IS RNA molecules (Figure 4.4a), although the samples were denatured in a 1:1 mixture of formamide and 8 M urea in boiling water for 3 minutes. The native electrophoresis condition probably induces the reformation of the secondary structures from the short nucleotides during the separation, resulting in multiple peaks, but secondary structure may not be the ultimate explanation for this phenomenon because only one product peak was detected in the case of *Phi*29 (Figure 4.4b). Nevertheless, the separation was very reproducible and we could easily identify the product peaks by comparing the patterns of the electropherograms from the blank and positive reactions (Figure 4.4a and 4.4b; also see Supporting Information Figure S 4.2 for the entire electropherograms). As shown in Figure 4a, peak areas of A1 and A2 increased with the small RNA amount, while other features in the CE traces

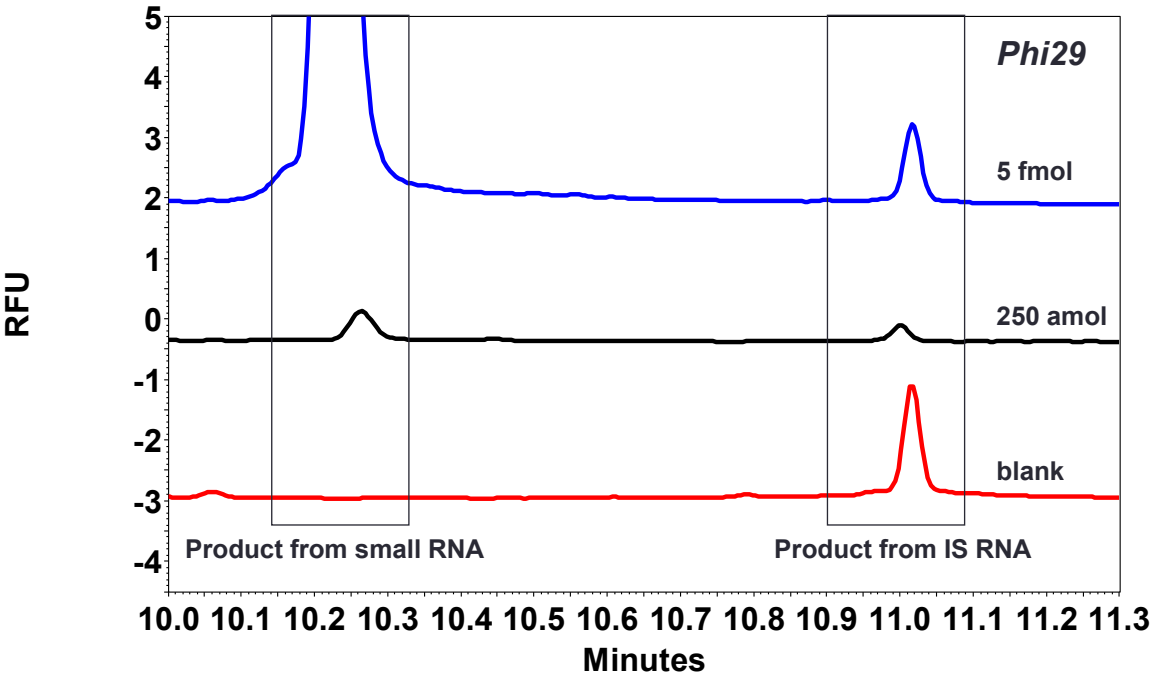
remained the same. Very low and no signal were detected at the positions for A1 and A2 in the blank trace. Similarly, A3 and A4 were reproducible peaks generated from the IS RNA as we examined the trace from the reaction with neither the small RNA target nor the IS RNA (data not shown). The peak in between A3 and A4 turned out to be not as reproducible and was discarded in our quantification. Therefore, we calculated the sum of A1 and A2, $A_{\text{small RNA}}$, and the total of A3 and A4, A_{IS}, and the calibration curve of $A_{\text{small RNA}}/A_{IS}$ vs. the amount of small RNA showed very good linearity with an $R^2 = 0.998$ and an average relative standard deviation (RSD) of 9 % (n = 3) (Supporting Information Figure S 4.3a). The theoretical mean-plus-3SD detection limit of the *Bst*-mediated amplification was determined to be 200 amol using the mean peak ratio of the blank reaction and the average standard deviation (SD) within the target concentration range of 0 – 500 amol. The detection limit was 10 fold lower than that of the ligation-RCA-CE assay for DNA detection reported by our group because of the exclusion of the ligation step.

Figure 4.4 Electropherograms from the CE analysis of the RCA products generated from different amounts of small RNA using *Bst* (a) or *Phi*29 (b) as the DNA polymerase.

(a)


Products from small RNA
Products from IS RNA
Bst
5 fmol
250 amol
blank
RFU
1.6
1.4
1.2
1.0
0.8
0.6
0.4
0.2
0.0
10.1 10.2 10.3 10.4 10.5 10.6 10.7 10.8 10.9 11.0 11.1 11.2 11.3 11.4
Minutes

(b)


Phi29
5 fmol
250 amol
blank
RFU
5
4
3
2
1
0
-1
-2
-3
-4
Product from small RNA
Product from IS RNA
10.0 10.1 10.2 10.3 10.4 10.5 10.6 10.7 10.8 10.9 11.0 11.1 11.2 11.3
Minutes

The overall signal intensity from *Phi*29 was higher than that from *Bst* and only one peak was detected for either the target small RNA or the IS RNA (Figure 4.4b). Therefore, it achieved a 5-time lower detection limit of 35 amol. The higher signal intensity with *Phi29* can be attributed to its high processivity[46] and the mild amplification temperature that stabilizes the RNA-circular probe hybridization and maintains the high affinity in the binding of dNTPs onto the circular template. However, the linearity and reproducibility of *Phi29* was not as good as *Bst*, with an $R^2 = 0.985$ and an average RSD of 12% (n = 3) (Supporting Information Figure S 4.3b). We observed large variations in the IS peak intensity while *Phi*29. Such variations could be originated from small deviations in manual solution preparation, fluctuation of reaction conditions inside each reaction vial, and loss of samples during the clean-up process. The assay procedure with *Phi29* is more complicated than that with *Bst*. An additional 15-min hybridization step at an elevated temperature of 65 °C was required by *Phi*29 before RCA, because 37 °C was not high enough to allow adequate hybridization of the target and circular probe. After amplification, *Phi29* should be deactivated at 70 °C for 10 min to ensure better reproducibility because the reaction could continue during the subsequent steps of restriction enzyme digestion which also took place at 37 °C and sample clean-up (at room temperature) with the active *Phi29*. More reaction steps lead to more random process variations and reduced reliability in detection, which should be corrected by the co-amplification of an internal standard.

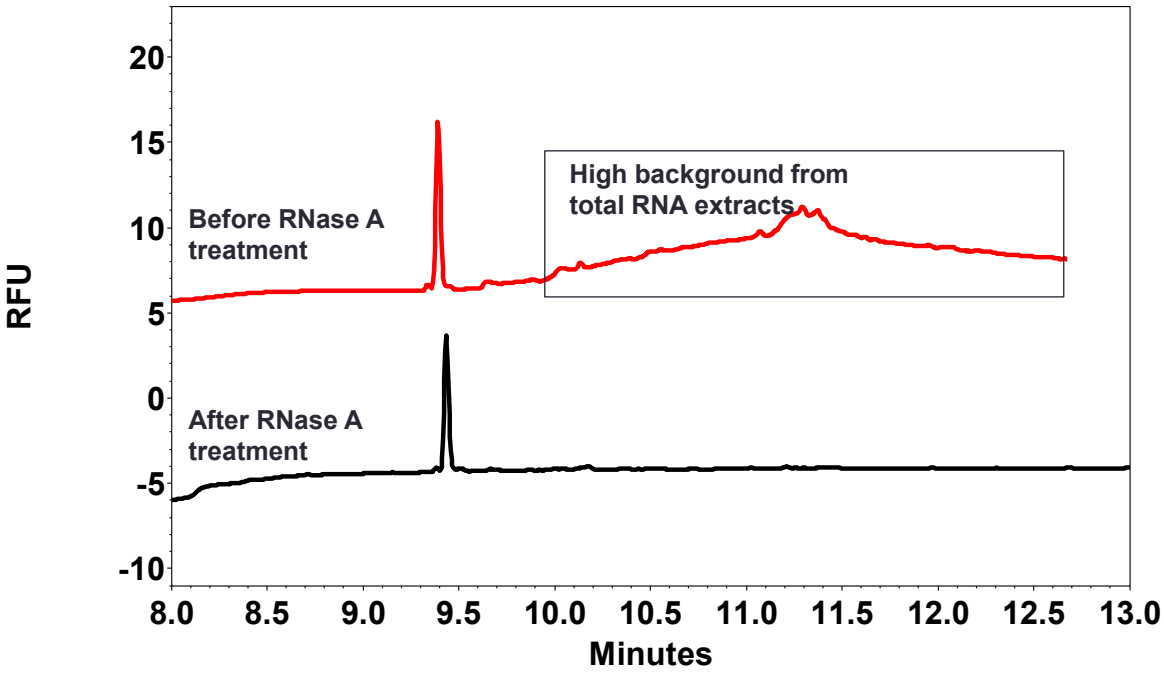
We also noticed that, the IS peak was much smaller than the target peak with either enzyme, probably because the IS circular template is 30% longer (17 nt longer) than that for the target. The longer circular template takes longer time to finish one round of the amplification and thus fewer numbers of repeated sequences are generated per unit reaction time, resulting in a lower overall yield.

4.3.4 Small RNA detection in plant total RNA extracts

After proving the specificity and sensitivity of our stand-alone RCA-CE assay, we applied it to detect the nat-siRNAATGB2 spiked into the plant total RNA extracts. The plant total RNA extracts was prepared from wild-type *Arabidopsis thaliana* without induction, in which the amount of endogenous nat-siRNAATGB2 was not detectible even with Northern blotting[123] Since the total RNA extract contains thousands types of different RNA molecules, extreme caution should be taken in its design to avoid amplification of the background RNA molecules that bind to other positions of the circular probe. The RNA molecules that can be used as the primer for RCA should meet several criteria. They should contain a complementary sequence to the circular probe with a considerable length (high T_m), have a free 3'-OH group, and have no over-hang at the 3'-terminus after hybridization to the circular probe, which exclude the long RNA molecules with matching sequences in regions other than the 3'-terminus. RNA molecules with modification on their free 3'end can not be amplified, either. With these considerations in mind, we performed a BLAST (Basic Local Alignment and Search Tool) search of the cDNA database of *Arabidopsis thaliana* (http://tigrblast.tigr.org), and

did not identify any sequence producing high-scoring segment pairs with our probes, indicating ultra-low chances in mistakenly amplifying the large population of messenger RNA in the sample.

Figure 4.5 Effect of RNase A treatment in removal of the high background signal in CE analysis.

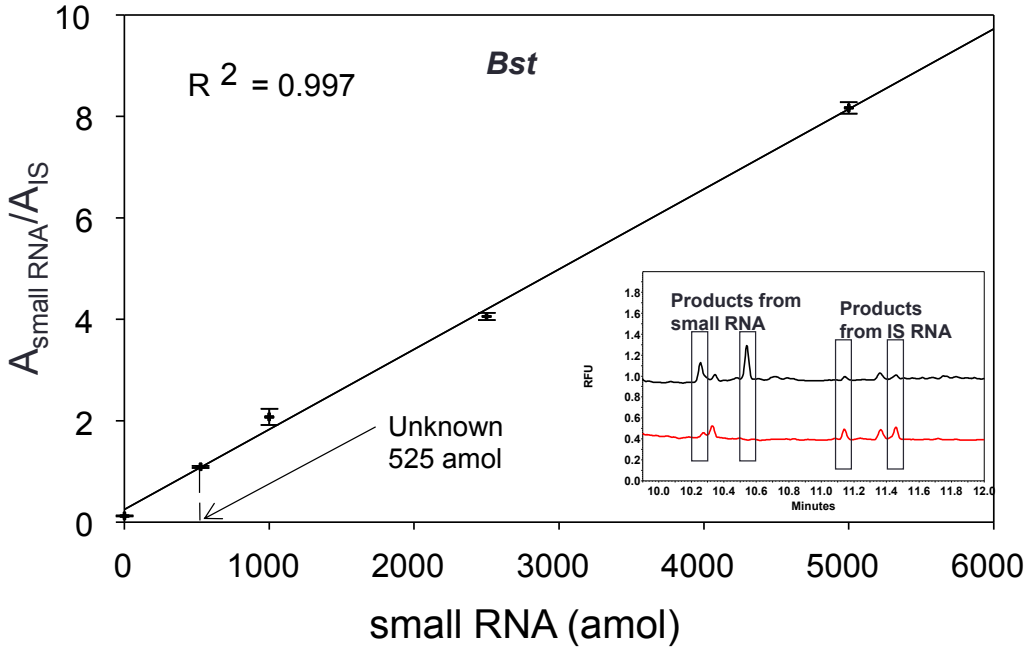


Another trouble accompanied with the high RNA content in the total RNA extract was the high detection background in CE because SYBR Green II is very sensitive to RNA, preventing clear detection of the RCA products (top trace in Figure 4.5). Therefore, an RNase A treatment was employed to digest any RNA molecule in the sample after the RCA and restriction enzyme digestion steps. The RCA products are DNA molecules and remain intact during the digestion. After the RNase treatment, a relatively flat base-line was detected in the blank reaction with the plant total RNA extract.

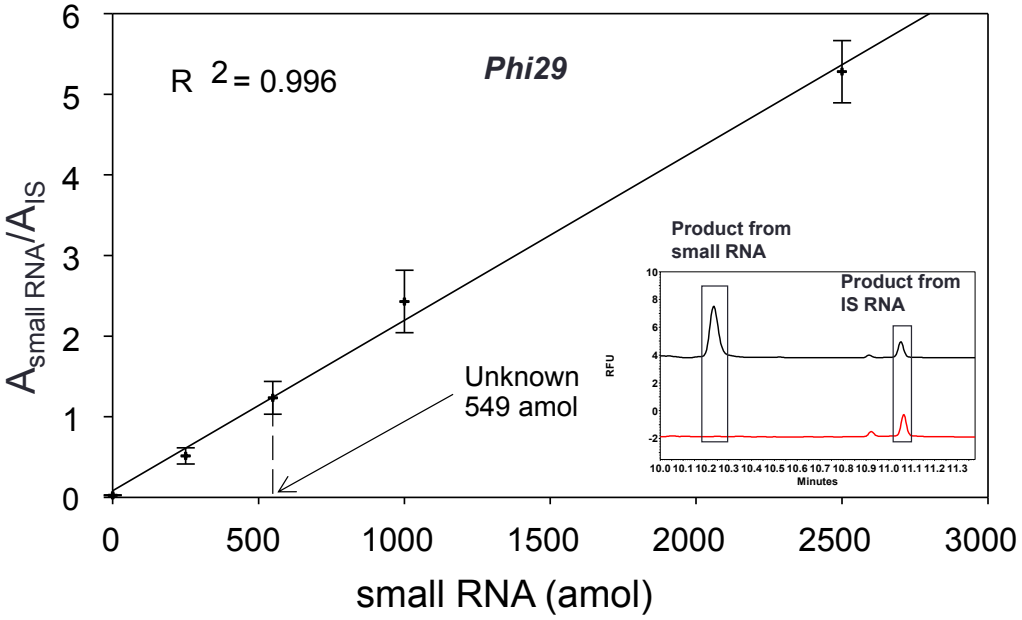
Then, different amount of the nat-siRNAATGB2 (0, 0.25 (only with *Phi*29), 0.5, 1, 2.5, and 5 fmol (only with *Bst*)) was spiked into 117 ng of the total RNA extract with 5 fmol of the IS RNA and detected with the RCA-CE assay. The one containing 500-amol target RNA was used as the artificial unknown to test the quantification accuracy of our assay, while the other four mixtures were used to construct the calibration curves shown in Figure 4.6. Inserts were the electropherograms with 0- (bottom trace) and 5-fmol (top trace) target RNA. The clean baselines signified that our stand-alone RCA-CE assay had sufficient specificity to avoid the amplification of any background RNA with detectible yield. The CE traces were not affected at all by the plant total RNA extract with the RNase A treatment, containing features greatly resemble to those obtained from pure small RNA samples. In addition, ultra high linearity with R^2 values larger than 0.99 were obtained (Figure 4.6). Again, *Bst* showed higher reproducibility with an average RSD value of 3.8% (n = 3), which increased to 14% for *Phi*29. Both enzymes accurately quantified the "unknown" small RNA sample with about 110% recovery.

Figure 4.6 The calibration curves for quantification of the 500 amol of target small RNA added to the plant total RNA extract using the stand-alone RCA-CE assay with *Bst* (a) or *Phi*29 (b) as the amplification enzyme. Inserted figures are the corresponding electropherograms. The traces on top are with the spiked-in small RNA and the bottom traces are without the spiked-in small RNA.

(a)


Bst
R 2 = 0.997
A small RNA/A IS
small RNA (amol)
Unknown
525 amol
Products from small RNA
Products from IS RNA
RFU
Minutes

(b)


Phi29
R 2 = 0.996
A small RNA/A IS
small RNA (amol)
Unknown
549 amol
Product from small RNA
Product from IS RNA
RFU
Minutes

4.4 Conclusions

A stand-alone RCA-CE assay was established for specific and sensitive detection of small RNA in total RNA extract. A ligation-less approach of using the target small RNA as the primer for direct rolling circle amplification simplified the assay procedure and lowered the detection limit to 200- or 35- amol with reasonable specificity. Highly reproducible detection and accurate quantification of the target small RNA in plant total RNA extracts was achieved with the complete digestion of the background RNA molecules by RNase A. Performance comparison of the two DNA polymerases, *Bst* and *Phi*29, showed that the *Bst*-based stand-alone RCA-CE had better specificity, simpler procedure, and higher reproducibility, but a 5-fold higher detection limit, compared to the *Phi*29-based RCA. Higher sensitivity with *Bst* is possible with further optimization of the assay. For example, the amplification efficiency could be improved by decreasing the amplification temperature of *Bst* to some extend, or by designing circular templates with higher GC content to which the dCTP and dGTP should have higher binding affinity even at elevated temperature. The speed-vac drying and formamide-urea-mediated DNA denaturing could be eliminated since multiple products were detected anyway, which can lead to about 5-fold signal enhancement (data not shown).

Our assay can be combined with automatic liquid handling station and a 96-capillary array instrument to improve sample throughput. It is also an appropriate technique for a fast initial screening on the expression levels of a large pool of small RNAs, because only the target strand binding sequence needs to be changed on the circular probe. The cost of

each assay is quite low because of the small reaction volume and the low sample consumption in CE analysis. Moreover, the simple and isothermal procedure makes it possible to apply our assay for on-column or on-chip[128] amplification of small RNA from very limited amount of the biological sample, because we actually detected products generated from less than 20 zeptomole molecules judging from the 20-nL injection volume in CE. Reliable detection of small RNA or other types of short RNA species in a small group of cells can greatly improve our understanding of the relationship between cell phenotypes and the expression of these non-coding RNA molecules and help with interpretation of their unique functions.

Supporting Information

Table S 4.1 Property comparison of commercially available enzymes with strand displacement activity. Information obtained from www.neb.com.

Name	**Strand Displacement Activity**	**Specific Activity (units/mg)**	**Amplification Temperature**
Phi29	+++++	100,000	37 ° C
DNA Polymerase I Large (Klenow) Fragment	++	20,000	37 ° C
M-MuLV Reverse Transcriptase	+++	500,000	37 ° C
Bst DNA Polymerase Large Fragment	++++	120,000	65 ° C
9 ° N_m	+++	35,000	72 °C
$Vent_{R®}$	+++	28,000	75 ° C

Figure S 4.1 PAGE gel image for separation of the ligation products generated by T4 DNA ligase or T4 RNA ligase 2. The gel was stained by SYBR Gold and the image was taken by the Typhoon Fluorescence Imager. *Lane 1 and lane10*: 10bp ladder; *Lane 2*: DNA version of the nat-siRNAATGB2; *Lane 3*: nat-siRNAATGB2; *Lane 4*: product from the RNA-templated ligation catalyzed by T4 RNA ligase 2; *Lane 5*: product from the DNA-templated ligation catalyzed by T4 RNA ligase 2; *Lane 6*: product from the RNA-templated ligation catalyzed by T4 DNA ligase; *Lane 7*: product from the DNA-templated ligation with T4 DNA ligase; *Lane 8*: preformed circular padlock probe, *Lane 9*: linear padlock probe.

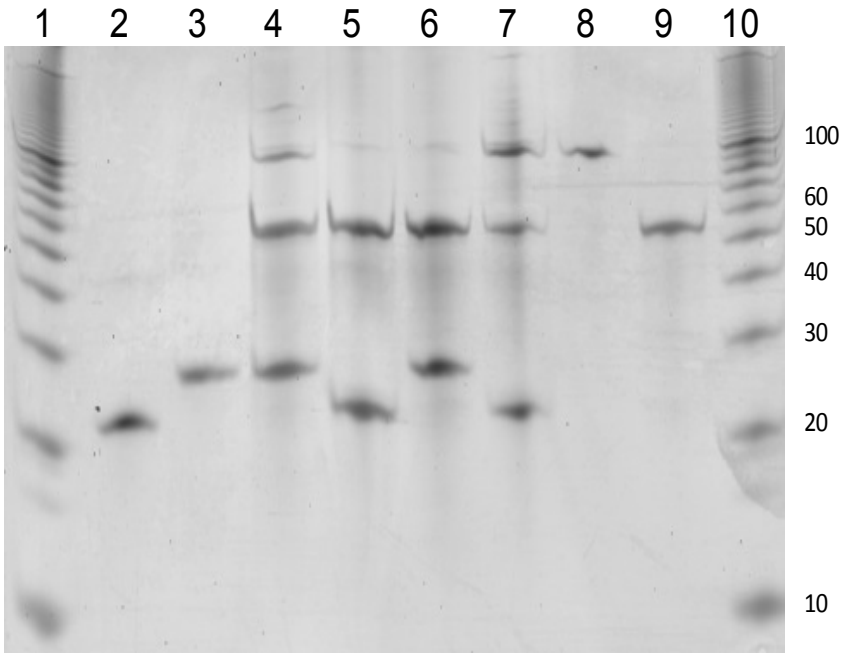


Figure S 4.2 The entire electrophoregrams of the reaction products from 250 amol small RNA and the corresponding blank. Amplification enzyme was *Bst*.

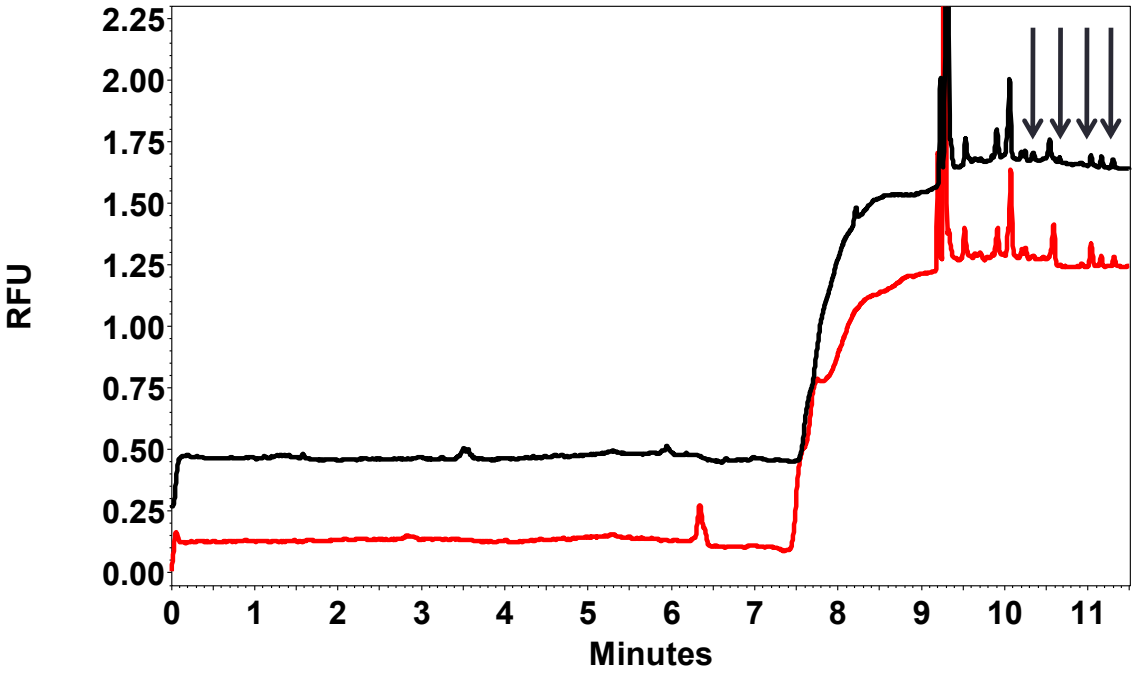
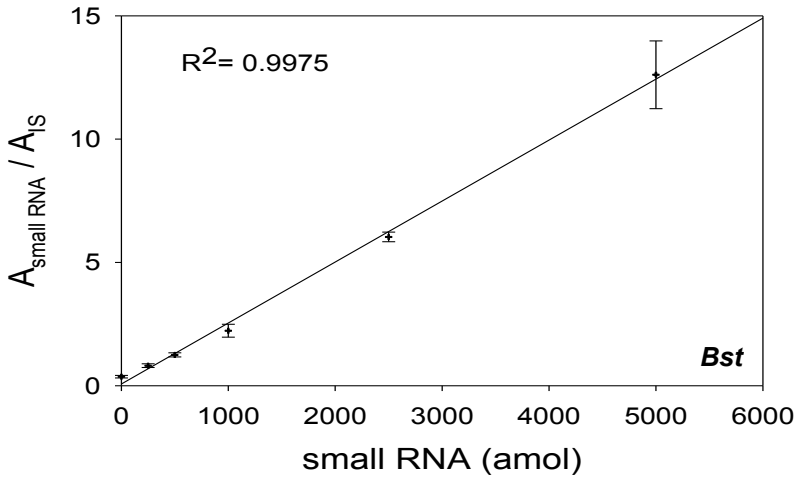
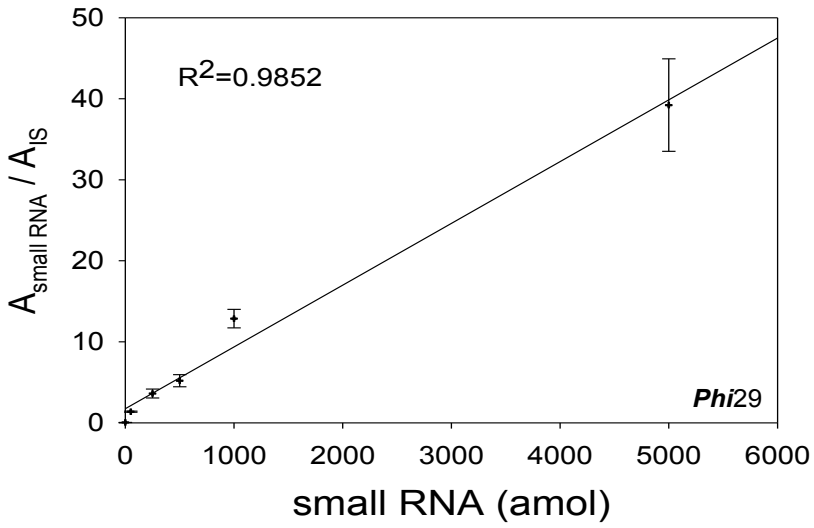


Figure S 4.3 The calibration curves for the CE analysis of the RCA products generated from different amounts of small RNA using either *Bst* (a) or *Phi29* (b) as the DNA polymerase.

(a)



(b)



Chapter 5

Analysis of the nano-bio interface

Within the past few years, tremendous developments have been made in nanomaterial synthesis. To be considered as nanomaterial, at least one dimension must be between one and one hundred nanometers. Various shapes of nanomaterials can be synthesized, such as commonly seen spherical, rod-shaped, hollow-tubular, tri-angular, square-shaped, and even more sophisticated shapes, such as tree-like and water-melon like. Material scientists have been exploring in the nano-scale world like artists and engineers so that delicate nanostructures can be achieved for specifically desired functions. High-yield, narrow-size distribution recipes are available for metal (i.e. Au, CdSe), metal oxide (i.e. iron oxide, titanium oxide), or carbon (carbon nanotube, graphene)-based nanomaterials. Rapid growth in nanotechnology is bringing nanometerials closer to biomolecules. The nano-bio interface is where inorganic nanomaterial interacts with biocomponents, such as protein. This interface is an interesting topic shared by nanomedicine, nanoengineering and nanotoxicity.[129] Most biocomponents are smaller than 100 nm. Many proteins, for instance, are under 10 nm in size, while DNA strands are even smaller. The comparable size of nanomaterials to biomolecules makes the nano-bio interface quite unique. It may have impact on both nanomateials and biomolecules, such as altering the behavior of nanomaterials and changing the biomolecule functionality. To have a predictive guidance

for the design of NPs for biological purposes, fundamental studies of the nano-bio interface are necessary. These studies include probing the interaction, measuring the affinity and kinetics, understanding the driving force and binding mechanisms, and predicting the effects based on both physical and chemical features of both parties.

For bio-related engineered nanomaterials, for example, bio-imaging tools, drug delivery cargos, therapeutic nano-roborts, *etc*., they can be homogenously dispersed in biological fluidics and living cells. They are usually designed to target specific cells or organs and be used to image, dose or kill the cells. However, when they are introduced to plasma by i.v., the most straightforward way to dose nanomaterials, they will immediately meet background plasma proteins. The resulted "corona" covered nanomaterials are seen and responded by cells. It has been reported that NPs could adsorb many plasma proteins.[130] The "corona" could bring in beneficial effects for NPs functioning as diagnostic or therapeutic substances, such as increasing the stability of NPs [131, 132] or assisting cell internalization.[133, 134] However, adsorption onto NP surface could induce protein aggregation,[89, 135] misfolding, and deactivation;[136] and could also subsequently affect protein-protein interaction.[137] Malfunctioning of proteins may ultimately lead to toxicity. In order to make engineered nanomaterials function in biological system as desired, a clear nano-bio interface understanding is urgently required. Not only those intentional exposures to nanomaterial, but also some unintential exposures to nanomaterials, such as pollutants in the air or natural water, greatly called attention on nanotoxicity study. Mechanism study on nano-bio interface is becoming a rising topic in nanotoxicity as well.

Currently, several techniques have been applied to the study of the nano-bio interface. Nanoparticle-protein interaction studies, either through interaction with the proteome or with individual proteins,[138] generally involve identifying which proteins are adsorbed on the surface by separation techniques (i.e. size exclusion chromatography, slab gel electrophoresis) and mass spectrometry (i.e. MALDI-TOF MS/MS),[130] quantifying the affinity strength and binding ratio by titration monitored by UV-vis, fluorescence spectroscopy,[139] dynamic light scattering, *etc.*, quantifying the binding kinetics by SPR, QCM, *etc.*, monitoring the conformational change of protein due to interaction with nanoparticles by CD,[140] fluorescence anisotropy, *etc*.. In this part of the thesis, we fully utilized the advantages of CE and MS, which will be further discussed in Chapter 6 and Chapter 7, and applied them in probing nanoparticle-protein interaction and understanding the mechanism (i.e. driving force and binding site identification).

Quantitative measurement of the biophysical parameters of nanoparticle−protein interaction could be conveniently performed by capillary electrophoresis (CE) as demonstrated in Chapter 6. Two interaction situations were identified. Stable nanoparticle−protein complexes were resolved from the free nanoparticles and the proteins by capillary zone electrophoresis (CZE). Transient complexes with fast association/dissociation rates showed distinct mobility change from the free nanoparticles in affinity capillary electrophoresis (ACE). Interactions of bovine serum albumin (BSA) with the Fe_3O_4 nanoparticles (average diameters of 8 and 10 nm) and with the Au

nanoparticles (average diameters of 5 and 10 nm) displayed slow and fast binding kinetics, respectively. Using the Hill equation, we could calculate the dissociation constants (K_D) and cooperativity coefficients (n). Impacts on nanoparticle−protein interaction from the physicochemical properties of nanoparticles and the incubation buffer were evaluated on the basis of the K_D and n values to interpret the interaction driving forces. Our study demonstrated the high simplicity and flexibility of CE in probing the interaction of proteins with diverse particles. The separation power of CE should also facilitate studies of the multicomponent interaction systems for investigating how adsorption onto nanoparticles could affect the protein−protein or protein−small molecule interactions.

Mechanism study on interaction driving force and interaction sites are presented in Chapter 7. First, we noticed that two Fe_3O_4 nanoparticles with similar size and similar zeta potentials displayed significant different K_D values when they interaction with the same protein. We realized that this could be attributed to the thermal degradation of PAA during NPs synthesis. Intramolecular loss of CO_2 and H_2O were revealed by mass spectrometry (MS) study of the surface ligands recovered from NPs. Along with the thermodynamic study, this result pointed out the importance of desolvation in driving forward the NP-protein interaction. Our study also highlighted the imperativeness of thorough characterization of the nanomaterials in probing the nano-bio interface. Second, cross-linking and mass spectrometry were adopted to study the binding site on human serum albumin when it interacts with PAA-Fe_3O_4 NPs. Peptides within HSA drug

binding site 2 were identified to interact with PAA-Fe_3O_4 NPs by comparing the mass spectra. Ibuprofen and naproxen, two representative drugs known to bind site 2 were tested and the results showed that both of them inhibited the binding between HSA and PAA-Fe_3O_4 NPs. In contrast, another drug, fusidic acid, which was known to bind HSA in a pocket away from site 2, did not affect the binding between HSA and PAA-Fe_3O_4 NPs at all. Those results further confirmed our findings via cross-linking and MS. Our strategy, borrowed from protein-protein interaction site identification, showed great capability on nanoparticle-protein interaction site identification and the results indicated that potential biological effects due to nanoparticle-protein interaction are calling attentions and in-depth studies would be significant for better design on nanomaterial for biological related applications.

Chapter 6

Probing nanoparticle-protein interaction by capillary electrophoresis

6.1 Introduction

In order to impose better control over both the advantageous and harmful effects from NPs, driving forces for NP-protein interaction need to be identified. Protein binding to surface involves synergetic work of non-covalent forces including electrostatic and hydrophobic interactions, hydrogen bonding, and π-π stacking. For NPs that are freely suspended, 3D subjects, other factors like solvation of NPs and NP-protein complexes, as well as NP surface curvature, also contribute to the interaction.[141] Further augmenting the number of variables playing roles in the interaction is the diverse physicochemical properties of NPs and proteins. To sort out how these many variables influence the NP-protein interaction, quantitative comparison of the interaction kinetics, affinity, and stoichiometry when systematically varying the types of protein or NP is highly demanded.

Presently, techniques like circular dichronism (CD),[140] surface plasmon resonance (SPR),[142] isothermal titration calorimetry (ITC),[141] and fluorescence correlated or quenching microscopy[139, 143] dominate the measurement of NP-protein interaction because of the high simplicity in direct measurement of the interaction mixture. However, low sensitivity, spectral interference from NPs in the background, requirement for protein

or NPs immobilization, and/or necessity for NPs to be luminescent or photoquenching, prevent the above techniques from studying NPs and proteins with wide ranges of physicochemical properties.[143] Moreover, it is difficult for these techniques to probe the interaction-induced changes in protein's binding capability to its ligands, substrates, or carrier molecules.[141, 143-145] Separation tools like size exclusion chromatrography (SEC), slab gel electrophoresis, and micellar electrokinetic chromatography have been applied to isolate proteins stably adsorbed onto NPs for downstream identification.[138, 146] SEC could be used to estimate the binding rates between single proteins and NPs, but the exclusion resin seemed to adsorb the NP-protein complex and interfere with the estimation. On the contrary, capillary electrophoresis (CE) operates in an open-column format without any packing materials, imposing the least impact to the NP-protein complex. This feature, in addition to other advantages it offers, such as high resolution power and rapid separation speed, makes CE highly suitable for quantitative measurement of the affinity between individual proteins and NPs. Additionally, CE can handle nanomaterials very well.[27-29] Polymeric and inorganic NPs ranging from 20 nm to 1.5 μm in diameter have been used as the stationary or pseudostationary phase in capillary eletrochromatography,[147, 148] and have demonstrated good performance in electrophoretic separation of small molecules[149], DNA[150], and proteins.[151, 152] Moreover, by adding the ligands to the running buffer, CE can conveniently study the transient complexes with fast association/dissociation rates.[153, 154] Diverse separation modes have been developed to facilitate analysis of molecules with different characteristics in charge, size, and hydrophobicity, and multichannel CE on

microchips can significantly enhance the analysis throughput, both adding extra values to the applicability of CE in studying NP-protein interaction.

In this chapter, we examined the effectiveness of CE in measuring the affinity between NPs and proteins with an appropriate interaction model. Interactions of bovine serum albumin (BSA) with the gold and superparamagnetic Fe_3O_4 NPs, which have shown great potential in biomedical applications, were investigated. Depending on the complex dissociation rate, binding situations could be studied with two CE operation modes: capillary zone electrophoresis (CZE) and affinity capillary electrophoresis (ACE). The response curves of peak area ratios in CZE or electrophoretic mobility shifts in ACE verse protein concentrations were fitted with the Hill equation; and the dissociation constants (K_D) and the Hill coefficients (n) were obtained. Our study demonstrates the great power of CE in studying NP-protein interaction, and paves the way for future investigation on the multi-component interaction systems to probe the binding of substrate, cargo molecules, ligands, receptors, *etc*. to proteins adsorbed on NP surface.

6.2 Experimental

6.2.1 Reagents and Materials

Gold colloid solutions (5-nm and 10-nm Au NPs) were from Sigma-Aldrich Corporation (St. Louis, MO), as well as all chemicals used for CE and PAA-Fe_3O_4 NPs synthesis. EMD OmniPur®10×PBS liquid concentrate (NaCl 137mM, KCl 2.7mM, Phosphate buffer

10 mM (Na_2HPO_4/KH_2PO_4 pH7.4) on 10× dilution) and molecular biology grade dimethyl sulfoxide (DMSO) was obtained from Fisher Scientific (Fairlawn, NJ). Solutions were prepared in the deionized water purified by the Milli ·Q water purification system (Billerica, MA).

6.2.2 Synthesis and characterization of NPs

Highly water-soluble superparamagnetic polyacrylic acid (PAA)-coated Fe_3O_4 NPs (average sizes of 8 nm and 10 nm) were synthesized by hydrolyzing $FeCl_3$ with NaOH/DEG in the presence of PAA (Mw 1800).[71, 155] A NaOH/Diethylene Glycol (DEG) stock solution was prepared by dissolving 50 mmol NaOH in 20 mL DEG. In a typical synthesis, a mixture of PAA (4 mmol), $FeCl_3$ (2 mmol), and DEG (15 mL) were heated up to 220 ˚C in a nitrogen atmosphere with stirring. A NaOH/DEG stock solution (4.5 mL) was then injected rapidly into the above hot mixture. The subsequent steps were different for the synthesis of PAA-Fe_3O_4 NPs with average diameters of 8- and 10-nm. The smaller NPs were obtained by continuously heating the resulted mixture for 12 hrs at 220˚C. The larger ones were achieved in several steps: heating the resulted mixture back to 220˚C; adding another 5 mL 0.4 M $FeCl_3$ stock solution that dropped the solution temperature to around 200˚C; heating the solution back to 220˚C again; and injecting another 3 mL 2.5 M NaOH/DEG and reacting for 10 min at 220˚C. Excess amount of PAA and other reagents in the reaction mixture were removed by centrifugation-assisted washing several times with a mixture of deionized water and ethanol. Finally, the PAA-Fe_3O_4 NPs were suspended in 10 mL water to form the stock solutions.

A Philips Tecnai 12 transmission electron microscope (TEM) was used to investigate the morphology of NPs. TEM images of NPs are shown in Supporting Information (Figure S 6.1). Inductively coupled plasma atomic emission spectroscopy (ICP-AES) tests were performed on a Perkin-Elmer Optima 2000 DV optical emission spectrometer to measure the concentration of Au or Fe element in NPs. With the size measured under TEM and the element content obtained from ICP-AES, molar concentration of the NPs stock solutions were obtained. Zeta potential and hydrodynamic size were measured with a ZetaPALS system (Brookhaven, Holtsville, NY) at 25°C, which was equipped with a 660-nm laser and a build-in precision Peltier temperature controller.

6.3.3 Capillary Electrophoresis

A P/ACE MDQ Capillary Electrophoresis System equipped with a diode array detector (Beckman Coulter, Fullerton, CA) was used for all CE experiments. The 50-cm fused-silica capillary (75 μm i.d., 365 μm o.d.; PolymicroTechnologies, Phoenix, AZ) with an effective length of 40 cm was sequentially rinsed at 30 psi with 0.1 M NaOH (2 min), deionized water (1 min), and the running buffer (6 min) prior to injection. All CE separations were done at 25 kV in room temperature. Peak area calculation was done by the 32Karat software provided by Beckman Coulter.

Capillary zone electrophoresis was performed in 10 mM borate buffer at pH 8.3. BSA at different concentrations (from 3.79 μM to 37.9 μM) was incubated with 194.8 nM 8-nm PAA-Fe_3O_4 at room temperature overnight before CZE analysis. For pH and salt effect

study, the 8-nm PAA-Fe_3O_4 and BSA (from 3.79 μM to 60.6 μM) were pre-incubated in 10 mM borate buffer at pH 8.3, 10 mM phosphate buffer at pH 7.5, or 1×PBS containing 150 mM NaCl.

In affinity capillary electrophoresis, NP was injected and different concentrations of proteins were included in the running buffer of 10 mM phosphate buffer (pH 7.5). The Au NPs (5.66 nM for the 10-nm Au NPs and 19.1 nM for the 5-nm Au NPs) were injected with 0.01% (v/v) DMSO.

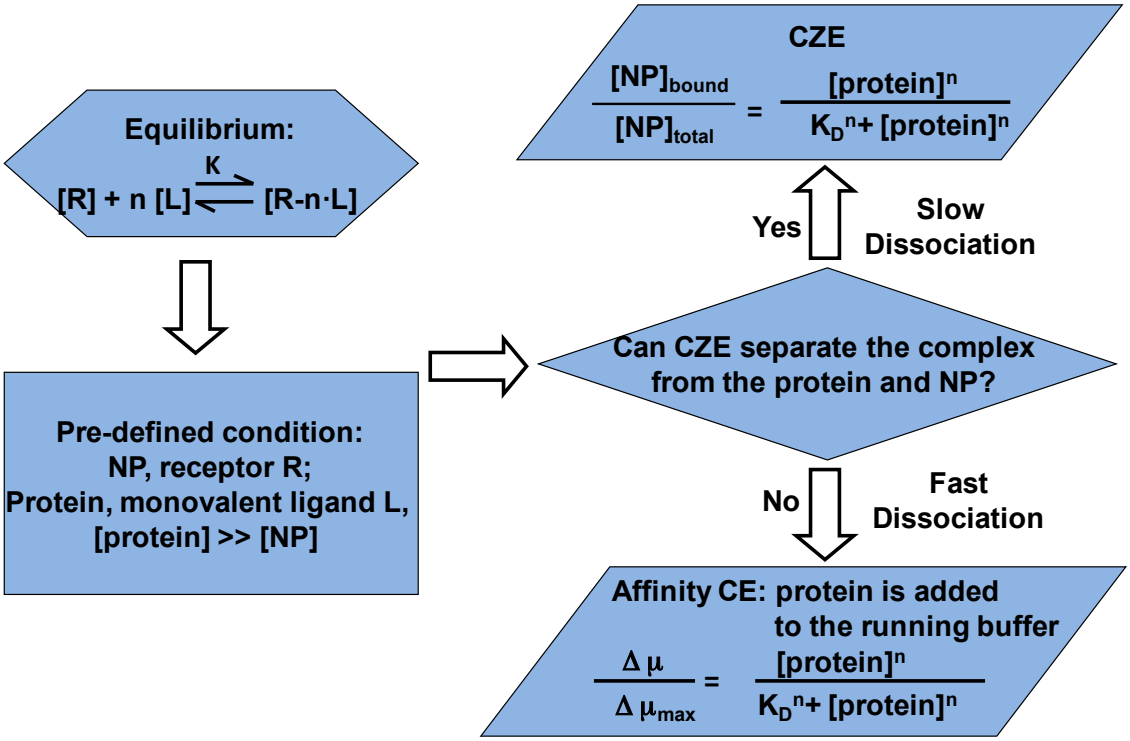
6.3 Results and discussions

6.3.1 CE modes and affinity calculation

The first important step in interaction study is to set up the roles of interactive components. Unlike the well defined ligand-receptor system, NPs could be the ligands or the receptors. NPs have uniform distribution of the same type of functional groups on their surface, forming multiple and possibly similar binding pockets for proteins. They range from 5 nm up to 100 nm,[134, 156, 157] much larger than proteins and thus able to accommodate more than 1 protein molecule on the surface. Additionally, NPs entering the circulation systems are present at small doses and face highly abundant proteins. The characteristics of NPs and the interaction circumstance make it more logical to consider each NP as a receptor having multiple binding sites for the protein which is the monovalent ligand (L) and present in excess. Moreover, this interaction model relies on measuring the NPs but not proteins as illustrated in below discussion, which lowers the

demand on detection methods because NPs usually have higher optical extinction coefficients in the UV-Vis range than proteins.

Figure 6.1 Flowchart of CE as a flexible probing platform for NP-protein interaction



The process of using CE to measure the binding affinity between NPs and proteins is described in Figure 6.1. The dissociation equilibrium constant of the NP-protein complex can be calculated from Hill equation [139, 143, 158, 159] using the protein-bound NP fraction (θ) and protein concentration:

$$\theta=[protein]^n/(K_d+[protein]^n)=[protein]^n/(K_D{}^n+[protein]^n)$$

In this equation, K_d and K_D are the macroscopic and microscopic dissociation constants, respectively, and n represents the binding cooperativeness. K_D is more descriptive for the

affinity of each binding site to the protein ligand. The multivalent nature of NP-protein interaction determines that competition or cooperation among the same protein molecules for the binding sites on NP surface would occur, which would be accurately described by n. However, the Hill equation assumes each binding site is occupied by one ligand and cannot reveal the adsorption of multiple protein layers on NP surface. This binding situation may happen when the protein concentration is very large or the protein tends to aggregate in the interaction buffer. It should be avoided by controlling the protein concentration, and aggregation could be monitored from the migration behaviour of the protein and NP-protein complexes in CE. Protein binding to NP surface can bring in significant change to the charge and size of NPs, affecting their migration behaviour in CE. If the dissociation rate is slower than the CE speed, the NP-protein complex remains stable during the separation and is resolved by CZE from the free ones. Then θ equals to the peak area ratio of the protein-bound and total NPs. For complexes formed and dissociated rapidly during CE, θ can be calculated from the apparent electrophoretic mobility (μ_{app}) of NP in ACE with different protein concentrations in the running buffer[37, 160]:

$$\mu_{app} = f_1 \cdot \mu_{max} + f_2 \cdot \mu_{free}$$

where f_1 and f_2 are the fractions of protein-bound and free NPs; μ_{free} and μ_{max} can be obtained when there is no protein and saturated protein in running buffer respectively. Thus, we have

$$\theta = NP_{bound}/NP_{total} = f_1 = (\mu - \mu_{free})/(\mu_{max} - \mu_{free})$$

For CZE study of the slow dissociation systems, NPs at a fixed concentration were incubated with different concentrations of BSA, and the equilibrium mixture was injected. The duration of incubation was determined by sampling the mixture at various times until no more change in the protein-bound NP peak was observed. Peak areas of the protein-bound and free NPs measured at the distinct wavelength of NPs with minimal interference from BSA were used to calculate the bound NP ratio. In the ACE mode, the mobility of NPs was monitored. Protein concentrations in running buffer would be increased until the maximum mobility shift was observed. A neutral marker, DMSO, was used to adjust the change in the electroosmotic flow (EOF).

6.3.2 Slow dissociation system

Interactions between BSA and the PAA-Fe_3O_4 (8 nm and 10 nm) NPs were typical slow dissociation systems. The interaction reached equilibrium after overnight incubation. The borate buffer (10 mM sodium borate, pH 8.3) provided the best separation of the bound- and free-NPs and thus was employed as the running buffer. We initially used water as the incubation buffer to promote BSA unfolding and facilitate its adsorption onto NP surface. Both the protein and the NPs were negatively charged. Under the normal electric field, BSA migrated faster than the NPs and its adsorption onto the NP surface slightly sped up the apparent migration of NPs. This is probably due to the increase in NP size after bound with BSA, because the total negative charges of NP or NP-protein complex should be majorly determined by the PAA which carried a large number of carboxyl groups. Hydration size and zeta potential measurement using the ZetaPALS confirmed this

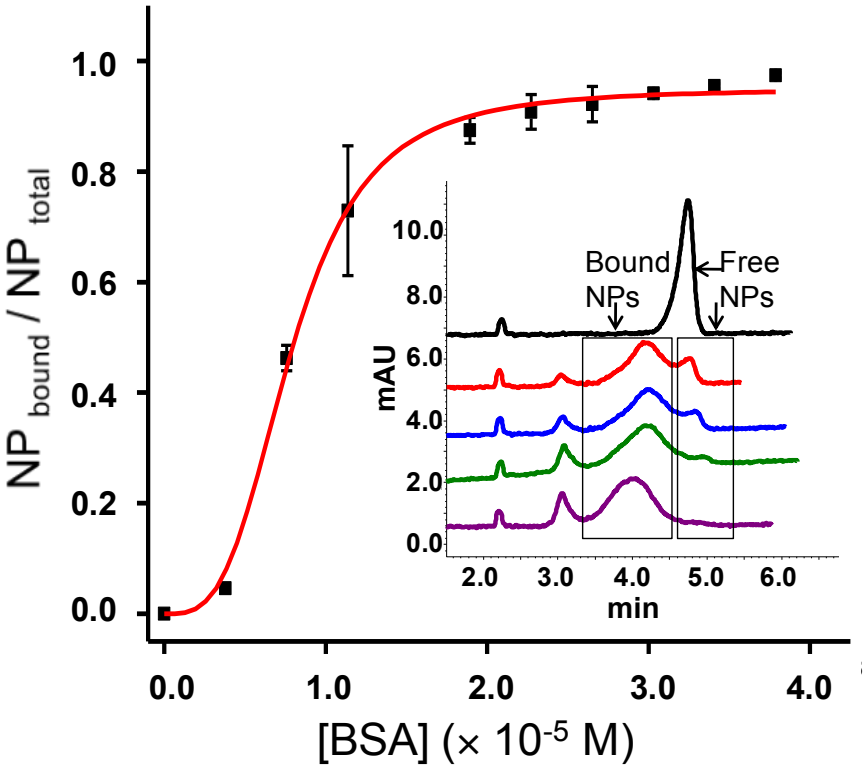
hypothesis. After mixing the 8-nm PAA-Fe_3O_4 NP with excess BSA in 10 mM borate buffer, a slight increment in the hydrodynamic size (from 47.5 nm to 49.1 nm) and a small decrease in ζ potential (from -26.55 mV to -23.14 mV) were observed. This comparison demonstrates another advantage of using CE to study NP-protein interaction, in that the μ of NPs can be used to calculate the ζ potential of NPs before and after interaction with proteins. Since the hydrodynamic size of NP is larger than 10 nm, it is appropriate to assume the NP diameter is much larger than the electrical double layer thickness (κ^{-1}) and apply the simplified Smoluchowski model in the calculation: [161]

$$\zeta = \mu\eta/\varepsilon$$

in which ε is the dielectric constant and η is the solution viscosity. The ζ potentials obtained from CE and the simplified Smoluchowshki model were 10-15% higher than those measured from Zetapals owing to the simplified calculation, but CE consumed much smaller volumes of samples.

The BSA-bound NP peak increased with the BSA concentration in the incubation, while the NP peak area decreased gradually. The peak area of the protein-bound NP should be dominantly from UV absorption of NPs. Therefore, we compared the electropherograms at different wavelengths. The electropherogram at 200 nm showed the largest signals for both the protein and the NPs (Figure S 6.2), suitable for monitoring of the separation process. The one obtained at 288 nm resulted in small signals from the protein at all concentrations used in our investigation and reasonable signals from the NPs, being selected for the calculation of θ. Moreover, our model employed high molar ratio of.

Figure 6.2 Representative electropherograms at 288 nm for an interaction study between BSA and 8 nm PAA-Fe_3O_4 NPs (1.94×10^{-7} M) by CZE and a model fitting curve (in triplicate). From top to bottom, traces were free 8 nm PAA-Fe_3O_4 NPs and mixtures of BSA and PAA-Fe_3O_4 NPs at molar ratios of 58.3:1, 97.2:1, 155.6:1, and 194.5:1. The peaks at around 2.2 min were from DMSO, and the peaks at around 3.0 min were for BSA.



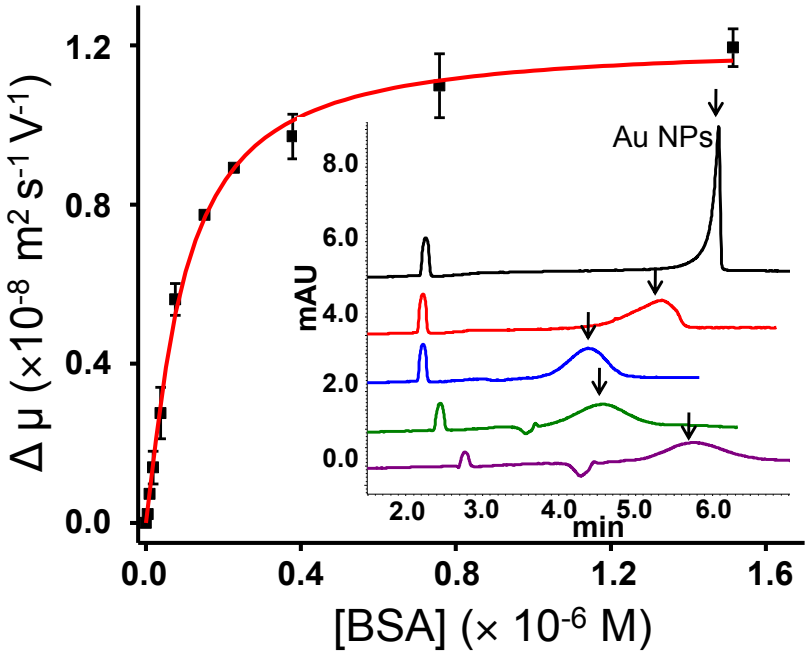
protein to NPs to validly approximate the equilibrium protein concentration using the initial concentration. The plot of θ (NP_{bound}/ NP_{total}) vs. BSA concentration fit to the Hill equation very well (Figure 6.2). By aligning the electropherograms (inserts in Figure 6.2), we observed a small shift of the NP-BSA complex peak to the left with increasing protein

concentration, which illustrated that the number of BSA molecules per NP increased with protein concentration until no more protein could be accommodated due to space hindrance. The representative electropherograms for the 10nm PAA-Fe_3O_4 NPs can be found in Figure S 6.3.

6.3.3 Fast dissociation system

Interaction between the Au NPs (5nm and 10nm) and BSA rendered only mobility shift but no separation of the complex and free NP peaks. The interaction was then investigated using ACE by adding BSA to the running buffer. Since no separation is involved, we employed the phosphate buffer (17.5 mM, pH 7.5) which was more resembling to the physiological conditions than the borate system. No additional NaCl was added to minimize band broadening from joule heating. Representative electropherograms and the curve fitting results for interaction of BSA with the 10-nm Au NP are shown in Figure 6.3, and those with the 5-nm Au NPs are displayed in Figure S 6.4. Again, association with BSA decreased the mobility of NPs and shortened their migration times inside the capillary, indicating the size of NP was enlarged. The change in mobility shift became smaller and smaller until no longer observable at high BSA concentrations. Along with higher protein contents, several phenomena were observed. First is the decrease in EOF due to the adsorption of BSA onto the capillary wall, judged from the migration time of the neutral marker DMSO. Secondly, the reduced EOF also contributed to a broader Au NP peak at higher protein concentrations. Thirdly, a negative peak before the Au NP peak appeared from the depletion of protein in the sample zone.

Figure 6.3 Representative electropherograms at 235 nm for an interaction study between BSA and 10 nm Au NPs (5.66×10^{-9} M) by ACE and a model fitting curve (in triplicate). From top to bottom, traces were an interaction study for BSA and 10 nm Au NPs at molar ratios of 0:1, 6.7:1, 26.8:1, 133.9:1, and 267.7:1.



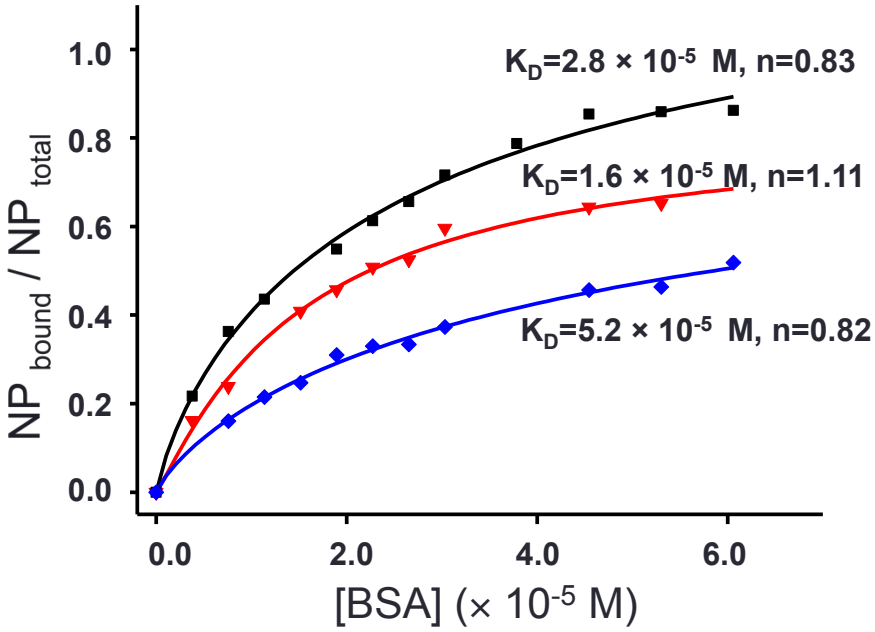
Though, all these changes did not affect the mobility measurement as long as the current and baseline remained stable. High measurement reproducibility (relative standard deviations of mobility shifts were smaller than 10%) and correlation constants close to 0.99 in curve fitting were still obtained.

6.3.4 Impact on affinity from incubation conditions

Because we employed different incubation buffers, i.e. water vs. phosphate buffer, in the above development of the slow and fast dissociation systems in CE measurement, we continued to explore how much difference in affinity would be caused by the buffers. It is very convenient to switch incubation buffers in the slow dissociation system because electrolyte variation within the small sample plug injected in CZE would not affect the separation. pH and ionic strength of the interaction buffer would affect the double layer thickness and the ζ-potential of both the protein and NPs, and therefore could alter the interaction. The 8-nm PAA-Fe_3O_4 NPs were pre-incubated in 17.5 mM phosphate buffer (pH 7.5), 10 mM sodium borate buffer (pH 8.3), or 1×PBS buffer, in which both proteins and NPs carried negative charges. The results were shown in Figure 6.4. Presence of 17.5 mM phosphate buffer in the incubation solution decreased the binding affinity by 3 fold in comparison with water (values reported in Table 4.1). Interaction occurred in 1× PBS showed almost the same Hill coefficient as and a 2-fold weaker affinity than that in 17.5mM phosphate buffer. The slight decrease in affinity in 1×PBS could be attributed to the more salt ions attached to the protein as well as to the NPs, which shielded the NPs from BSA better. Additionally, the physiological condition of PBS can well reserve the structure of BSA and impede with its unfolding on NP surface. Both effect reduced the non-specific binding between BSA and NPs. Still, the differences in the binding values by using 17.5mM phosphate buffer and 1× PBS were small. This result illustrated that the interaction values obtained in the fast-dissociation/ACE model with 17.5mM phosphate

as the running buffer could be used to approximate the binding situations under physiological conditions.

Figure 6.4 The salt and pH effects from pre-incubation buffer for interaction between BSA and 8-nm PAA-Fe_3O_4 NPs. ■: in 17.5 mM phosphate buffer ;▼: in 10 mM borate buffer ;◆: in 1× PBS buffer.



Affinity variations observed in different buffers should be considered in interaction study. If possible, similar buffer conditions, like the type of buffer components, pH, and salt level, should be maintained. The phosphate buffer and the PBS exhibited around 1.8 fold change in the affinities, with identical n values. Thus, affinities measured in the

phosphate buffer without NaCl added could be used to approximate the situation in PBS, simplifying the CE study.

6.3.5 Understanding the interaction from K_D and n

In this study, we used BSA and four types of NPs to demonstrate the effectiveness of CE in quantitatively measuring the affinity and cooperativity of NP-protein interaction. K_D and n values obtained from fitting the data to the Hill equation were listed in Table 6.1. Besides affinity, which reflects the strength of binding, the multivalent nature of NP-protein interaction determines that competition or cooperation among the same protein molecules for the binding sites on NP surface would occur, which would be accurately described by n, the cooperativity. Size and surface functionalization are probably the most important physicochemical NP properties that are related to the affinity and cooperativity, because they define the surface curvature, the formation of electrical double layer, and the geometrical accommodation of proteins.

Table 6.1. Model fitting parameters for interaction between BSA and PAA-Fe_3O_4 NP, Au NP (In triplicate)

NPs interacted with BSA	K_D (M)	n	R^2
8 nm PAA-Fe_3O_4 NP	$7.9 \times 10^{-6} \pm 2.1 \times 10^{-7}$	3.3 ± 0.3	0.988
10 nm PAA-Fe_3O_4 NP	$1.9 \times 10^{-7} \pm 7.3 \times 10^{-9}$	2.4 ± 0.3	0.996
5 nm Au NP	$2.3 \times 10^{-7} \pm 1.9 \times 10^{-8}$	2.3 ± 0.4	0.979
10 nm Au NP	$9.5 \times 10^{-8} \pm 6.8 \times 10^{-9}$	1.2± 0.1	0.997

Our results pointed out that relatively strong interactions existed between BSA and the investigated NPs, all K_D values in the range between 10 – 0.01 μM (including those shown in Figure 6.4). The affinity increased with the size of NPs: the 8-nm Fe_3O_4 NPs yielded a K_D value 40 times larger than the 10-nm ones; and the 5-nm Au had a 2-fold higher K_D than the 10-nm Au NPs. The affinity scale and its dependence on the size of NPs matched with values reported on Au NPs in the literature which were measured with spectroscopic methods, [156, 162] but no systematic study of BSA with the Fe_3O_4 NPs was found. The reduction in affinity for the smaller NPs might be related to the higher space hindrance to accommodate the relatively large BSA molecule around the NPs (in neutral solutions, the crystal structure of BSA was found to have a heart-shaped structure with dimensions of 8.4 nm × 8.4 nm × 8.4 nm × 3.15 nm).[163] The sharper curvature of the smaller NPs may also impede the refolding of BSA molecule on surface.

Within the scope of our study, Au NPs displayed averagely higher affinity to BSA than the Fe_3O_4 NPs. The difference in surface coating may be one of the driven forces for the relative strength in affinity. The electrostatic repulsion from negatively charged BSA and NPs did not prevent the relatively strong interaction between them. The high structure flexibility of BSA probably allowed easy refolding of the BSA molecule to adapt to the surface. A conformational change in BSA upon its adsorption onto the 2D surface or NPs has been well documented.[156, 164-168] The Au NPs were coated with citrate, and the Fe_3O_4 NPs were stabilized by PAA. The longer chain of PAA than the citrate groups on Au surface would extend the thickness of the diffuse layer and prevent the BSA molecules to

get closer to the Fe_3O_4 NPs surface. Indeed, hydration size measurement indicated that the 5- and 10-nm Au NPs had hydrodynamic sizes of 22.6 nm and 37.7 nm, respectively, both smaller than the 47.5-nm hydrated Fe_3O_4 NPs. Furthermore, the polymer layer provided adequate shielding of the iron oxide core[169] that may have prevented the coordination between the metal oxide core and the functional groups on BSA. A difference in surface coating may also exist within the Fe_3O_4 NPs, even though they were both coated with PAA. The PAA difference was studied in Chapter 7. The Au NPs were produced by a modified tannic acid/citrate method[170] with different amounts of reducing tannic acid added to the reaction. However, the synthesis procedures for the 8- and 10-nm iron oxide NPs were significantly different after the seeds had formed. The 12-hr pyrolysis duration may load a considerably higher amount of PAA on the surface of the 8-nm NPs, contributing to the 40-fold affinity reduction.[71, 155] The exact contribution from the core or surface coating needs to be further explored with the preparation of a series of NPs with only one physicochemical property being changed at a time. The could-be-tedious, systematic comparison of a large numbers of different NPs is simplified with the straightforward but effective CE platform, and will reveal more information about the driving forces for the interaction.

The dependence of interaction cooperativeness, i.e. the n value, on the physicochemical properties of NPs is also evaluated.[171] Interaction between BSA and the Au NPs were cooperative, with $n > 1$. This result is contradictory to that reported previously when the Au NPs and proteins were viewed as ligands and receptors,[156] respectively, opposite to

our model. We believe our model could reflect the real situation better by accommodating proteins on NP surface. The cooperativity indicates that the surface functional groups of NP may be reorganized upon the binding of the first BSA molecule to expose more sites for interaction with the subsequent BSA molecules. In addition, for NPs with the same core material, e.g. Au NPs, the larger NPs showed weaker cooperativity (smaller n). Same trend was observed in the previous study using fluorescence quenching spectroscopy.[156] The larger surface area available for binding may lead to only local reorganization of the surface groups and thus less impact on the subsequent binding. Decrease in steric hindrance between BSA molecules packed on the surface could be another important contributor to the reduced cooperativity as well

.

Interactions of BSA with the iron oxide NPs taking place in water (Table 6.1) showed positive cooperativity, i.e. $n > 1$, while those in buffers (Figure 6.4) were non-cooperative. This again could be related to the more rigid structure of BSA in the buffered solutions than in water, which reduced the influence from peer BSA molecules co-adsorbed onto the same NP. The non-cooperativity of the 8-nm iron oxide NPs measured in phosphate buffer is significantly different than the situation for Au NPs in the same buffer. The larger hydration size and thicker polymer layers, i.e. more flexible structure and less stringency on reorganization, on the iron oxide particles could both contribute to such a big variation. The cooperativity also deceased with the size of the Fe_3O_4 NPs.

6.4 Conclusions

We demonstrated here that CE can be employed for quantitative study of the interaction between protein and NPs. Interaction systems with slow dissociation rates relative to CE speed can be analyzed by CZE where bound and free NP can be separated and quantified. Systems with fast dissociation rates can be analyzed by ACE where mobility shift of NP is monitored. The interaction endures no disturbance in the open separation channel of CE. The fast separation speed significantly improves the study efficiency. The separation-based platform will permit study of the more complicated systems which involve multiple interactive components.

Diverse CE running modes make it possible to investigate various protein and NP combinations. CZE is more suitable for the study of binding under physiological condition because high salt concentrations can be employed in the incubation buffer, which is not applicable in ACE due to the peak dispersion with increased running current. Therefore, ultra-fast CE, such as microsecond CE[172, 173], can be developed to separate the transient NP-protein complex from the free NPs. For proteins with high pI values and nanoparticles carrying positive charges, coated capillary will be considered to minimize the adsorption of proteins and NPs on the capillary wall. Fluorescence detector would be useful for the study involving fluorescent NP like quantum dots or proteins labelled fluorescently. Lower protein and NP concentrations are then needed to avoid side effects accompanied with high protein concentrations in the running buffer in ACE, such as EOF alteration, peak distortion, and low peak intensity. Adsorption of multiple protein layers

on NPs and the possible disturbance to the NP-protein complex by the strong electric field of CE should be paid attention as well in future studies.

Supporting Information

Figure S 6.1. TEM images for PAA-Fe_3O_4 NPs (A: 8-nm, B: 10-nm) and Au NPs (C: 5-nm, D: 10-nm) with 50nm.

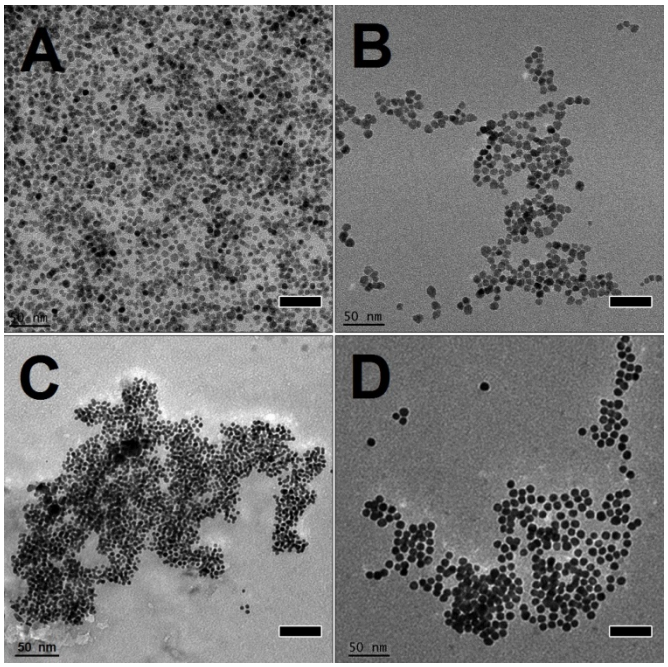


Figure S 6.2. Electropherogram at 200 nm for pre-incubated mixture of BSA and 8-nm PAA-Fe_3O_4 (molar ratio 58.3:1).

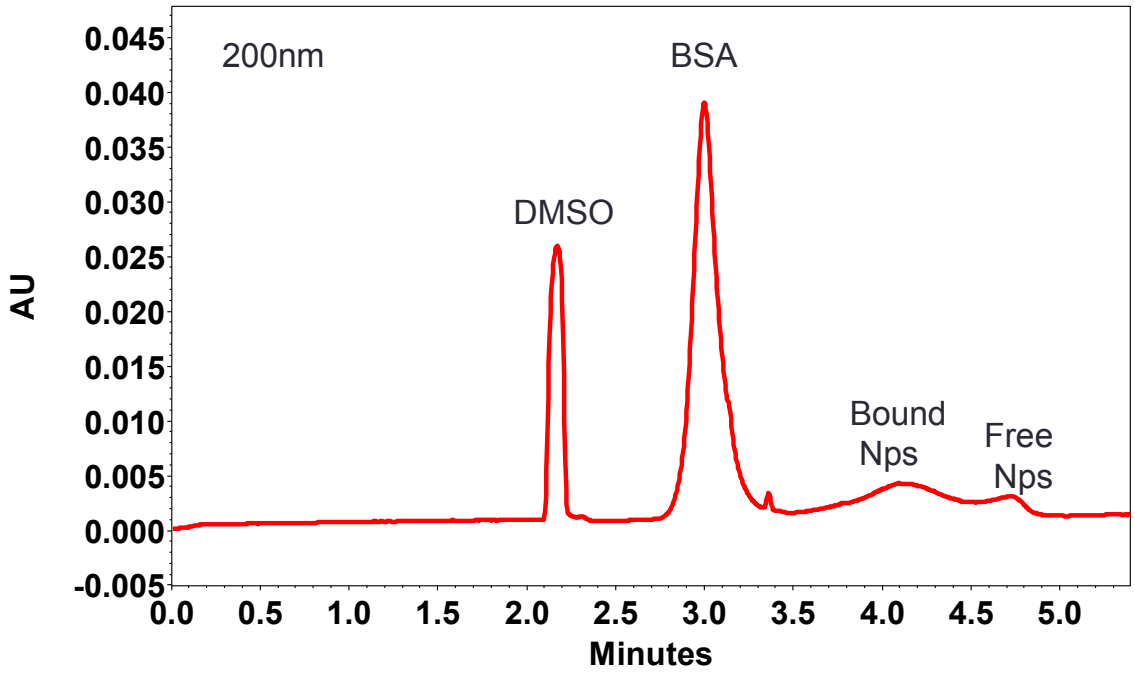


Figure S 6.3. Representative electropherograms at 288 nm for interaction study between BSA and 10-nm PAA-Fe_3O_4 NPs (1.08×10^{-7} M) at different molar ratio (from top to bottom: 0:1, 2.8:1, 4.2:1, 5.6:1 and 17.5:1) by CZE.

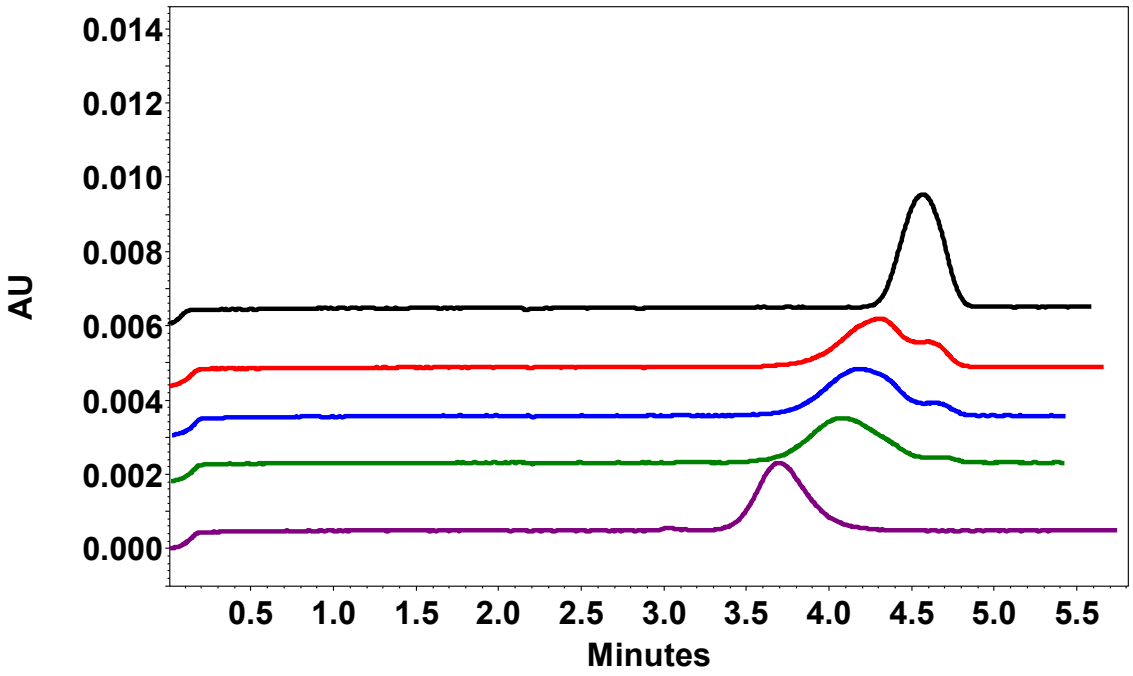
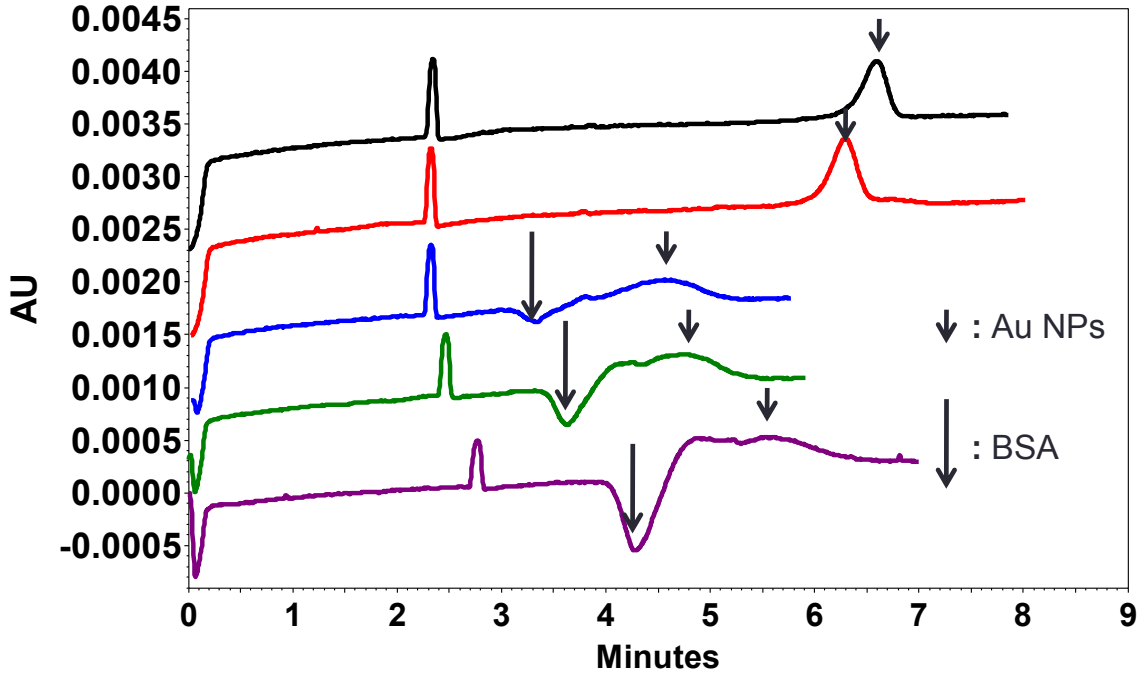


Figure S 6.4. Representative electropherogram at 235 nm for interaction study between BSA and 5-nm Au NPs (1.91×10^{-8} M) at different molar ratios (from top to bottom: 0:1, 2.0:1, 15.9:1, 39.7:1, 79.3:1) by ACE.



Chapter 7

Mechanism study on nanoparticle-protein interaction by capillary electrophoresis and mass spectrometry

7.1 Introduction

The increasing human exposure to the engineered nanomaterials either as biomedical substances[174, 175] or environmental pollutants[176, 177] demands better understanding of the nano-bio interface. The knowledge can help to ensure safe implementation of nanomaterials[178, 179] and increase efficacy of nano-medicine.[174, 180, 181] Since protein adsorption is believed to be the primary event when nanoparticles (NPs) encounter a biological environment,[182, 183] the cell probably "sees" and reacts to the stable protein corona instead of the original inorganic surface.[30, 184] Indeed, binding to proteins could affect the behaviors of NPs in cells, such as cytotoxicity and cellular uptake[144, 185-187] Therefore, NPs-protein interaction is the front line of the nano-bio interface, and needs to be studied for rendering better control of the protein adsorption on nanomaterials for different application purposes.[188]

Nanoparticles with quite different sizes, shapes, and surface coatings have been compared for their behaviors in cells or organisms[187, 189, 190] and in interaction with proteins.[185 143, 191, 192] Still, no general consensus has been reached.[193-195] The

discrepancies were blamed on variations in material preparation,[196] purity,[197] distribution in the biological matrices,[198] and surface coating.[199] Such phenomena hint that even subtle alteration in the physicochemical properties of NPs could affect the NPs-protein binding and subsequently their performance in the biosystems.[186, 192] What exactly the nanoparticle surface ligands are and how they behave at the nano-bio interface are two of the major topics of interest on the nanoparticle side.

An in-depth knowledge of the binding sites on the protein is also desired. Few attempts have explored the binding interface of nanoparticles and proteins at the amino acid level, employing techniques that are powerful in the determination of protein folding and protein-ligand interaction in solution, like hydrogen/deuterium (H/D) exchange-mass spectrometry[137] and nuclear magnetic resonance (NMR).[200] NMR demands high material concentration and is limited to proteins smaller than 50-60 kDa, which restricts its applications in the study of nanoparticle-protein interaction: nanoparticles tend to aggregate at high concentrations and proteins of biomaterial and medical interest are often large, such as human serum albumin and immunoglobulin. H/D exchange mass spectrometry (HXMS) coupled with proteolytic digestion is a more sensitive approach with a relatively lower resolution than NMR. However, rapid and efficient proteolysis at low pH and low temperature is essential for the success of HXMS. Proteases active at pH 2.5 should be used and denaturant for unfolding of protein structure is needed. These requirements may not be met easily with the presence of NPs that might interfere with the proteolytic digestion and extend the digestion duration. Chemical surface labeling, cross-

linking and mass spectrometry has been applied on probing surface topology,[201-203] protein function,[204] as well as to determine protein-peptide, protein-protein,[205] protein-cofactor, protein-drug[206] and protein-DNA[207] interaction due to the advantages such as low sample consumption, rapid and variety of chemistry targeting diverse functional groups and good qualification ability ensured by mass spectrometry.[208] All of these make it a facile method to study the binding interface of NPs and proteins. Moreover, data analysis is simplified when one of the cross-linking parties is NP that has lower possibility of self-cross-linking and can be removed easily by centrifugation or filtration. Besides, covalent attachment of proteins to NPs is one dominant approach to obtain stable NP-protein construct.

In this chapter, we first demonstrated that chemical changes in the surface ligand molecules could indeed bring in big difference in NP-protein binding. Detailed study of the surface molecule structure and the corresponding affinity with proteins led us to more insights about the importance of desolvation in strengthening the binding between the negatively charged NPs and proteins. Next, cross-linking followed by mass spectrometry has been for the first time explored to reveal the nature of molecular interface within nanoparticle-protein complex by examining the amino acid residues involved in particular cross-linking reactions. Drug binding site 2 on human serum albumin was found to bind to 8.2-nm PAA Fe_3O_4 NPs. Drug binding tests further confirmed our findings.

7.2 Experimental

7.2.1 Synthesis of PAA-Fe_3O_4 NPs

The reagents for synthesis are from Sigma-Aldrich Corporation (St. Louis, MO, USA). A NaOH/DEG stock solution was prepared by dissolving 50 mmol of NaOH in 20 mL of DEG. In a typical synthesis, a mixture of PAA (4 mmol), $FeCl_3$ (2 mmol), and DEG (15 mL) was heated up to 220 °C in a nitrogen atmosphere with stirring. A NaOH / DEG stock solution (4.5 mL) was then injected rapidly into the above hot mixture. The subsequent steps were different for the synthesis of PAA-Fe_3O_4 NPs with average diameters of 7.5- and 8.2-nm. The resulting mixture was further heated for 10 min to yield magnetite nanocrystals with an average size of ~7.5nm. In contrast, the 8.2-nm NPs were obtained by continuously heating the mixture for 12 h at 220 °C. An excess amount of PAA and other reagents in the reaction mixture were removed by centrifugation-assisted washing several times with a mixture of deionized water and ethanol. Finally, the PAA-Fe_3O_4 NPs were suspended in 10 mL of water to form the stock solutions.

7.2.2 Capillary Electrophoresis

The capillary electrophoresis separation for K_D measurement was reported in our previous work.[209] Briefly, a 50 cm fused-silica capillary (75 μm i.d., 365 μm o.d.; PolymicroTechnologies, Phoenix, AZ, USA) with an effective length of 40 cm was sequentially rinsed at 30 psi with 0.1 M NaOH (2 min), deionized water (1 min), and the running buffer (6 min) prior to injection. All CE separations were done at 25 kV in room temperature. Capillary zone electrophoresis was performed using 10 mM borate buffer at

pH 8.3 as separating buffer. Samples analyzed by CZE were pre-incubated in17.5 mM phosphate buffer (pH 7.5). In affinity capillary electrophoresis experiments, 17.5 mM phosphate buffer (pH 7.5) was adopted to dilute proteins and nanoparticles. Therefore, all the K_D data presented in Table 7.1 were measured in 17.5 mM phosphate buffer (pH 7.5). For drug binding tests, CE separation was done in 10mM borate buffer (pH 8.3).

7.2.3 MALDI-TOF MS for PAA characterization

MALDI-TOF MS experiment was carried out on a Voyager-DE STR MALDI-TOF mass spectrometer (Applied Biosystems, Framingham, MA, USA) operating in negative reflective mode. The spectrometer is equipped with a pulsed nitrogen laser operated at 337 nm with 3 ns duration pulses. MS spectra were acquired as an average of 100 laser shots. Mass resolution is greater than 10,000. Sample spotting procedure was slightly modified from the published work.[210] In brief, 1 μL of 125mM trans-3-indoleacrylic acid (IAA, 98%, Acros Organics) in THF, 1μL of PAA aqueous solution (standard PAA in water, or PAA solutions obtained by all the mentioned treatment in results and discussion part), and 1 μL of THF were sequentially spotted on MALDI plate. Between each depot, enough time was allowed for solvent evaporation. Sample preparation for MALDI-TOF MS analysis is summarized as follows. For nanoparticles, ~10 μL stock solutions were mixed with 20 μL TFA (99.5%, biochemistry grade, Acros Organics), sonicated at room temperature for 1h and then the mixtures were set on the bench for ~3 days until all nanoparticles dissolved. The samples were diluted with 90 μL deionized water and then dialyzed against deionized water for 24 h using Tube-O-dialyzer (Micro, 1k MWCO,

Gbiosciences, MO, USA). The resulting solutions were ready for MALDI-TOF MS analysis. For pseudo reactions without adding $FeCl_3$, after one week, ~10 µl of bottom solutions were taken out and then treated in the same way as the nanoparticles.

7.2.4 Cross-linking and MALDI-TOF MS for binding site identification

Human serum albumin was incubated with NPs at a molar ratio of 1:1.2 in de-ionized water at room temperature overnight to ensure large percent of HSA could bind to NPs. Then EDC/2-(N-morpholino)ethanesulfonic acid (MES) buffer (50 mM, pH=6.2) or SDAD/phosphate buffer (17.5 mM, pH=7.5) was added to cross-link the adsorbed protein onto NPs. EDC reacted with the protein and NPs for 4 hours at room temperature, and then the extra EDC and buffer salts were removed by a 30 kDa centrifugal filter. The reaction with SDAD took two steps: a 0.5-h incubation at room temperature attached SDAD to the primary amine on HSA and the excess SDAD was removed by filter; the photochemistry toward the carbon atom on PAA chain was triggered by 360-nm UV light for 15 min to couple the protein to the NPs via SDAD. Finally, the cross-linking product was cleaned by the 30 k Da filter, and trypsin was introduced into the recovered protein-NPs mixture in the present of NH_4HCO_3 buffer (50 mM, pH=8.0) to digest the cross-linked protein at 37 ℃ overnight. After digestion, another centrifugation separated the supernatant containing free peptides from NPs. The supernatant was then dried, cleaned by the C18 ziptip, and analyzed by MALDI-TOF-MS. Positive, reflective mode was used. The saturated CHCA matrix solution was prepared in ACN: 0.1% TFA (50:50, v/v).

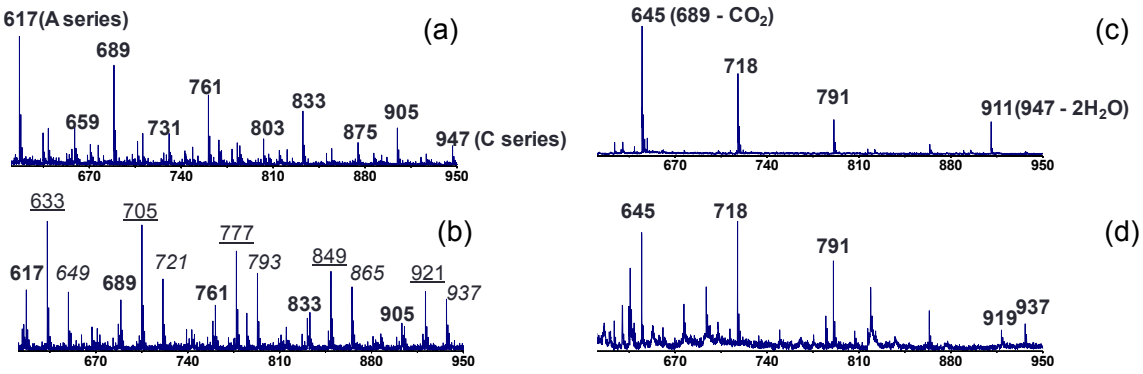
7.3 Results and discussions

7.3.1 PAA pyrolysis identified by MS and affinity differences

A brief, 10-min heating step obtained the NPs with an average size of 7.5-nm; while a long, 12-hr heating period yielded a slightly larger diameter of 8.2 nm (Figure S 7.1a). Besides the comparable average diameter, these NPs also shared similar size distribution profiles (Figure S 7.1b) and zeta potentials (Figure S 7.2). However, further analysis of the surface ligand molecules revealed significant alteration in PAA structure after the elongated heating. We detached the PAA molecules from NPs by dissolving the Fe_3O_4 core with trifluoroacetic acid (TFA), and analyzed them by matrix-assisted laser-desorption ionization time-of-flight mass spectrometry (MALDI-TOF-MS) after removing the ions and excess acid by extensive dialysis process. The mass spectrum of PAA recovered from the 8.2-nm NPs was shown in Figure 7.1, along with those from standard PAA and PAA gone through the same heating procedures as in NP synthesis but without addition of $FeCl_3$. Negative controls can be found in Supporting Information Figure S 7.3. Within the m/z range from 600 to 950, in which we observed clear MS signal in all of our samples, PAA collected from NPs exhibited only a few discernable peaks (Figure 7.1d). On the contrary, the intact PAA sample contained three series of peaks with Δm/z equal to 72, the exact mass of the acrylic acid monomer (Figure 7.1a). Based on previous reports, these series are acrylic acid homopolymer with different head groups, each named as A, B, or C (Structures shown in Figure S 7.4).[39-40] These series polymer peaks were still present after PAA being heated at 220 ºC for 10 minutes (the same heating durations as making the 7.5-nm NPs), while peaks of the A series with +16

or +32 were also observed, indicating the addition of 1 or 2 oxygen atoms to the polymer chains during the heating (Figure 7.1b). Much fewer peaks were identified in the PAA sample heated for 12 hrs (Figure 7.1c), and these peaks matched with those found in the PAA sample collected from the 8.2-nm NPs. By comparing the mass difference between

Figure 7.1 Mass spectra of (a) standard PAA (1 mg/mL in water); PAA underwent (b) 10-min (**Bold**: A series; Underline : A series + O; *Italic*: A series + 2O), or (c) 12-hrs heating with no $FeCl_3$ addition, and (d) PAA recovered from 8.2-nm nanoparticle treated with TFA and dialysis.

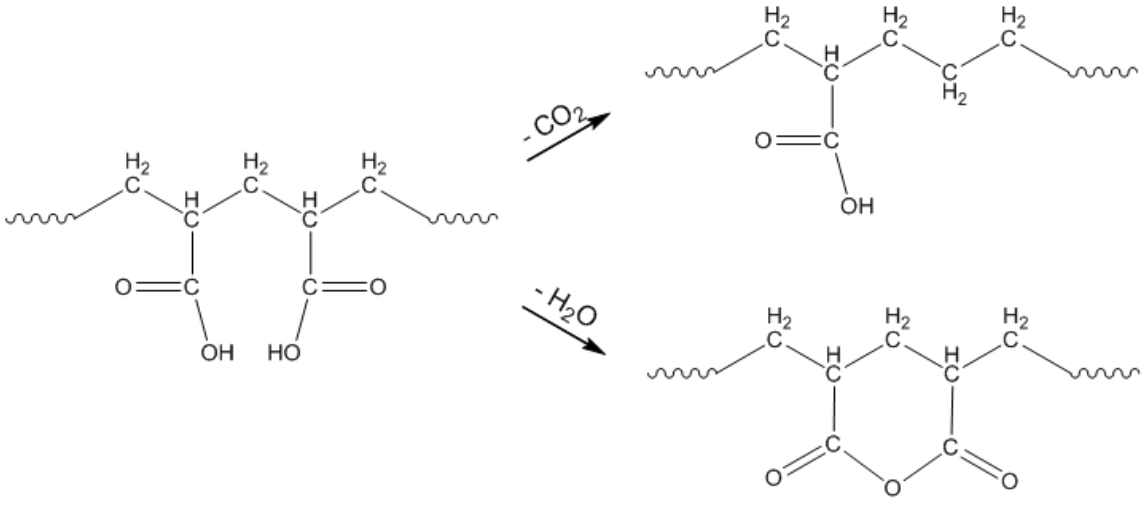


the original PAA series and the peaks in the heated PAA samples, we concluded that the m/z 645 peak could be the decarboxylation product of m/z 689 and m/z 911 be the dehydration product of the C series m/z 947. For still unknown reasons, following m/z 645 and 911, two peaks groups, m/z (718, 791) and m/z (984, 1057), respectively (Figure

7.1c and Supporting Information Figures S 7.5), were seen with a m/z increase of 73 instead of 72.

Water and carbon dioxide have already been found to be the major and only volatile pyrolysis products of PAA in 160 – 240 °C.[36] The intramolecular loss of CO_2 and H_2O, and the hypothesized H addition to the C=O resulted in fewer COOH groups in the PAA () molecules that coated the 8.2-nm Fe_3O_4 NPs. We were not able to obtain clear MS signals from the PAA eluted off the 7.5- and 10-nm NPs, probably owing to the stronger repulsion among $–COO^-$ of the intact PAA chains at basic pH that led to a lower density of PAA on NPs.[211] The 8.2-nm NPs had more modified PAA molecules with fewer carboxyl groups, so still a similar zeta potential as the 7.5-nm NPs.

Figure 7.2 Pyrolysis reactions of PAA



Interestingly, such structure difference in PAA could significantly change the protein binding affinity of the PAA-coated NPs. We measured the binding affinity of the 7.5- and 8.2-nm NPs with three acidic proteins using a capillary electrophoresis (CE)-based method that was previously established in our group.[209] The results are listed in Table 7.1. CE directly studies binding between the freely suspended proteins and NPs with negligible perturbation to the complex, and does not rely on any interaction-induced alteration in spectral properties.[138] The microscopic dissociation constant, K_D, and the binding cooperativeness, n, were obtained using the Hill equation:[212]

$$\theta = [\text{protein}]^n/(K_D^n + [\text{protein}]^n)$$

in which θ is the protein-bound NP fraction. A larger-than-1 n represents positive cooperative binding, i.e. adsorption of the 1st protein molecule facilitates subsequent protein binding; and an n smaller than 1 indicates negative cooperative interaction. The exchange kinetics was judged by the behavior of the protein-NP complex in CE. Complexes with slow exchange kinetics show clear separation of the protein-bound and free NPs peaks, and the protein-bound NP fraction, θ, is calculated from the peak area ratio. On the other hand, no separation of the protein-bound and free NPs could be obtained for complexes with fast on-and-off rates, and the change of the NP electrophoretic mobility under different protein concentration is measured to obtain θ. Even though the NPs had similar sizes and zeta potentials, their affinities to the same protein were different by up to 20 times (Table 7.1). The three chosen proteins have been known to be adsorbed easily on solid surface due to their high structure flexibility, and

Table 7.1 Summary on protein interaction of the PAA-Fe_3O_4 nanoparticles investigated.

Protein	**NPs Diameter**	**K_D (M)**	**n**	**Exchange Kinetics**
BSA	7.5 nm	2.60×10^{-6}	1.0	Fast
66 kDa, pI 4.8	8.2 nm	1.37×10^{-5}	1.1	Slow
β-casein	7.5 nm	2.31×10^{-7}	2.7	Fast
24 kDa, pI 4.6	8.2 nm	4.60×10^{-6}	1.3	Slow
Calmodulin	7.5 nm	2.84×10^{-7}	0.4	Fast
17 kDa, pI 3.9	8.2 nm	1.51×10^{-8}	2.1	Fast

they all carry negative charges under neutral pH.[166, 213] The 7.5-nm Fe_3O_4 NPs bound stronger to bovine serum albumin (BSA) and β-casein than the 8.2-nm NPs, which showed higher affinity to calmodulin. Moreover, the 7.5-nm NPs bound to proteins with fast exchange kinetics, but the kinetics of the 8.2-nm NPs was slow except with calmodulin.

7.3.2 Driving force of desolvation

We believe that the decarboxylation and dehydration of PAA had caused the distinct protein binding behaviors of the 8.2-nm NPs in comparison to the 7.5-nm ones, which were coated by more intact PAA molecules. PAA and its salts have been well known to

be super-absorbents.[214] The consecutive carboxyl groups of PAA could trap a high number of water molecules and counter ions.[215-217] When the NPs interact with proteins, the trapped molecules would be released from the interface, which dramatically increase the system entropy (Figure 7.3). Such a large increase in entropy could overcome the electrostatic repulsion between the negatively charged NPs and proteins, and facilitate the interaction.[218] Indeed, the van't Hoff plot (Figure 7.4) showed the positive entropy and enthalpy changes for the adsorption of BSA on the 8.2-nm Fe_3O_4 NPs in 1×PBS. Between 22 and 37 ºC, ΔH was calculated to be + 50.17 kJ and ΔS was + 241.69 J/K. This temperature range was selected for two reasons: one is to minimize the errors brought by changes in specific heat capacity of water (ΔC_p)[219, 220] because by standard chart C_p values at 20, 25, 30, 35, 40 ºC are quite close to each other; the other is to cover our experimental and physiological temperature range. The adsorption process could involve noncovalent bonding and solvent reorganization.[141, 213] Non-covalent bonding is exothermic, and the system losses entropy with the conformational restriction of both proteins and NPs upon complexation.[141, 213] By contrast, solvent reorganization needs extra thermal energy to disrupt the initial well-ordered hydration shells and release the hydration water into the bulk solution, which is an endothermic process with entropy gain.[141, 213] The positive entropy change overcame the electrostatic repulsion between the negatively charged NPs and proteins in our case and drove forward the spontaneous binding process. Fewer carboxyl groups due to the decarboxylation and dehydration of PAA reduced the total number of trapped molecules and thus the 8.2-nm NPs showed lower affinity to BSA and β-casein compared to the 7.5-nm NPs.

Figure 7.3 Schematic illustration on desolvation driving force on nanoparticle-protein interaction

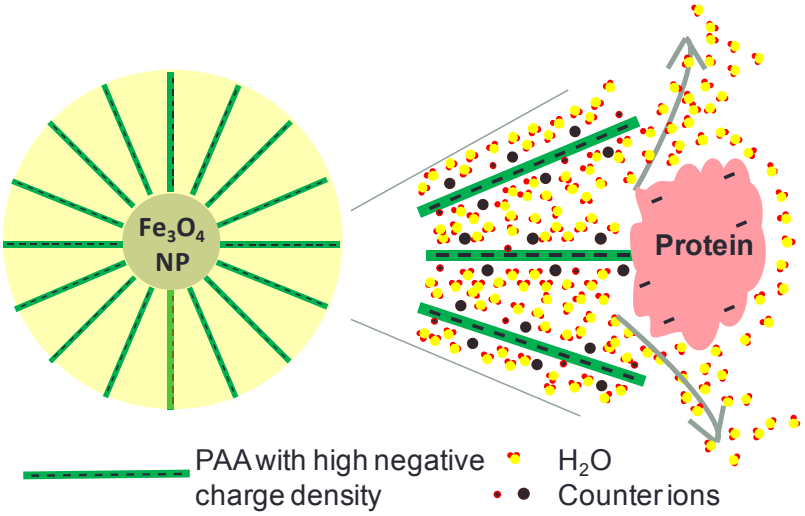
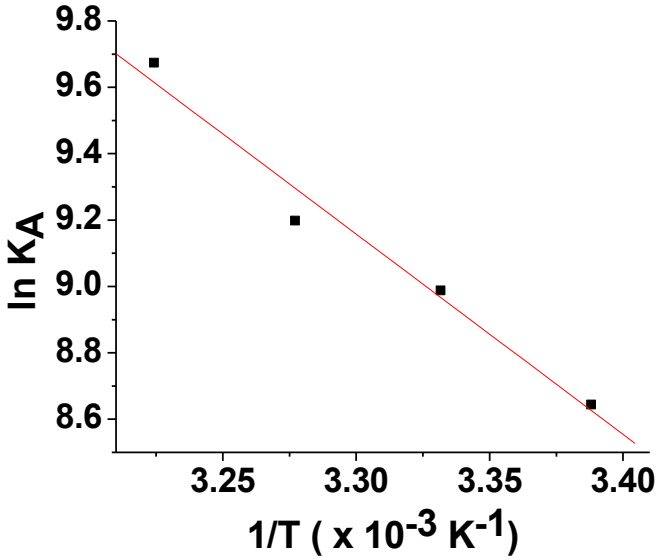


Figure 7.4 The van't Hoff plot for interaction between BSA and 8.2-nm PAA-Fe_3O_4 nanoparticles in 1 × PBS.



On the contrary, the fewer carboxyl groups on the 8.2-nm NPs resulted in stronger interaction with calmodulin, a protein with lower pI than BSA and β-casein, owing to the weaker repulsion between the NPs and the protein. The strong repulsion with the 7.5-nm particles even yielded a negative binding cooperativity (n = 0.4) for the interaction. However, the overall affinity of calmodulin with the negatively charged NPs is strong, hinting that other driving forces must have been involved. For example, we found out that more flexible the protein is, higher binding affinity it has to the NPs (unpublished data), similar to protein adsorption onto flat surface.[213] Calmodulin has the most flexible structure among the proteins selected in our study. It may be able to wrap around the sharp surface curvature of the small NPs to stabilize the interaction.

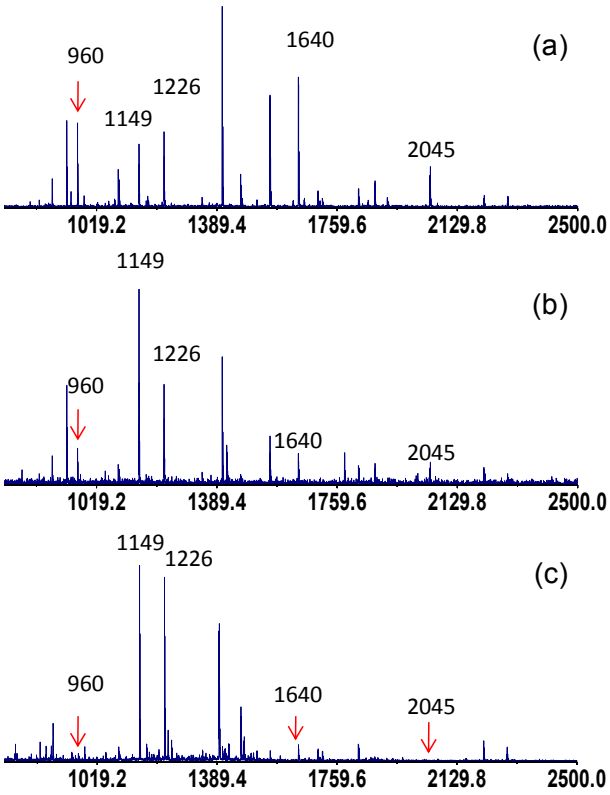
7.3.3 Peptides associated with nanoparticle-protein interaction interface identified by cross-linking and mass spectrometry

Two cross-linkers were adopted in this study. The first one, [1-ethyl-3-(3-dimethylaminopropyl)-carbodiimide hydrochloride], EDC, is a widely used zero-length, amine-reactive cross-linker to facilitate the direct conjugation of carboxyls to primary amines.[221] In our case, EDC could activate the carboxyl groups of PAA on the surface of NPs, which would react with the primary amino residues in HSA and form amide bonds. Since only the primary amino residues within the maximum cross-linking distance of EDC could react with the active EDC-PAA intermediates and be cross-linked onto NPs, those residues should be at the NP-HSA binding interface. The second one, succinimidyl 2-([4,4'-azipentanamido]ethyl)-1,3'-dithioproprionate, SDAD, is a heterobifunctional

cross-linker combining the proven amine-reactive chemistry with the diazirine-based photochemistry for conjugating amine-containing molecules to nearly any other functional group.[222] In our case, the primary amines on HSA were linked to the carbon atom on the PAA polymer chain locating within the cross-linkable distance. The spacer arm of SDAD is 13.5 angstrom.[222] While EDC is effective for NPs with carboxyl groups on the surface and targets the amino acid residues very close to NPs, SDAD can work on NPs with any types of surface groups and link residues within 13.5 Å from the NP surface if no primary amine is available right at the interface. The cross-linking was performed after HSA was adsorbed onto NPs and followed by tryptic digestion of HSA and removal of NPs. The affected residues should be removed by NPs, causing a decrease signal observed in MALDI-MS analysis.

Based on our previous study, the PAA-Fe_3O_4 NPs could form stable complex with HSA after overnight incubation. HSA was incubated with NPs at a molar ratio of 1:1.2 at room temperature overnight. Two types of incubation buffers were tested. One was the deionized water and the other was the 1 × phosphate buffered saline (PBS). The NPs bind to HSA with a higher affinity in water ($K_D = 5.1 \times 10^{-6}$ M) than in PBS ($K_D = 2.4 \times 10^{-5}$ M). A higher portion of protein could be adsorbed by the NPs in water, and thus a higher amount of peptides could be recovered at the end for MALDI-MS analysis to yield higher signals. Figure 7.5 shows the MALDI-MS results for the analysis of HSA adsorbed in absence of cross-linker (Figure 7.5 a) or cross-linked to NPs by EDC (Figure 7.5 b) or SDAD (Figure 7.5c). Control results were displayed in Figure S 7.6, including that for the

Figure 7.5 Mass spectra of HSA and 8.2-nm PAA-Fe_3O_4 NPs pre-incubated in water then treated with (a) no cross-linking, trypsin digestion (b) EDC cross-linking and trypsin digestion (c) SDAD cross-linking, trypsin digestion.



trypsin digestion of HSA, of the cross-linked HSA, and for the trypsin self-digestion. A total of fourteen peptides peaks were identified in Figure 7.5 a. The intensity of m/z 1640 decreased dramatically, after HSA was adsorbed and cross-linked to the NPs by EDC. If SDAD, the cross-linker with a longer spacer, was used, three peptides (m/z 960, 1640, and 2045) were either missing or appeared at much lower intensity. These results indicated that the peptide of m/z 1640 could locate right at the interface and thus be

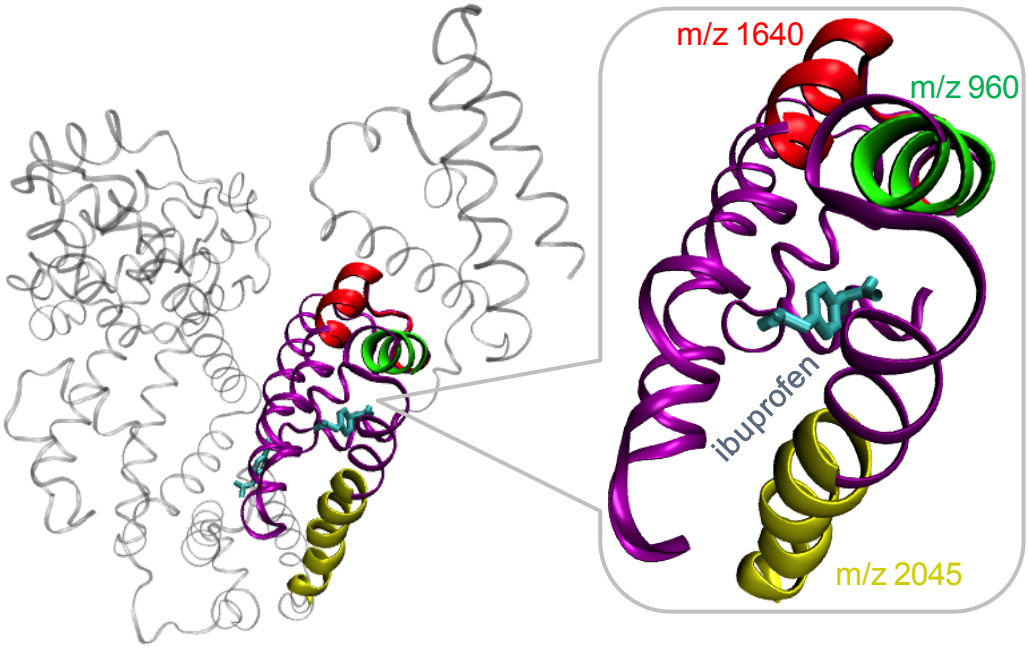
attached to the NP surface by the zero-length cross-linker EDC. The two additional peptides identified with SDAD cross-linking should be further away from the NP surface but still within 13.5 Å distance, the length of the spacer arm of SDAD. MALDI-TOF-MS/MS analysis verified that the sequences of m/z 960, 1640, 2045 featured amino acid sequences as FQNALLVR (403-410), **K**VPQVSTPTLVEVSR (414-428), and VFDEF**K**PLVEEPQNLI**K** (373-389), respectively. They all have a preceding K residue (K402, K413, and K372) which could be cross-linked to NPs and not cleavable by trypsin. We mapped the location of these peptides on the crystal structure of HSA (PDB ID: 1AO6) (Figure S 7.7). They were all surface peptides with m/z 960 in subdomain IIIA-h2, m/z 1640 in subdomain IIIA-h2 and h3, m/z 2046 in subdomain IIB-h4 and IIIA-h1.

7.3.4 Binding site further confirmed by drug binding tests

It is worth to note that subdomian IIIA is a putative binding site, the so-called drug-binding site 2, for drugs with acidic or electronegative features like ibuprofen, naproxen, and diflunisal.[223] Therefore, to verify the identification, we tested the competitive binding to HSA between NPs and ibuprofen or naproxen. Ibuprofen binds to HSA with a binding affinity of 2.8×10^4 M^{-1},[224, 225] and its crystal structure has also been reported (PDB ID: 2BXG) (Figure 7.6). Ibuprofen has a secondary binding site locating outside of site 2 on HSA but with a much lower affinity.[226] The affinity of naproxen to HSA is relatively higher than that of ibuprofen, at $1.2\text{-}1.8\times10^6$ M^{-1}.[227] HSA was first incubated with ibuprofen or naproxen at different drug concentrations for 30 mins. Then a constant

amount of NPs was added to the HSA-drug mixture, and the samples were incubated at room temperature overnight before analyzed by capillary zone electrophoresis (CZE).

Figure 7.6 Identified peptides in HSA-ibuprofen complex 3-D crystal structure.

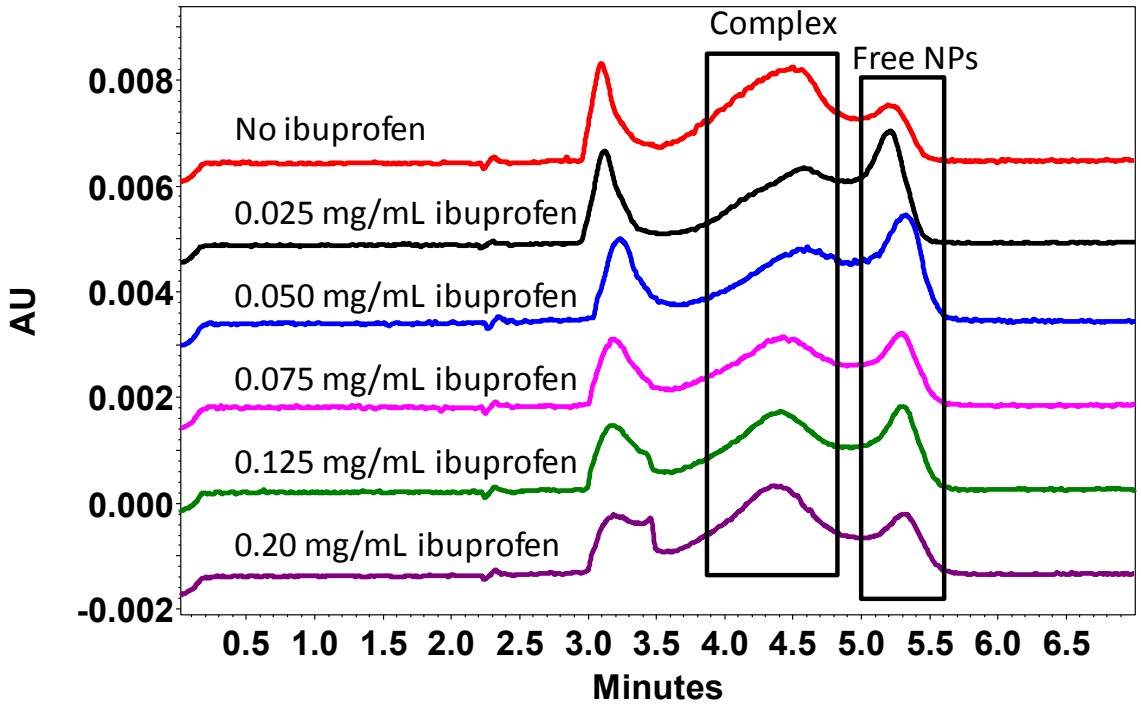


Since the HSA-NPs complexes could be well separated from the free HSA and NPs, the fraction of protein-bound NPs, θ, obtained from the peak area ratio of the protein-bound and free NPs, could be used to judge the HSA-NP interaction strength: a smaller θ represents weaker binding. The selected electropherograms and the plots of the normalized θ vs. drug concentration were shown in Figure 7.7 and Figure S 7.9. Both ibuprofen (Figure 7.7 b) and naproxen (Figure S 7.9 a) caused the maximum of 28% and

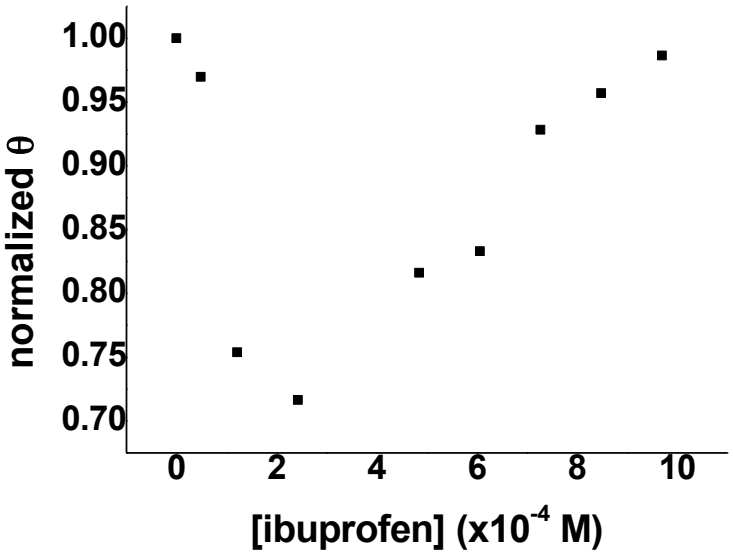
31%, respectively, reduction in θ when the drug concentration was lower than 3×10^{-4} M. Detailed studies on the structure of HSA after the binding of small drugs like ibuprofen have revealed very little conformational change in HSA. Therefore, the inhibition of HSA-NP interaction by these two drugs could not be due to the exposure of new epitopes

Figure 7.7 Effects from pre-incubating HSA and ibuprofen on NP-HSA interaction: (a) representative electropherograms; (b) normalized bound percentage of PAA-Fe_3O_4 NPs when interacting with HSA.

(a)



(b)



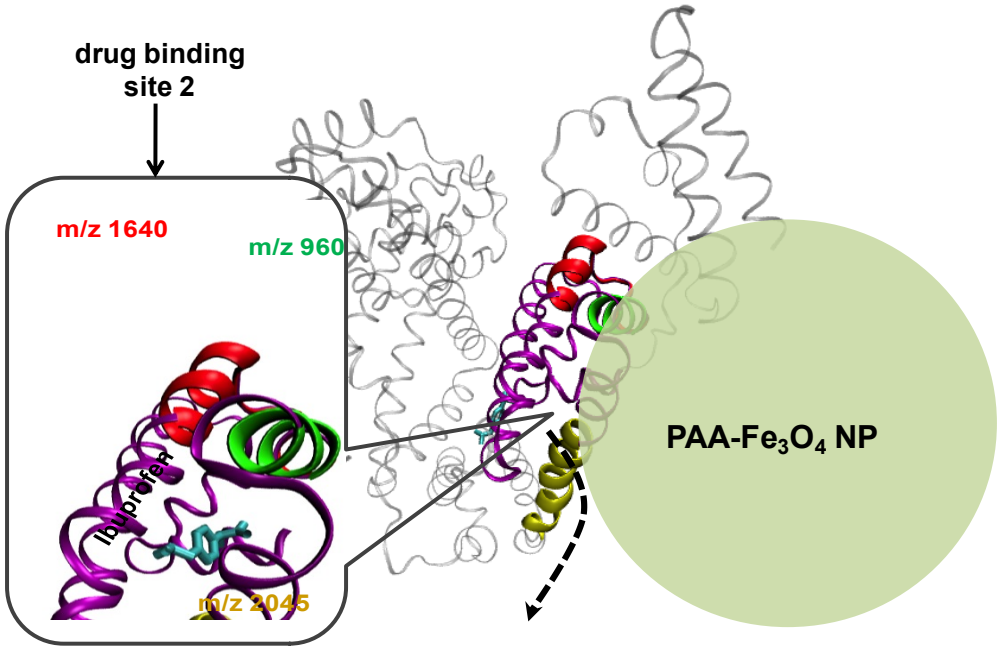
on HSA upon drug binding, but could be attributed to the competition of the same binding site 2 on HSA between the drug molecules and the NPs. The stronger affinity of naproxen to HSA led to a larger reduction in the protein-bound NP portion. However, when drug concentration increased further, θ started to increase and the complex showed a shift in the migration position in CE, indicating the formation of a different complex than the original HSA-NP complex. It may be a three-party complex with both the drug and the NP binding simultaneously on HS. More study is needed to verify this hypothesis. Furthermore, we examined the competition effect from fusidic acid on the HSA-NP interaction. Fusidic acid binds to either subdomain IIIB or subdomain IB of HSA (PDB ID: 2VUF) (Figure S 7.8), [228] a site further away from the binding pocket of ibuprofen and the three peptides we identified at the HSA-NP interface. Indeed, fusidic acid did not show any inhibition effect on the binding of HSA to NPs (Figure S 7.9 b).

The competitive binding to HSA between the NPs and ibuprofen or naproxen verified that the NPs bound to HSA at a position very close to the drug-binding site 2.(Schematically shown as Figure 7.8) Site 2 is mainly in subdomain IIIA, having a pre-formed hydrophobic cavity with distinct polar features and a single main polar patch at the pocket entrance. The patch contains residues R410, Y411, K414 and S489; and the side chain of R410 is right at the mouth of the pocket and the hydroxyl of Y411 faces towards the inside of the pocket. The distribution of basic and polar residues on the largely hydrophobic interior walls attracts for the electronegative drugs, attributed to the general selectivity of this binding pocket. In this study, the PAA molecules on the NPs surface carried negative charges under our experiment conditions, which could be pulled closer to site 1 through electrostatic interaction through the basic residues of R410, Y411, and K414. In addition, the entrance of site 2 is not encumbered by the following subdomain IIIB. It rotates further away and leaves the pocket entrance more solvent-accessible. Our previous study on the binding between bovine serum albumin (BSA) and the PAA-coated NPs has revealed the main driving force for the interaction is the desolvation effect. The release of a large number of solvent molecules from the binding interface resulted in large entropy increase and drove forward the spontaneous interaction. The high solvent exposure of the site 2 well explains the specific selectivity of the PAA-Fe_3O_4 NPs to this binding site.

However, the selective binding of the NPs to the drug-binding site 2 could not be simply explained by electrostatic interaction, because the drug-binding site 1 also has two

clusters of polar residues. The residues of the first cluster, Y150, H242, and R257, locates towards the bottom of the pocket, and those of the second cluster (K195, K199, R218, R222) are at the entrance of the pocket. All K residuess in site 1 are located on the surface of HSA, which should be accessible to EDC and SDAD. However, out of the identified 14 peptides in Figure 7.5 a, three peptides (m/z 673 AWAVAR, m/z 649 CASLQK, m/z 789 LVTDLTK, m/z 1386 YICENQDSISSK) are mapped in site 1, but all of them did not show significant decreasing trends in Figure 7.5 b and c. Three other peptides (m/z 645 LDELR, m/z 715 AACLLPK, m/z 1074 LDELRDEGK) close to site 1 did not decrease. From these phenomena, we concluded that that it was unlikely that the NPs could bind to site 1.

Figure 7.8 Scheme of the identified binding site



At a concentration of 0.6 mM, HSA is the most abundant protein in human plasma. Binding to HSA by a wide variety of endogenous ligands or drug molecules could increase their solubility, extend their circulation duration, help with their biodistribution, and even reduce their toxicity via transportation to disposal sites. Thus, identification of the binding site of NPs on HSA can lead to better prediction of the pharmacokinetic behaviors of NPs in human plasma. It can also enhance our understanding on the dependence of binding site selectivity towards the surface coating of NPs as well as their other physicochemical properties, such as size and shape. The knowledge is definitely useful for the design of nanomaterials to be employed as drug carriers or medical imaging reagents. Our study also demonstrated the power of cross-linking chemistry coupled with MS in binding site identification, which can be adopted to study the interface of proteins and the functional nanomaterials with the availability of diverse cross-linking chemicals and the high performance mass spectrometers.

7.4 Conclusions

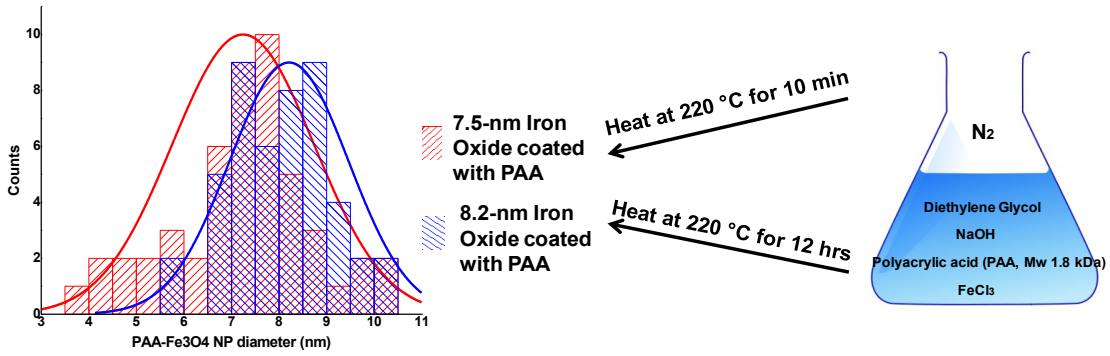
There is no doubt that for better understanding of the interaction phenomena we observed, more studies with wider particle diameter range and better control on the PAA structures, as well as investigations with techniques other than CE and MS are needed. Nevertheless, our study highlights the significance of surface coating to the interaction between proteins and nanomaterials. Subtle change in particle preparation could lead to big difference in protein binding behavior which could affect the interaction of NPs with biosystems. Thorough characterization of structure change in the coating molecules after

NPs synthesis is definitely desired prior to the study of their interactions with biomolecules and biosystems. The methodology of using cross-linking and mass spectrometry to identify the nano-bio interface peptide was successfully developed and 8.2-nm PAA-Fe_3O_4 NPs were found to bind to drug binding site 2 on human serum albumin. This strategy could be applied to identify the interaction sites in aqueous environment. When the interaction sites occupy the biologically functioning domain of a protein, it may lead to biological effects due to bio-function adjusted and it may change the behavior of nanoparticles in living systems. To get a clear view of nano-bio interface, various techniques should be involved and even new methodology needs to be developed to meet the requirement of this complicated topic.

Supporting Information

Figure S 7.1 (a) Scheme of synthesis difference between 7.5-nm and 8.2-nm PAA-Fe_3O_4 NPs and size distribution based on TEM images.(b) TEM images for PAA-Fe_3O_4 NPs (A: 7.5-nm, B: 8.2-nm) with a 50-nm scale bar.

(a)



(b)

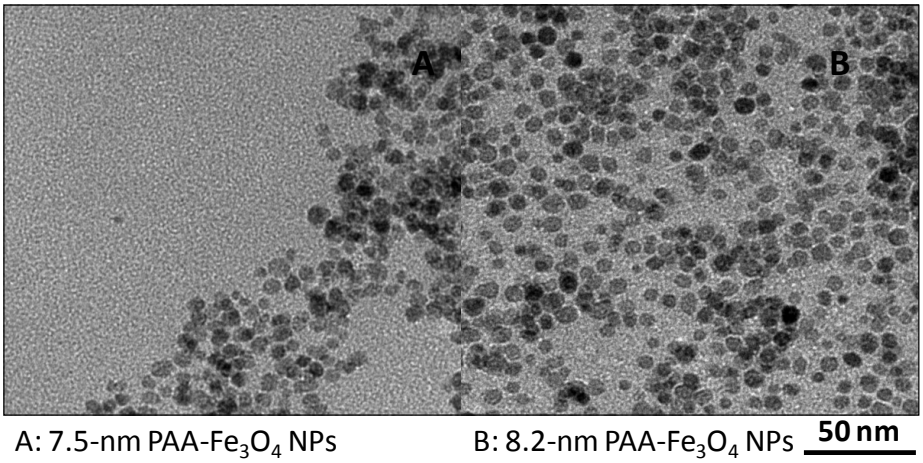
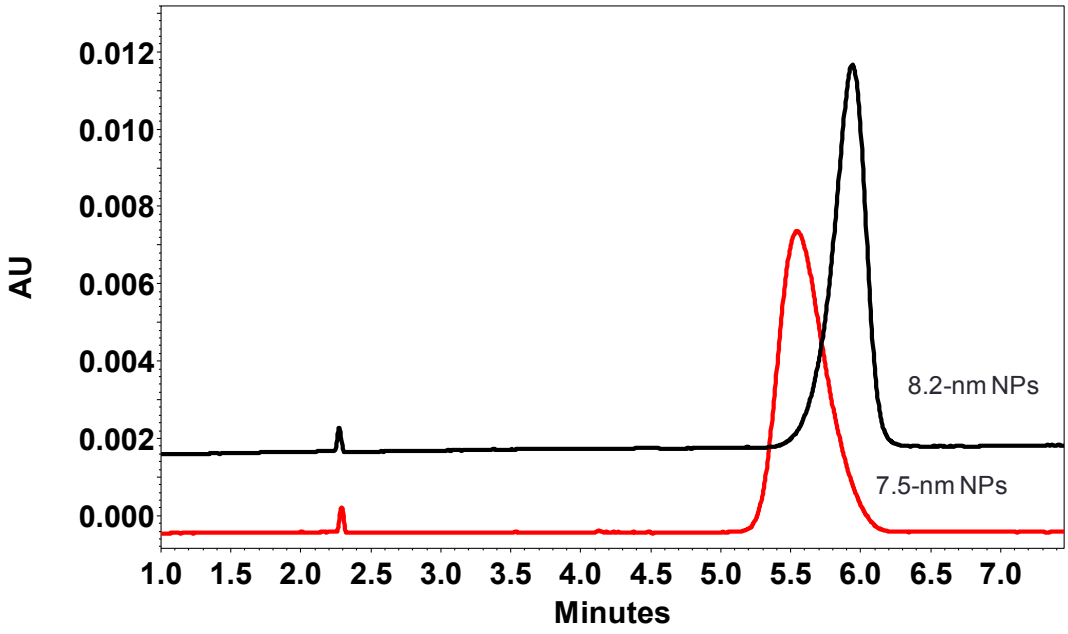


Figure S 7.2. Zeta potential calculation from CE data.(a). electropherograms of the 7.5- and 8.2-nm NPs; (b) zeta potentials calculated from the equation[3] shown in the plot.

(a)



(b)

Fe_3O_4 NPs	Electrophoretic mobility ($m^2 V^{-1} S^{-1}$)	Zeta potential (mV)
7.5-nm	-3.42×10^{-8}	-43.79
8.2-nm	-3.61×10^{-8}	-46.22

$$\xi = \frac{\mu_e \cdot \eta}{\varepsilon} = \frac{\mu_e \cdot \eta}{\varepsilon_0 \cdot \varepsilon_r} = \frac{\mu_e \cdot 8.90 \times 10^{-4} \cdot 10^3}{8.854187817 \times 10^{-12} \cdot 78.4}$$

Figure S 7.3. Mass spectra for (a) PAA solution treated with TFA and dialysis, (b) IAA matrix, (c) empty tube treated with TFA and dialysis.

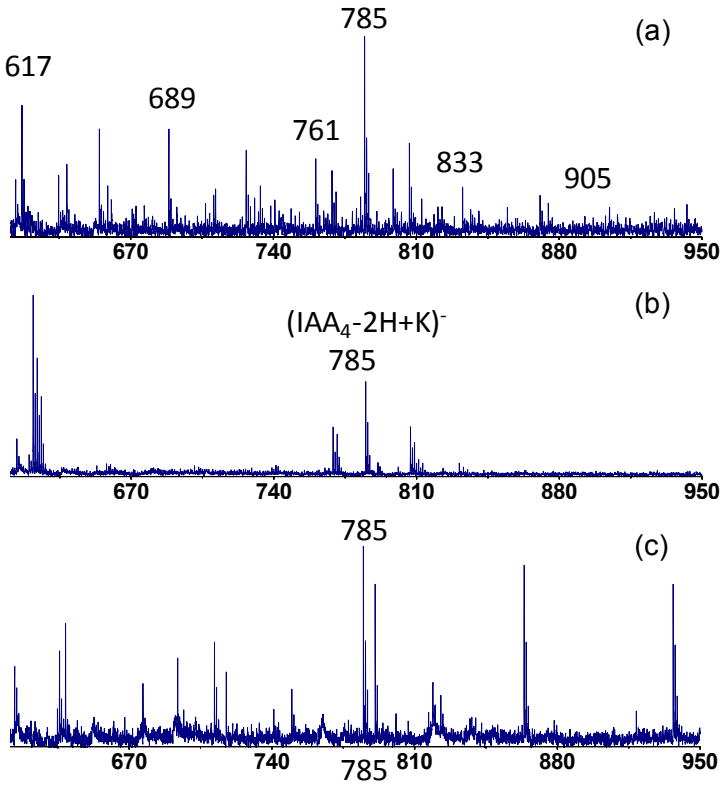


Figure S 7.4 Structures of A, B, and C series (from top to bottom) of PAA.

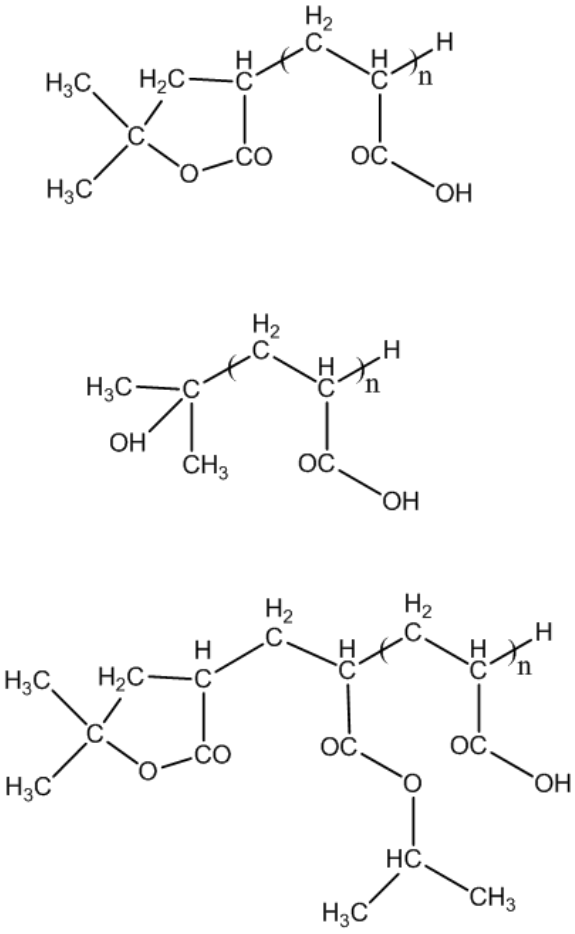


Figure S 7.5. Mass spectrum with wider m/z range for pseudo 8.2-nm reaction in which PAA underwent the same heating procedures as 8.2-nm nanoparticle synthesis with no $FeCl_3$ addition.

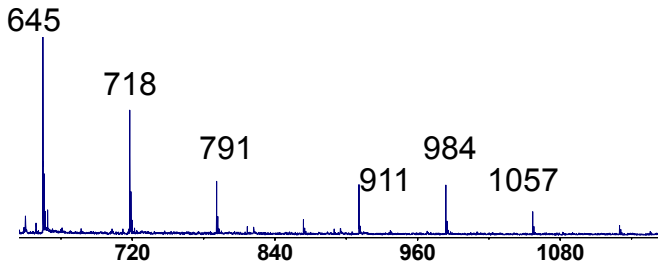


Figure S 7.6 Controls for binding site identification: (a) HSA trypsin digestion (b)Trypsin self digestion (c) Tryptic digestion of SDAD-cross-linked HSA (d) Tryptic digestion of EDC-cross-linked HSA (e) Tryptic digestion of HSA followed by adsorption to NPs (f) Tryptic digestion of EDC-cross-linked HSA followed by adsorption to NPs.

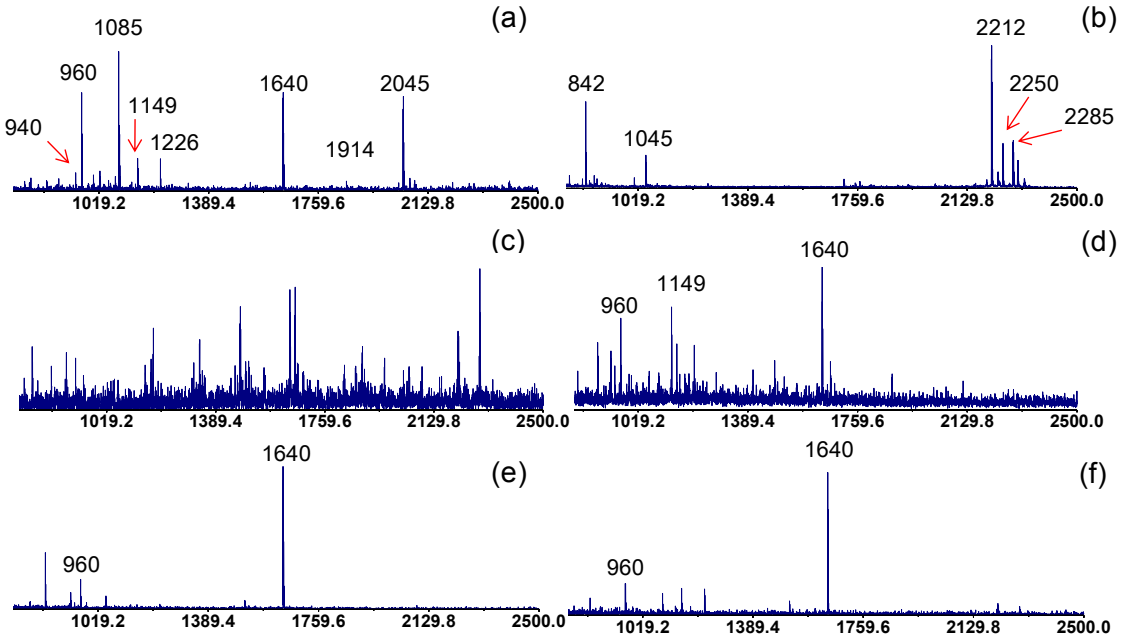


Figure S 7.7 3-D crystal structure of HSA (Chain A and Chain B)

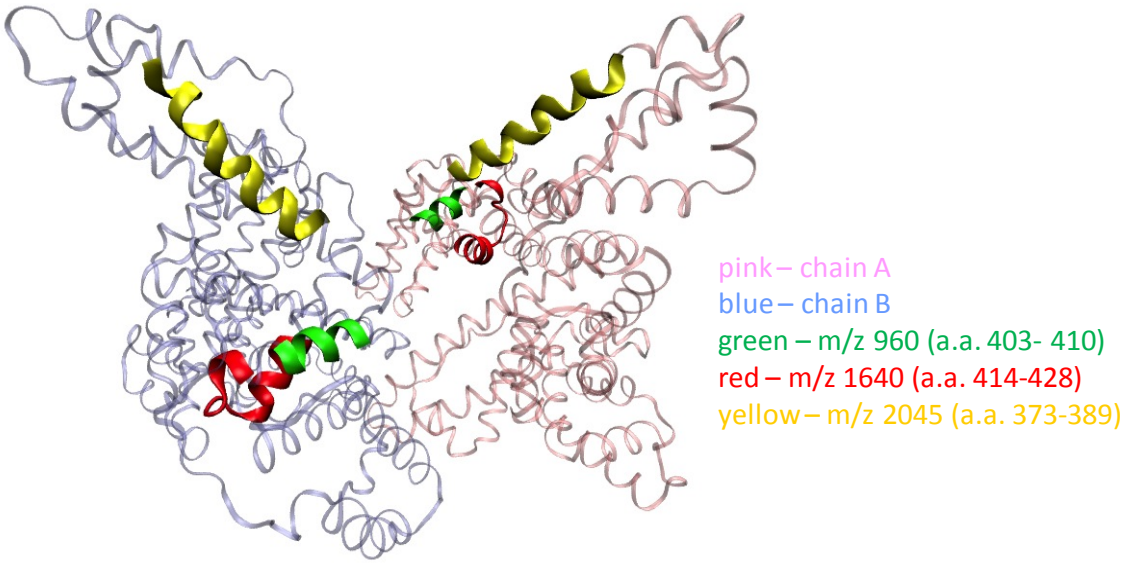


Figure S 7.8 3-D crystal structure of fusidic acid bound to HSA at sites away from drug binding site 1 and 2

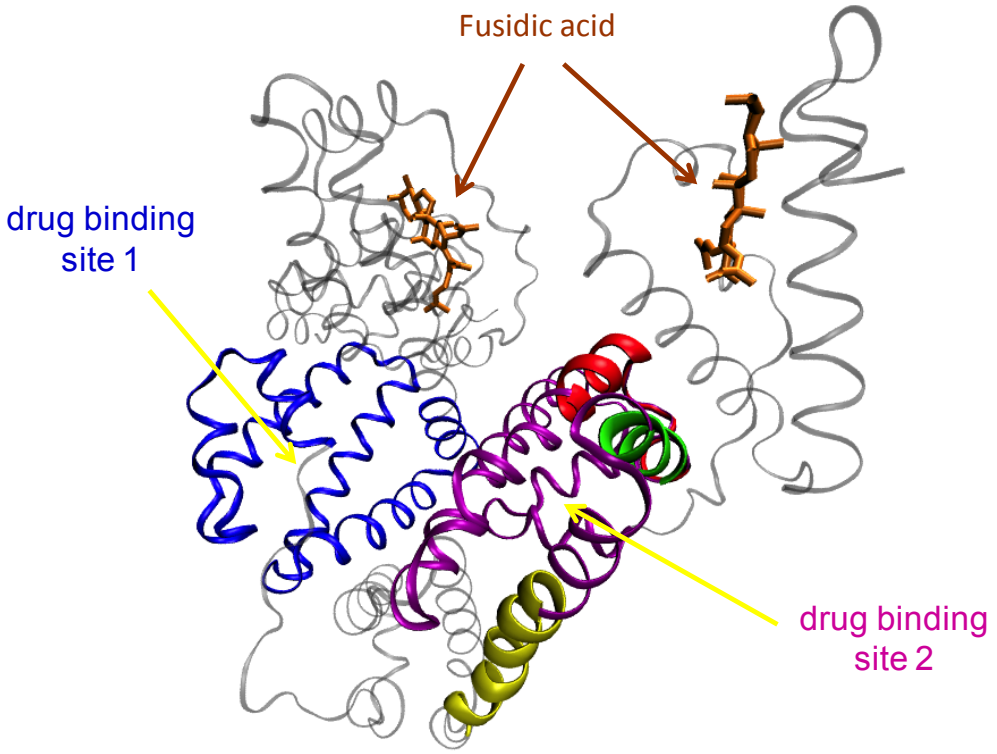
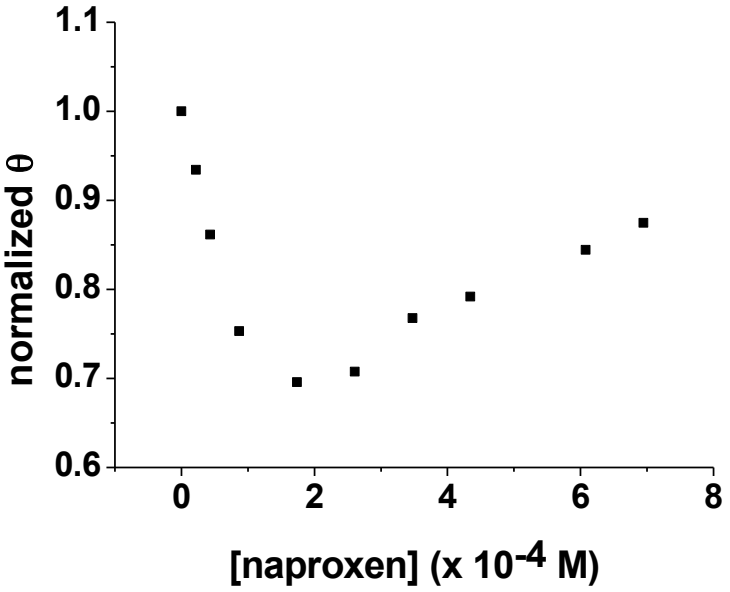


Figure S 7.9 Effects of pre-incubating HSA and (a) naproxen (b) fusidic acid on normalized binding percentage between HSA and PAA-Fe_3O_4 NPs.

(a)



(b)

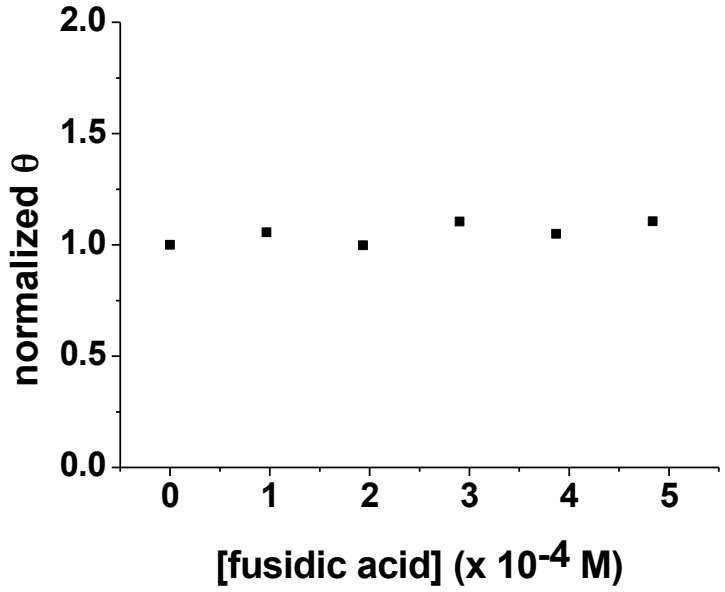
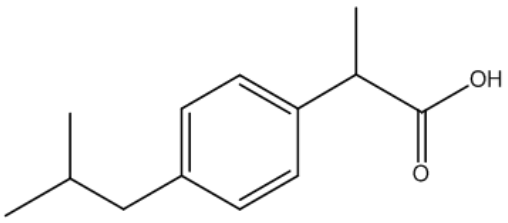
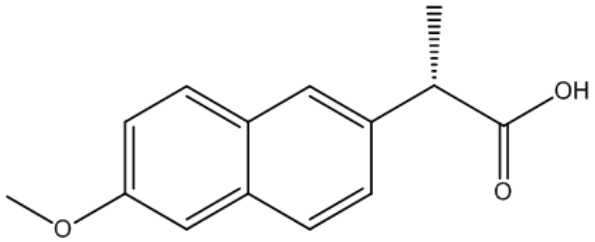


Figure S 7. 10 Chemical structures of (a) ibuprofen, (b) naproxen and (c) fusidic acid.

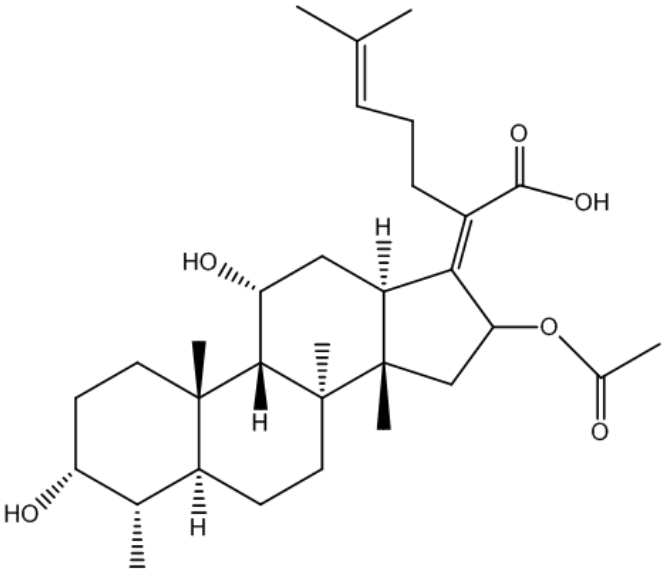
(a)



(b)



(c)



Chapter 8

Conclusions

This thesis was focused on CE-based methodology development and applications on biomolecule analysis, mainly utilizing high resolution separation power of CE to study systems containing multi-components. On one hand, the CE separation can resolve target biomolecules of interest in presence of background biomolecules; on the other hand CE can be used to quantify the affinity of stable and transient interaction complexes composed of biomolecule and inorganic nanomaterial.

In part I, for sensitive detection of short DNA, RCA catalyzed by *Phi29* was adopted to generate long products which were then digested into identical short DNA strands by endonuclease. Those fragments were ready for CE-LIF analysis for sensitive and accurate quantitation. High specificity was achieved by ligation step. To further improve the sensitivity for small RNA detection, ligation step was eliminated. Careful circular probe designing was required to avoid non-specific amplification theoretically. Experimentally, two polymerases working at different temperature (37˚C and 65˚C) were compared on their performance in terms of sensitivity and selectivity. The best LOD achieved was 35 amol for small RNA target.

In part II, CE was developed as a flexible platform to measure the affinity between engineered nanoparticles and proteins. Two modes, CZE and ACE were adopted for slow and fast on-and-off systems respectively. Mechanism study on driving force and binding site identification was carried out by using CE and mass spectrometry. Mass spectrometry was informative for nanoparticle surface ligand characterization. Based on our experimental results, desolvation can overcome the electrostatic repulsion and drive the interaction between nanoparticles and proteins. Binding sites were then identified by cross-linking followed by mass spectrometry and further verified by drug binding tests.

This thesis work has demonstrated the advantages, capabilities and potentials of CE-based assays for biomolecule analysis. When combined or coupled with other techniques, CE has been enabled with great power on solving problems related to biomolecule analysis in presence of other biomolecules, inorganic nanomaterial, small drug molecule, *etc.*. The methodology we developed on commercial CE instrument can be applied to micro-chip based CE systems in the future. This will provide high throughput, high automation and short analysis time.

References

(1) Tiselius, A. *Trans. Faraday Soc.* **1937**, *33*, 524-531.
(2) Hjerten, S. *Chromatogr. Rev.* **1967**, *9*, 122-219.
(3) Jorgenson, J. W.; Lukacs, K. D. *Clin. Chem. (Winston-Salem, N. C.)* **1981**, *27*, 1551-1553.
(4) Kleparnik, K.; Bocek, P. *Bioessays* **2010**, *32*, 218-226.
(5) Lin, C. E.; Hsueh, C. C.; Wang, T. Z.; Chiu, T. C.; Chen, Y. C. *Journal of Chromatography A* **1999**, *835*, 197-207.
(6) FurtosMatei, A.; Li, J. J.; Waldron, K. C. *Journal of Chromatography B* **1997**, *695*, 39-47.
(7) Vespalec, R.; Bocek, P. *Chemical Reviews* **2000**, *100*, 3715-3753.
(8) Heegaard, N. H. H.; Nilsson, S.; Guzman, N. A. *Journal of Chromatography B-Analytical Technologies in the Biomedical and Life Sciences* **1998**, *715*, 29-54.
(9) Chu, Y. H.; Avila, L. Z.; Gao, J. M.; Whitesides, G. M. *Accounts of Chemical Research* **1995**, *28*, 461-468.
(10) Colton, I. J.; Carbeck, J. D.; Rao, J.; Whitesides, G. M. *Electrophoresis* **1998**, *19*, 367-382.
(11) Morozova, O.; Marra, M. A. *Genomics* **2008**, *92*, 255-264.
(12) Altria, K. D.; Elder, D. *J. Chromatogr., A* **2004**, *1023*, 1-14.
(13) Radko, S. P.; Chrambach, A. *J. Chromatogr., B: Biomed. Sci. Appl.* **1999**, *722*, 1-10.
(14) Kraly, J.; Fazal, M. A.; Schoenherr, R. M.; Bonn, R.; Harwood, M. M.; Turner, E.; Jones, M.; Dovichi, N. J. *Anal. Chem.* **2006**, *78*, 4097-4110.
(15) Toledo-Rodriguez, M.; Markram, H. *Methods Mol. Biol. (Totowa, NJ, U. S.)* **2007**, *403*, 123-139.
(16) Li, H.; Yeung, E. S. *Electrophoresis* **2002**, *23*, 3372-3380.
(17) Pang, H.-M.; Yeung, E. S. *Nucleic Acids Res.* **2000**, *28*, e73, ii-viii.
(18) Chen, S.; Lillard, S. J. *Anal. Chem.* **2001**, *73*, 111-118.
(19) Zabzdyr, J. L.; Lillard, S. J. *Anal. Chem.* **2001**, *73*, 5771-5775.
(20) Hashimoto, M.; He, Y.; Yeung, E. S. *Nucleic Acids Res.* **2003**, *31*, e41/41-e41/17.
(21) Santoro, M. M.; Liu, Y.; Khan, S. M. A.; Hou, L. X.; Bolen, D. W. *Biochemistry* **1992**, *31*, 5278-5283.
(22) Salata, O. V. *J. Nanobiotechnol.* **2004**, *2*, No pp. given.
(23) Liu, W.-T. *J. Biosci. Bioeng.* **2006**, *102*, 1-7.
(24) Schmid, K.; Riediker, M. *Environ. Sci. Technol.* **2008**, *42*, 2253-2260.
(25) McNeil, S. E. *Methods Mol. Biol. (N. Y., NY, U. S.)* **2011**, *697*, 9-15.
(26) Scheffer, A.; Engelhard, C.; Sperling, M.; Buscher, W. *Anal. Bioanal. Chem.* **2008**, *390*, 249-252.
(27) d'Orlye, F.; Varenne, A.; Georgelin, T.; Siaugue, J.-M.; Teste, B.; Descroix, S.; Gareil, P. *Electrophoresis* **2009**, *30*, 2572-2582.
(28) Pyell, U. *Electrophoresis* **2008**, *29*, 576-589.
(29) Vicente, G.; Colon, L. A. *Anal. Chem. (Washington, DC, U. S.)* **2008**, *80*, 1988-1994.
(30) Walczyk, D.; Bombelli, F. B.; Monopoli, M. P.; Lynch, I.; Dawson, K. A. *J. Am. Chem. Soc.* **2010**, *132*, 5761-5768.
(31) *Electrophoresis Supplementary Issue S1'09*, 2009.
(32) Strege, M. A.; Lagu, A. L. *Anal. Biochem.* **1993**, *210*, 402-410.
(33) Ding, W.; Fritz, J. S. *J. High Resolut. Chromatogr.* **1997**, *20*, 575-580.
(34) Cifuentes, A.; Rodriguez, M. A.; Garcia-Montelongo, F. J. *J. Chromatogr., A* **1996**, *742*, 257-266.

(35) Baryla, N. E.; Melanson, J. E.; McDermott, M. T.; Lucy, C. A. *Anal. Chem.* **2001**, *73*, 4558-4565.
(36) Jones, M. N. *Chem. Soc. Rev.* **1992**, *21*, 127-136.
(37) Liu, Q.; Yang, Y.; Huang, Y.; Pan, C.; Nie, Z.; Yao, S. *Electrophoresis* **2009**, *30*, 2151-2158.
(38) Barron, A. E.; Sunada, W. M.; Blanch, H. W. *Electrophoresis* **1996**, *17*, 744-757.
(39) Barron, A. E.; Soane, D. S.; Blanch, H. W. *J. Chromatogr., A* **1993**, *652*, 3-16.
(40) Albarghouthi, M. N.; Buchholz, B. A.; Doherty, E. A. S.; Bogdan, F. M.; Zhou, H.; Barron, A. E. *Electrophoresis* **2001**, *22*, 737-747.
(41) Baba, Y.; Ishimaru, N.; Samata, K.; Tsuhako, M. *J. Chromatogr., A* **1993**, *653*, 329-335.
(42) Kondo, K.; Kaji, N.; Toita, S.; Okamoto, Y.; Tokeshi, M.; Akiyoshi, K.; Baba, Y. *Biomicrofluidics* **2010**, *4*, 032210.
(43) Dolnik, V.; Xu, D.; Yadav, A.; Bashkin, J.; Marsh, M.; Tu, O.; Mansfield, E.; Vainer, M.; Madabhushi, R.; Barker, D.; Harris, D. *J. Microcolumn Sep.* **1998**, *10*, 175-184.
(44) Lucy, C. A.; MacDonald, A. M.; Gulcev, M. D. *J. Chromatogr., A* **2008**, *1184*, 81-105.
(45) Madabhushi, R. S. *Electrophoresis* **1998**, *19*, 224-230.
(46) Cretich, M.; Chiari, M.; Pirri, G.; Crippa, A. *Electrophoresis* **2005**, *26*, 1913-1919.
(47) Schweitzer, B.; Roberts, S.; Grimwade, B.; Shao, W.; Wang, M.; Fu, Q.; Shu, Q.; Laroche, I.; Zhou, Z.; Tchernev, V. T.; Christiansen, J.; Velleca, M.; Kingsmore, S. F. *Nat. Biotechnol.* **2002**, *20*, 359-365.
(48) Kato, M.; Sakai-Kato, K.; Jin, H.; Kubota, K.; Miyano, H.; Toyo'oka, T.; Dulay, M. T.; Zare, R. N. *Anal. Chem.* **2004**, *76*, 1896-1902.
(49) Dahm, R. *Hum. Genet.* **2008**, *122*, 565-581.
(50) Crick, F. H. C. *Nature (London)* **1970**, *227*, 561-563.
(51) Palecek, E. *Talanta* **2002**, *56*, 809-819.
(52) Epstein, J. R.; Biran, I.; Walt, D. R. *Anal. Chim. Acta* **2002**, *469*, 3-36.
(53) Chen, C.; Ridzon, D. A.; Broomer, A. J.; Zhou, Z.; Lee, D. H.; Nguyen, J. T.; Barbisin, M.; Xu, N. L.; Mahuvakar, V. R.; Andersen, M. R.; Lao, K. Q.; Livak, K. J.; Guegler, K. J. *Nucleic Acids Res.* **2005**, *33*, e179/171-e179/179.
(54) Liu, J.; Tian, S.; Tiefenauer, L.; Nielsen, P. E.; Knoll, W. *Anal. Chem.* **2005**, *77*, 2756-2761.
(55) Uslu, F.; Ingebrandt, S.; Mayer, D.; Bocker-Meffert, S.; Odenthal, M.; Offenhausser, A. *Biosens. Bioelectron.* **2004**, *19*, 1723-1731.
(56) Tombelli, S.; Mascini, M.; Sacco, C.; Turner, A. P. F. *Anal. Chim. Acta* **2000**, *418*, 1-9.
(57) Thaitrong, N.; Liu, P.; Briese, T.; Lipkin, W. I.; Chiesl, T. N.; Higa, Y.; Mathies, R. A. *Anal. Chem. (Washington, DC, U. S.)*, *82*, 10102-10109.
(58) Palecek, E.; Fojta, M. *Talanta* **2007**, *74*, 276-290.
(59) Schopf, E.; Fischer, N. O.; Chen, Y.; Tok, J. B. H. *Bioorg. Med. Chem. Lett.* **2008**, *18*, 5871-5874.
(60) Chapman, E. J.; Carrington, J. C. *Nat. Rev. Genet.* **2007**, *8*, 884-896.
(61) Rana, T. M. *Nat. Rev. Mol. Cell Biol.* **2007**, *8*, 23-36.
(62) Costa, F. F. *Gene* **2008**, *410*, 9-17.
(63) Young, R. F., III *Science (Washington, DC, U. S.)* **2008**, *321*, 922-923.
(64) Ding, S.-W.; Voinnet, O. *Cell (Cambridge, MA, U. S.)* **2007**, *130*, 413-426.
(65) Phillips, J. R.; Dalmay, T.; Bartels, D. *FEBS Lett.* **2007**, *581*, 3592-3597.
(66) Sunkar, R.; Chinnusamy, V.; Zhu, J.; Zhu, J.-K. *Trends Plant Sci.* **2007**, *12*, 301-309.
(67) Bejerano-Sagie, M.; Xavier, K. B. *Curr. Opin. Microbiol.* **2007**, *10*, 189-198.

(68) Valentin-Hansen, P.; Johansen, J.; Rasmussen, A. A. *Curr. Opin. Microbiol.* **2007**, *10*, 152-155.
(69) Masse, E.; Salvail, H.; Desnoyers, G.; Arguin, M. *Curr. Opin. Microbiol.* **2007**, *10*, 140-145.
(70) Xia, M. H. P. *J. Cancer Mol.* **2008**, *4*, 79-89.
(71) Sever, N. I.; Younan, S.; Wojcik, S. E.; Spizzo, R.; Fabbri, M.; Calin, G. A. *Pers. Med.* **2007**, *4*, 147-155.
(72) Voorhoeve, P. M.; Agami, R. *Biochim. Biophys. Acta, Rev. Cancer* **2007**, *1775*, 274-282.
(73) Tricoli, J. V.; Jacobson, J. W. *Cancer Res.* **2007**, *67*, 4553-4555.
(74) Calin, G. A.; Croce, C. M. *Nat. Rev. Cancer* **2006**, *6*, 857-866.
(75) Cummins, J. M.; Velculescu, V. E. *Oncogene* **2006**, *25*, 6220-6227.
(76) Stadler, B. M.; Ruohola-Baker, H. *Cell (Cambridge, MA, U. S.)* **2008**, *132*, 563-566.
(77) Fire, A.; Xu, S.-Q. *Proc. Natl. Acad. Sci. U. S. A.* **1995**, *92*, 4641-4645.
(78) Schweitzer, B.; Wiltshire, S.; Lambert, J.; O'Malley, S.; Kukanskis, K.; Zhu, Z.; Kingsmore, S. F.; Lizardi, P. M.; Ward, D. C. *Proc. Natl. Acad. Sci. U. S. A.* **2000**, *97*, 10113-10119.
(79) Baner, J.; Nilsson, M.; Mendel-Hartvig, M.; Landegren, U. *Nucleic Acids Res.* **1998**, *26*, 5073-5078.
(80) Nilsson, M.; Malmgren, H.; Samiotaki, M.; Kwiatkowski, M.; Chowdhary, B. P.; Landegen, U. *Science (Washington, D. C.)* **1994**, *265*, 2085-2088.
(81) Hashimoto, M.; Hupert, M. L.; Murphy, M. C.; Soper, S. A.; Cheng, Y.-W.; Barany, F. *Anal. Chem.* **2005**, *77*, 3243-3255.
(82) Gerry, N. P.; Witowski, N. E.; Day, J.; Hammer, R. P.; Barany, G.; Barany, F. *J. Mol. Biol.* **1999**, *292*, 251-262.
(83) Li, M.; Diehl, F.; Dressman, D.; Vogelstein, B.; Kinzler, K. W. *Nat. Methods* **2006**, *3*, 95-97.
(84) Nallur, G.; Luo, C.; Fang, L.; Cooley, S.; Dave, V.; Lambert, J.; Kukanskis, K.; Kingsmore, S.; Lasken, R.; Schweitzer, B. *Nucleic Acids Res.* **2001**, *29*, e118/111-e118/119.
(85) Jarvius, J.; Melin, J.; Goeransson, J.; Stenberg, J.; Fredriksson, S.; Gonzalez-Rey, C.; Bertilsson, S.; Nilsson, M. *Nat. Methods* **2006**, *3*, 725-727.
(86) Jonstrup, S. P.; Koch, J.; Kjems, J. *RNA* **2006**, *12*, 1747-1752.
(87) Blab, G. A.; Schmidt, T.; Nilsson, M. *Anal. Chem.* **2004**, *76*, 495-498.
(88) Hunh, H., Demidov, V.V In *DNA Amplification: Current Technologies and Applications*; Demidov, V. V., Broude, N.E., Ed.; Horizon Bioscience: Norfolk, UK, 2004, pp 245-266.
(89) Li, J.; Chu, X.; Liu, Y.; Jiang, J.-H.; He, Z.; Zhang, Z.; Shen, G.; Yu, R.-Q. *Nucleic Acids Res.* **2005**, *33*, e168/161-e168/169.
(90) Favis, R.; Huang, J.; Gerry, N. P.; Culliford, A.; Paty, P.; Soussi, T.; Barany, F. *Hum. Mutat.* **2004**, *24*, 63-75.
(91) Yang, L.; Fung, C. W.; Cho, E. J.; Ellington, A. D. *Anal. Chem. (Washington, DC, U. S.)* **2007**, *79*, 3320-3329.
(92) Lin, C.; Xie, M.; Chen, J. J. L.; Liu, Y.; Yan, H. *Angew. Chem., Int. Ed.* **2006**, *45*, 7537-7539.
(93) Grossman, P. D., Colburn, J.C. *Capillary Electrophoresis Theory and Practice*; Academic Press, Inc: London, UK, 1992.
(94) Radko, S. P.; Chrambach, A. *Electrophoresis* **2002**, *23*, 1957-1972.
(95) Dahl, F.; Baner, J.; Gullberg, M.; Mendel-Hartvig, M.; Landegren, U.; Nilsson, M. *Proc. Natl. Acad. Sci. U. S. A.* **2004**, *101*, 4548-4553.
(96) Reckmann, B.; Krauss, G. *Biochim. Biophys. Acta, Gene Struct. Expression* **1987**, *908*, 90-96.

(97) Kourkine, I. V.; Hestekin, C. N.; Barron, A. E. *Electrophoresis* **2002**, *23*, 1375-1385.
(98) Chen, J.; Kadlubar, F. F.; Chen, J. Z. *Nucleic Acids Res.* **2007**, *35*, 1377-1388.
(99) Jaeger, J.; Spang, R. *BMC Bioinformatics* **2006**, *7*, 388.
(100) Harvey, J. J.; Lee, S. P.; Chan, E. K.; Kim, J. H.; Hwang, E.-S.; Cha, C.-Y.; Knutson, J. R.; Han, M. K. *Anal. Biochem.* **2004**, *333*, 246-255.
(101) Nilsson, M.; Gullberg, M.; Dahl, F.; Szuhai, K.; Raap, A. K. *Nucleic Acids Res.* **2002**, *30*, e66/61-e66/67.
(102) Hamilton, A. J.; Baulcombe, D. C. *Science (Washington, D. C.)* **1999**, *286*, 950-952.
(103) Pall, G. S.; Codony-Servat, C.; Byrne, J.; Ritchie, L.; Hamilton, A. *Nucleic Acids Res.* **2007**, *35*, e60/61-e60/69.
(104) Tang, X.; Gal, J.; Zhuang, X.; Wang, W.; Zhu, H.; Tang, G. *RNA* **2007**, *13*, 1803-1822.
(105) Wark, A. W.; Lee, H. J.; Corn, R. M. *Angew. Chem., Int. Ed.* **2008**, *47*, 644-652.
(106) Wark, A. W.; Lee, H. J.; Qavi, A. J.; Corn, R. M. *Anal. Chem. (Washington, DC, U. S.)* **2007**, *79*, 6697-6701.
(107) Neely, L. A.; Patel, S.; Garver, J.; Gallo, M.; Hackett, M.; McLaughlin, S.; Nadel, M.; Harris, J.; Gullans, S.; Rooke, J. *Nat. Methods* **2006**, *3*, 41-46.
(108) Fang, S.; Lee, H. J.; Wark, A. W.; Corn, R. M. *J. Am. Chem. Soc.* **2006**, *128*, 14044-14046.
(109) Saba, R.; Booth, S. A. *BMC Biotechnol* **2006**, *6*, 47.
(110) Hu, Z.; Zhang, A.; Storz, G.; Gottesman, S.; Leppla, S. H. *Nucleic Acids Res.* **2006**, *34*, e52/51-e52/57.
(111) Su, X.; Teh, H. F.; Lieu, X.; Gao, Z. *Anal. Chem. (Washington, DC, U. S.)* **2007**, *79*, 7192-7197.
(112) Cissell, K. A.; Rahimi, Y.; Shrestha, S.; Hunt, E. A.; Deo, S. K. *Anal. Chem. (Washington, DC, U. S.)* **2008**, *80*, 2319-2325.
(113) Blanco, L.; Bernad, A.; Lazaro, J. M.; Martin, G.; Garmendia, C.; Salas, M. *J. Biol. Chem.* **1989**, *264*, 8935-8940.
(114) Blanco, L.; Bernad, A.; Lazaro, J. M.; Martin, G.; Garmendia, C.; Salas, M. *J Biol Chem* **1989**, *264*, 8935-8940.
(115) Dean, F. B.; Nelson, J. R.; Giesler, T. L.; Lasken, R. S. *Genome Res.* **2001**, *11*, 1095-1099.
(116) Zhao, W.; Ali, M. M.; Brook, M. A.; Li, Y. *Angew. Chem., Int. Ed.* **2008**, *47*, 6330-6337.
(117) Nilsson, M.; Antson, D.-O.; Barbany, G.; Landegren, U. *Nucleic Acids Res.* **2001**, *29*, 578-581.
(118) Sriskanda, V.; Shuman, S. *Nucleic Acids Res* **1998**, *26*, 3536-3541.
(119) Nilsson, M.; Antson, D. O.; Barbany, G.; Landegren, U. *Nucleic Acids Res* **2001**, *29*, 578-581.
(120) Bullard, D. R.; Bowater, R. P. *Biochem. J.* **2006**, *398*, 135-144.
(121) Liu, D.; Daubendiek, S. L.; Zillman, M. A.; Ryan, K.; Kool, E. T. *J. Am. Chem. Soc.* **1996**, *118*, 1587-1594.
(122) Li, N.; Li, J.; Zhong, W. *Electrophoresis* **2008**, *29*, 424-432.
(123) Katiyar-Agarwal, S.; Morgan, R.; Dahlbeck, D.; Borsani, O.; Villegas, A., Jr.; Zhu, J.-K.; Staskawicz, B. J.; Jin, H. *Proc. Natl. Acad. Sci. U. S. A.* **2006**, *103*, 18002-18007.
(124) Blasco, M. A.; Blanco, L.; Pares, E.; Salas, M.; Bernad, A. *Nucleic Acids Res.* **1990**, *18*, 4763-4770.
(125) Torrisani, J.; Parmentier, L.; Buscail, L.; Cordelier, P. *Curr. Genomics* **2007**, *8*, 229-233.
(126) Roush, S.; Slack, F. J. *Trends Cell Biol.* **2008**, *18*, 505-516.

(127) Miska, E. A.; Alvarez-Saavedra, E.; Townsend, M.; Yoshii, A.; Sestan, N.; Rakic, P.; Constantine-Paton, M.; Horvitz, H. R. *Genome Biol* **2004**, *5*, R68.
(128) Mahmoudian, L.; Kaji, N.; Tokeshi, M.; Nilsson, M.; Baba, Y. *Anal. Chem. (Washington, DC, U. S.)* **2008**, *80*, 2483-2490.
(129) Nel, A. E.; Madler, L.; Velegol, D.; Xia, T.; Hoek, E. M. V.; Somasundaran, P.; Klaessig, F.; Castranova, V.; Thompson, M. *Nat. Mater.* **2009**, *8*, 543-557.
(130) Cedervall, T.; Lynch, I.; Lindman, S.; Berggard, T.; Thulin, E.; Nilsson, H.; Dawson, K. A.; Linse, S. *Proc. Natl. Acad. Sci. U. S. A.* **2007**, *104*, 2050-2055.
(131) Deguchi, S.; Yamazaki, T.; Mukai, S.-a.; Usami, R.; Horikoshi, K. *Chem. Res. Toxicol.* **2007**, *20*, 854-858.
(132) Samanta, B.; Yan, H.; Fischer, N. O.; Shi, J.; Jerry, D. J.; Rotello, V. M. *J. Mater. Chem.* **2008**, *18*, 1204-1208.
(133) Lynch, I.; Cedervall, T.; Lundqvist, M.; Cabaleiro-Lago, C.; Linse, S.; Dawson, K. A. *Adv. Colloid Interface Sci.* **2007**, *134-135*, 167-174.
(134) Aggarwal, P.; Hall, J. B.; McLeland, C. B.; Dobrovolskaia, M. A.; McNeil, S. E. *Adv. Drug Delivery Rev.* **2009**, *61*, 428-437.
(135) Zhang, D.; Neumann, O.; Wang, H.; Yuwono, V. M.; Barhoumi, A.; Perham, M.; Hartgerink, J. D.; Wittung-Stafshede, P.; Halas, N. J. *Nano Lett.* **2009**, *9*, 666-671.
(136) You, C.-C.; De, M.; Han, G.; Rotello, V. M. *J. Am. Chem. Soc.* **2005**, *127*, 12873-12881.
(137) Bayraktar, H.; You, C.-C.; Rotello, V. M.; Knapp, M. J. *J. Am. Chem. Soc.* **2007**, *129*, 2732-2733.
(138) Li, L.; Mu, Q.; Zhang, B.; Yan, B. *Analyst (Cambridge, U. K.)* **2010**, *135*, 1519-1530.
(139) Roecker, C.; Poetzl, M.; Zhang, F.; Parak, W. J.; Nienhaus, G. U. *Nat. Nanotechnol.* **2009**, *4*, 577-580.
(140) Lundqvist, M.; Sethson, I.; Jonsson, B.-H. *Langmuir* **2004**, *20*, 10639-10647.
(141) De, M.; You, C.-C.; Srivastava, S.; Rotello, V. M. *J. Am. Chem. Soc.* **2007**, *129*, 10747-10753.
(142) Doyle, G.; Ashall, B.; Galvin, M.; Berndt, M.; Crosbie, S.; Zerulla, D. *Appl. Phys. A: Mater. Sci. Process.* **2007**, *89*, 351-355.
(143) De, P. L. S. H.; Park, J.-J.; Meuse, C.; Pristinski, D.; Becker, M. L.; Karim, A.; Douglas, J. F. *ACS Nano* **2010**, *4*, 365-379.
(144) Aggarwal, P.; Hall, J. B.; McLeland, C. B.; Dobrovolskaia, M. A.; McNeil, S. E. *Adv. Drug Delivery Rev.* **2009**, *61*, 428-437.
(145) Chen, Y.; Flowers, K.; Calizo, M.; Bishnoi, S. W. *Colloids Surf., B* **2010**, *76*, 241-247.
(146) Kim, H. R.; Andrieux, K.; Delomenie, C.; Chacun, H.; Appel, M.; Desmaele, D.; Taran, F.; Georgin, D.; Couvreur, P.; Taverna, M. *Electrophoresis* **2007**, *28*, 2252-2261.
(147) Nilsson, C.; Birnbaum, S.; Nilsson, S. *J. Chromatogr., A* **2007**, *1168*, 212-224.
(148) Nilsson, C.; Nilsson, S. *Electrophoresis* **2006**, *27*, 76-83.
(149) Luong, J. H. T.; Bouvrette, P.; Liu, Y.; Yang, D.-Q.; Sacher, E. *J. Chromatogr., A* **2005**, *1074*, 187-194.
(150) Huang, M.-F.; Kuo, Y.-C.; Huang, C.-C.; Chang, H.-T. *Anal. Chem.* **2004**, *76*, 192-196.
(151) Stathakis, C.; Arriaga, E. A.; Dovichi, N. J. *J. Chromatogr., A* **1998**, *817*, 233-238.
(152) Nilsson, C.; Becker, K.; Harwigsson, I.; Bulow, L.; Birnbaum, S.; Nilsson, S. *Anal. Chem. (Washington, DC, U. S.)* **2009**, *81*, 315-321.
(153) Heegaard, N. H. *J Chromatogr A* **1994**, *680*, 405-412.

(154) Heegaard, N. H. H. *Electrophoresis* **2009**, *30 Suppl 1*, S229-239.
(155) Ge, J.; Hu, Y.; Biasini, M.; Dong, C.; Guo, J.; Beyermann, W. P.; Yin, Y. *Chem.--Eur. J.* **2007**, *13*, 7153-7161.
(156) De Paoli Lacerda, S. H.; Park, J.-J.; Meuse, C.; Pristinski, D.; Becker, M. L.; Karim, A.; Douglas, J. F. *ACS Nano*, *4*, 365-379.
(157) Dobrovolskaia, M. A.; Patri, A. K.; Zheng, J.; Clogston, J. D.; Ayub, N.; Aggarwal, P.; Neun, B. W.; Hall, J. B.; McNeil, S. E. *Nanomed-Nanotechnol.* **2009**, *5*, 106-117.
(158) Hill, A. V. **1910**, *40*, iv-vii.
(159) Weiss, J. N. *FASEB J* **1997**, *11*, 835-841.
(160) Chu, Y. H.; Lees, W. J.; Stassinopoulos, A.; Walsh, C. T. *Biochemistry* **1994**, *33*, 10616-10621.
(161) Schnabel, U.; Fischer, C.-H.; Kenndler, E. *J. Microcolumn Sep.* **1997**, *9*, 529-534.
(162) Brewer, S. H.; Glomm, W. R.; Johnson, M. C.; Knag, M. K.; Franzen, S. *Langmuir* **2005**, *21*, 9303-9307.
(163) Ferrer, M. L.; Duchowicz, R.; Carrasco, B.; de la Torre, J. G.; Acuña, A. U. *Biophys. J.* **2001**, *80*, 2422-2430.
(164) Chen, Y.; Flowers, K.; Calizo, M.; Bishnoi, S. W. *Colloids Surf., B*, *76*, 241-247.
(165) Turci, F.; Ghibaudi, E.; Colonna, M.; Boscolo, B.; Fenoglio, I.; Fubini, B. *Langmuir* **2010**, *26*, 8336-8346.
(166) Gray, J. J. *Curr. Opin. Struct. Biol.* **2004**, *14*, 110-115.
(167) Latour, R. A. *J. Biomed. Mater. Res., Part A* **2006**, *78A*, 843-854.
(168) Lu, J. R. 2006; Springer GmbH; 265-282.
(169) Baigorri, R.; Garcia-Mina, J. M.; Gonzalez-Gaitano, G. *Colloids Surf., A* **2007**, *292*, 212-216.
(170) Slot, J. W.; Geuze, H. J. *Eur J Cell Biol* **1985**, *38*, 87-93.
(171) Weiss, J. N. *FASEB J.* **1997**, *11*, 835-841.
(172) Plenert, M. L.; Shear, J. B. *Proc. Natl. Acad. Sci. U. S. A.* **2003**, *100*, 3853-3857.
(173) Ritschdorff, E. T.; Plenert, M. L.; Shear, J. B. *Anal. Chem.* **2009**, 11860-11864.
(174) Grainger, D. W.; Castner, D. G. *Adv. Mater. (Weinheim, Ger.)* **2008**, *20*, 867-877.
(175) Riehemann, K.; Schneider, S. W.; Luger, T. A.; Godin, B.; Ferrari, M.; Fuchs, H. *Angew. Chem., Int. Ed.* **2009**, *48*, 872-897.
(176) Simonet, B. M.; Valcarcel, M. *Anal. Bioanal. Chem.* **2009**, *393*, 17-21.
(177) Lee, J.; Mahendra, S.; Alvarez, P. J. J. *ACS Nano* **2010**, *4*, 3580-3590.
(178) Balshaw, D. M.; Philbert, M.; Suk, W. A. *Toxicol. Sci.* **2005**, *88*, 298-306.
(179) Stern, S. T.; McNeil, S. E. *Toxicol. Sci.* **2008**, *101*, 4-21.
(180) Faunce, T. A. *Expert Opin. Drug Saf.* **2008**, *7*, 103-106.
(181) Sanhai, W. R.; Sakamoto, J. H.; Canady, R.; Ferrari, M. *Nat. Nanotechnol.* **2008**, *3*, 242-244.
(182) Asuri, P.; Bale, S. S.; Karajanagi, S. S.; Kane, R. S. *Curr. Opin. Biotechnol.* **2006**, *17*, 562-568.
(183) Lynch, I.; Dawson, K. A. *Nano Today* **2008**, *3*, 40-47.
(184) Lynch, I.; Cedervall, T.; Lundqvist, M.; Cabaleiro-Lago, C.; Linse, S.; Dawson, K. A. *Adv. Colloid Interface Sci.* **2007**, *134-135*, 167-174.
(185) Mu, Q.; Li, Z.; Li, X.; Mishra, S. R.; Zhang, B.; Si, Z.; Yang, L.; Jiang, W.; Yan, B. *J. Phys. Chem. C* **2009**, *113*, 5390-5395.

(186) Lesniak, A.; Campbell, A.; Monopoli, M. P.; Lynch, I.; Salvati, A.; Dawson, K. A. *Biomaterials* **2010**, *31*, 9511-9518.
(187) Zhu, Z.-J.; Carboni, R.; Quercio, J. M. J.; Yan, B.; Miranda, O. R.; Anderton, D. L.; Arcaro, K. F.; Rotello, V. M.; Vachet, R. W. *Small* **2010**, *6*, 2261-2265.
(188) Rana, S.; Yeh, Y.-C.; Rotello, V. M. *Curr. Opin. Chem. Biol.* **2010**, *14*, 828-834.
(189) Xia, T.; Kovochich, M.; Brant, J.; Hotze, M.; Sempf, J.; Oberley, T.; Sioutas, C.; Yeh, J. I.; Wiesner, M. R.; Nel, A. E. *Nano Lett.* **2006**, *6*, 1794-1807.
(190) Rejman, J.; Oberle, V.; Zuhorn, I. S.; Hoekstra, D. *Biochem. J.* **2004**, *377*, 159-169.
(191) Lind, K.; Kresse, M.; Muller, R. H. *Electrophoresis* **2001**, *22*, 3514-3521.
(192) Lundqvist, M.; Stigler, J.; Elia, G.; Lynch, I.; Cedervall, T.; Dawson, K. A. *Proc. Natl. Acad. Sci. U. S. A.* **2008**, *105*, 14265-14270,S14265/14261-S14265/14211.
(193) Dobrovolskaia, M. A.; McNeil, S. E. *Nat. Nanotechnol.* **2007**, *2*, 469-478.
(194) Card, J. W.; Magnuson, B. A. *Int. J. Toxicol.* **2010**, *29*, 402-410.
(195) Rabolli, V.; Thomassen, L. C. J.; Princen, C.; Napierska, D.; Gonzalez, L.; Kirsch-Volders, M.; Hoet, P. H.; Huaux, F.; Kirschhock, C. E. A.; Martens, J. A.; Lison, D. *Nanotoxicology* **2010**, *4*, 307-318.
(196) Thode, K.; Lueck, M.; Schroeder, W.; Blunk, T.; Mueller, R. H.; Kresse, M. *J. Drug Targeting* **1998**, *5*, 459-469.
(197) Alkilany, A. M.; Nagaria, P. K.; Hexel, C. R.; Shaw, T. J.; Murphy, C. J.; Wyatt, M. D. *Small* **2009**, *5*, 701-708.
(198) Fubini, B.; Ghiazza, M.; Fenoglio, I. *Nanotoxicology* **2010**, *4*, 347-363.
(199) Zeineldin, R.; Al-Haik, M.; Hudson, L. G. *Nano Lett.* **2009**, *9*, 751-757.
(200) Calzolai, L.; Franchini, F.; Gilliland, D.; Rossi, F. *Nano Lett.* **2010**, *10*, 3101-3105.
(201) Zappacosta, F.; Ingallinella, P.; Scaloni, A.; Pessi, A.; Bianchi, E.; Sollazzo, M.; Tramontano, A.; Marino, G.; Pucci, P. *Protein Sci.* **1997**, *6*, 1901-1909.
(202) Ohguro, H.; Palczewski, K.; Walsh, K. A.; Johnson, R. S. *Protein Sci.* **1994**, *3*, 2428-2434.
(203) Suckau, D.; Mak, M.; Przybylski, M. *Proc. Natl. Acad. Sci. U. S. A.* **1992**, *89*, 5630-5634.
(204) Krell, T.; Chackrewarthy, S.; Pitt, A. R.; Elwell, A.; Coggins, J. R. *J. Pept. Res.* **1998**, *51*, 201-209.
(205) Steiner, R. F.; Albaugh, S.; Fenselau, C.; Murphy, C.; Vestling, M. *Anal Biochem* **1991**, *196*, 120-125.
(206) Ganguly, A. K.; Pramanik, B. N.; Huang, E. C.; Liberles, S.; Heimark, L.; Liu, Y. H.; Tsarbopoulos, A.; Doll, R. J.; Taveras, A. G.; Remiszewski, S.; Snow, M. E.; Wang, Y. S.; Vibulbhan, B.; Cesarz, D.; Brown, J. E.; del, R. J.; James, L.; Kirschmeier, P.; Girijavallabhan, V. *Bioorg. Med. Chem.* **1997**, *5*, 817-820.
(207) Wong, D. L.; Pavlovich, J. G.; Reich, N. O. *Nucleic Acids Res.* **1998**, *26*, 645-649.
(208) Bennett, K. L.; Matthiesen, T.; Roepstorff, P. *Methods Mol. Biol. (Totowa, N. J.)* **2000**, *146*, 113-131.
(209) Li, N.; Zeng, S.; He, L.; Zhong, W. *Anal. Chem. (Washington, DC, U. S.)* **2010**, *82*, 7460-7466.
(210) Loiseau, J.; Doeerr, N.; Suau, J. M.; Egraz, J. B.; Llauro, M. F.; Ladaviere, C.; Claverie, J. *Macromolecules* **2003**, *36*, 3066-3077.
(211) Sarkar, D.; Somasundaran, P. *Langmuir* **2004**, *20*, 4657-4664.
(212) Weiss, J. N. *FASEB J.* **1997**, *11*, 835-841.

(213) Claesson, P. M.; Blomberg, E.; Froberg, J. C.; Nylander, T.; Arnebrant, T. *Adv. Colloid Interface Sci.* **1995**, *57*, 161-227.
(214) *Ullmann's Encyclopedia of Industrial Chemistry*; VCH: Weinheim, 1992.
(215) Wittemann, A.; Haupt, B.; Ballauff, M. *Phys. Chem. Chem. Phys.* **2003**, *5*, 1671-1677.
(216) Quintero, S. M. M.; Ponce, F. R. V.; Cremona, M.; Triques, A. L. C.; d'Almeida, A. R.; Braga, A. M. B. *Polymer* **2011**, *51*, 953-958.
(217) Wittemann, A.; Ballauff, M. *Phys. Chem. Chem. Phys.* **2006**, *8*, 5269-5275.
(218) Lemieux, R. U. *Acc. Chem. Res.* **1996**, *29*, 373-380.
(219) Tellinghuisen, J. *Biophys. Chem.* **2006**, *120*, 114-120.
(220) Liu, Y.; Sturtevant, J. M. *Biophys. Chem.* **1997**, *64*, 121-126.
(221) Hermanson, G. T. *Bioconjugation Techniques*, 2nd ed.; Academic Press: New York, 2008.
(222) Bomgardon, R. *Previews* **2008**, *12*, 2-3.
(223) Sugio, S.; Kashima, A.; Mochizuki, S.; Noda, M.; Kobayashi, K. *Protein Eng.* **1999**, *12*, 439-446.
(224) Jin, L.; Choi, D. Y.; Liu, H.; Row, K. H. *Bull. Korean Chem. Soc.* **2005**, *26*, 136-138.
(225) Yamasaki, K.; Rahman, M. H.; Tsutsumi, Y.; Maruyama, T.; Ahmed, S.; Kragh-Hansen, U.; Otagiri, M. *AAPS PharmSciTech* **2000**, *1*, No pp. given.
(226) Ghuman, J.; Zunszain, P. A.; Petitpas, I.; Bhattacharya, A. A.; Otagiri, M.; Curry, S. *J. Mol. Biol.* **2005**, *353*, 38-52.
(227) Rahman, M. M.; Rahman, M. H.; Rahman, N. N. *Pak. J. Pharm. Sci.* **2005**, *18*, 43-47.
(228) Zunszain, P. A.; Ghuman, J.; McDonagh, A. F.; Curry, S. *J. Mol. Biol.* **2008**, *381*, 394-406.